EXPERIMENTS ON ROTATIONAL RESTRAINT OF SHEATHING

Schafer, B.W., Sangree, R.H., Guan, Y.

FINAL REPORT

FOR:

American Iron and Steel Institute – Committee on Framing Standards

July 2007

TABLE OF CONTENTS

EXECUTIVE SUMMARY

A series of cantilever tests on joist-sheathing assemblies were conducted to determine the rotational restraint that sheathing provides to the compression flange of a floor joist in bending. This rotational restraint, which is characterized by the stiffness k_ϕ, can partially or fully retard distortional buckling. Distortional buckling is a mode of instability in which the flange undergoes rotation about the flange/web juncture of a member and the web locally bends. This mode of buckling has recently been recognized as a separate strength limit state in the North American Specification and design rules for its prediction adopted.

The cantilever tests reported herein (pictured to the right) covered joist thicknesses from 0.033 in. to 0.097 in., joist depths from 3.62 to 12 in., flange widths from 1.62 to 2.50 in., fasteners from #6 to #10, and plywood, OSB, and gypsum board sheathing. A total of 36 independent tests (and 6 re-tests) were conducted. The majority of the tests were completed with plywood sheathing and exhibited well behaved results through large rotations of the assembly. However, large variation in the total rotational stiffness was observed in the tests. The OSB tests exhibited less scatter than their plywood counterparts, but one test failed in pull-through at a rotation well beyond expected levels required. All of the gypsum tests failed via pull-through of the fasteners and large variations in the strength of the assembly were observed.

In this report a new method is proposed and validated for extending the cantilever tests such that the rotations associated with the sheathing and those associated with the connection may be decomposed. For example, shown to the right are the moment-rotation curves for a plywood sheathed specimen showing the overall rotation (θ_2) as well as the sheathing rotation (θ_w) and connection rotation (θ_{c2}) from which the overall rotation is composed; in this example the connection is quite a bit stiffer than the sheathing. Through this decomposition a number of findings are illustrated, including (1) variability in plywood sheathed specimens is due to the plywood, not the connection stiffness, (2) variability in OSB specimens is low, but primarily due to the connection stiffness, not the OSB, (3) gypsum board connection stiffness is high and consistent; but strength is low and variable, (4) joist thickness is the most important variable for determining connection stiffness, far more important than joist depth, joist flange width, or even fastener size and fastener spacing.
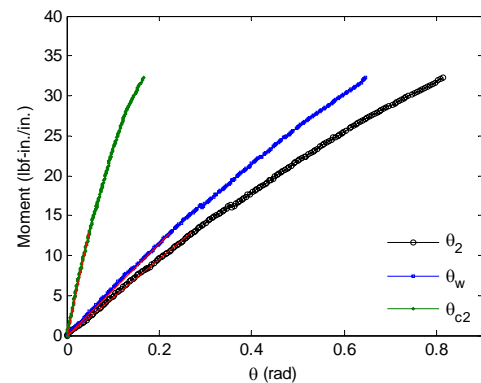
A design method is proposed for adoption that characterizes the available rotational stiffness as two rotational springs in series, i.e.: $k_\phi = (1/k_{\phi_w} + 1/k_{\phi_c})^{-1}$ where k_{ϕ_w} is the sheathing (wood) rotational stiffness, estimated as EI_w/L where EI_w is the bending rigidity of the sheathing (industry standard APA, Gypsum Assoc., etc. tables may be used) and L is ½ the joist spacing; k_{ϕ_c} is the connection rotational stiffness, estimated as a function of the joist thickness based on the experimental results herein and assuming fastener spacing of at least 12 in. o.c. to the sheathing. Section 13 of this report provides the complete methodology for determining k_ϕ in draft specification form.

1   INTRODUCTION AND BACKGROUND

A cold-formed steel floor joist may potentially suffer from a number of member instabilities that limit its ultimate strength. The most common concern is lateral-torsional buckling of the joist; blocking and bridging combined with fastened sheathing is employed to stabilize the members from the global translation and twist associated with lateral-torsional buckling, as shown in Figure 1. Local buckling, where the strength and rigidity of portions of the member are partially lost due to plate buckling, must also be accounted for. Local buckling reductions are handled through the use of the effective width method and appropriate effective cross-section properties. The strength in local buckling is largely independent of the floor framing details as the instability occurs over a short length of the joist. The final member instability of concern is distortional buckling (Figure 2); distortional buckling is a combination of local and lateral-torsional buckling, involving large rotations of the flange and large plate bending deformations in the web. The floor sheathing provides a beneficial restraint for the joist against distortional buckling, but the magnitude of this restraint is poorly understood. This report details testing performed to quantify the provided rotational restraint.

(a) floor framing   (b)sub floor sheathing
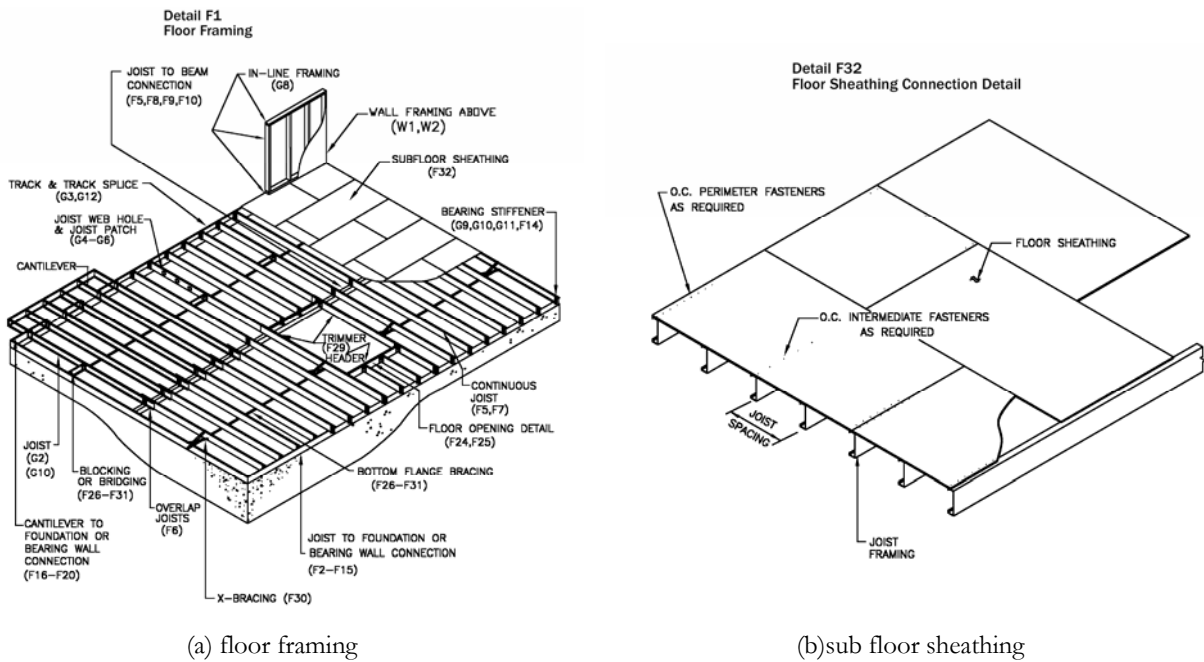
Figure 1 Typical floor framing showing
(a) overall floor system including blocking/bridging to stabilize joists and (b) sheathing of joists
Source: Low-rise residential construction details, Steel Framing Alliance (2000)

(a) distortional buckling of an exterior joist

(b) distortional buckling of interior joist (sheathing provides twice the restraint of exterior case)
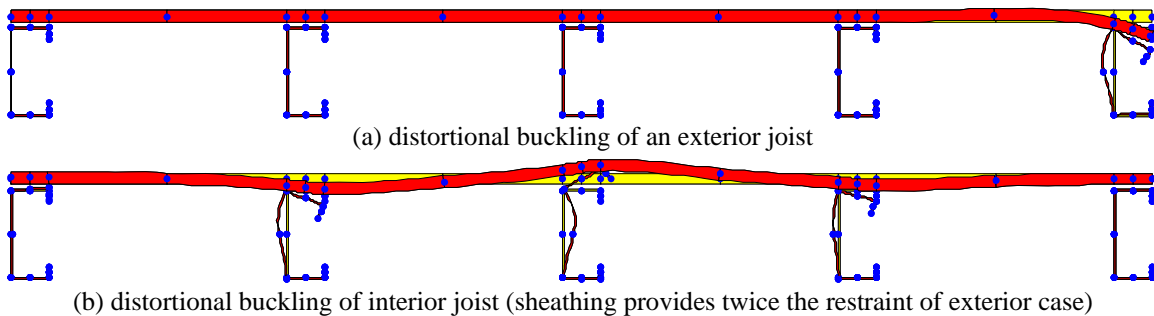
Figure 2 Finite strip model of a floor joist system

An investigation into the restraint that sheathing provides against distortional buckling is timely as new provisions to account for distortional buckling have just (2006) been adopted in the AISI-S100 (2007). These provisions, section C3.1.6 of AISI-S100, were developed through a series of 4-point bending tests conducted by Yu and Schafer (2003, 2006) in which distortional and local buckling of bending members were examined. The distortional buckling tests, as shown in Figure 3, did not include any compression flange restraint and generally resulted in distortional buckling failures. When the metal panel shown in the shear spans of Figure 3(a) was extended into the center region and fastened to the compression flange with pairs of fasteners, the failure mode changed to local buckling. In these latter tests the metal panel was engaged and distortional buckling was restricted. The rotational restraint provided by the metal deck was the key to avoiding distortional buckling. The new provisions for distortional buckling in C3.1.6 of AISI-S100 include a term, k_ϕ, which increases the distortional buckling capacity as a function of available rotational restraint (stiffness).

(a) test setup of Yu and Schafer (2006) to investigate unrestrained distortional buckling

(b) 800S200-054 C with unrestrained compression flange exhibiting distortional buckling
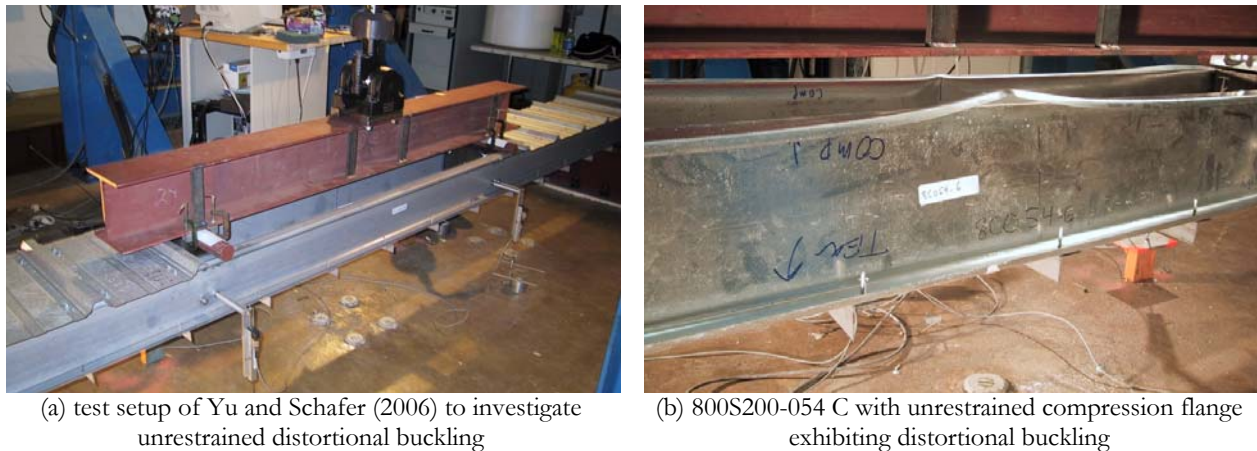
Figure 3 Tests on distortional buckling of C-sections

In the early 1980's the Metal Building Manufacturer's Association (MBMA) examined available rotational restraint in their systems: purlins fastened through insulation to metal deck. MBMA developed the "F" test (MRI 1981, Hausler and Pabers 1973) which later was formalized as AISI TS-1-02 (AISI 2002). The test uses a small cantilevered segment of panel with a purlin attached, and pulls on the free flange of the purlin such that a moment and rotation is induced at the panel-purlin connection. This test provides an estimate of the panel-purlin rotational restraint (k_ϕ) and was intended to provide reliable estimates of the bracing provided by the panel to restrict lateral-torsional buckling of the purlin, and to restrict rolling of the Z-section as it attempts to respond in its principal plane. LaBoube summarized the available MBMA testing with metal panels and demonstrated the critical role of purlin thickness on the available rotational restraint (LaBoube 1986). The important role of thickness in the conducted tests (as opposed to purlin depth, deck thickness, insulation, etc.) suggests that the panel-purlin connection flexibility, and local flange deformations at the connection, played a dominant role.

The restraint provided by metal deck was further explored in Yu's thesis (Yu 2005) and the existing MBMA tests were found to provide a conservative prediction of developed restraint and suggested for use as k_ϕ in the distortional buckling design check in the commentary of AISI-S100. However, no equivalent data for cold-formed steel framing systems is available. The tests conducted herein use the "F" test to examine cold-formed steel framing systems: steel joists sheathed with plywood and OSB, as well as steel joists sheathed with gypsum board as might exist in walls and ceilings.

2   DESIRED ROTATIONAL RESTRAINT (k_ϕ)

2.1   Distortional buckling with k_ϕ vs. local and lateral-torsional buckling

From the standpoint of simplifying design, the desired rotational restraint is the k_ϕ that will eliminate the distortional buckling limit state. For the sections initially selected to be tested, the k_ϕ such that M_n for distortional buckling per C3.1.6(b) of AISI-S100 (2007) is always greater than M_n for a fully laterally braced ($L_b=0$) section is determined and reported in Table 1. The k_ϕ values reported in Table 1 provide estimates of the desired rotational restraint for the testing; in addition they indicate the relative complexity in determining the desired k_ϕ for eliminating distortional buckling. In general, thicker members with higher yield stress require larger k_ϕ's to eliminate distortional buckling, but this is a very approximate statement and not universally true.

Table 1 Minimum k_f and L_b to avoid distortional buckling for example sections[1]

| | avoid distortional bucking via | |
| | k_ϕ | L_b |
Section	(lbf-in./in./rad)	(ft)
362S162-33	36	4.4
362S162-33 (50ksi)	76	4.2
362S162-68	*DB never controls*	*DB never controls*
362S162-68 (50ksi)	*DB never controls*	*DB never controls*
800S200-33	31	6.6
800S200-33 (50ksi)	30	5.3
800S162-54	92	4.1
800S162-54 (50ksi)	190	4.1
800S200-54	300	6.1
800S200-54 (50ksi)	326	6.0
800S250-54	190	7.8
800S250-54 (50ksi)	233	7.1
800S200-97	*DB never controls*	*DB never controls*
800S200-97 (50ksi)	400	3.8
1200S200-54	128	5.9
1200S200-54 (50ksi)	123	5.6
1200S200-97	118	4.1
1200S200-97 (50ksi)	770	4.4

k_ϕ determined such that M_n for distortional buckling per C3.1.6(b)
   is greater than M_n for a fully laterally braced ($L_b=0$) section
L_b determined such that M_n for distortional buckling per C3.1.6(b)
   is greater than M_n for a section braced at any $L > L_b$

At longer unbraced lengths, lateral-torsional buckling will control and distortional buckling will not matter even if $k_\phi=0$, thus Table 1 also reports the unbraced length L_b at which M_n for distortional buckling per C3.1.6(b) of AISI-S100 (2007) is greater than M_n for lateral-torsional buckling. The length at which distortional buckling does not control is relatively short, so if blocking or bracing is spaced at lengths greater than L_b in Table 1 and the sheathing contribution is ignored in the strength calculation, then distortional buckling can also be ignored.

---

[1] These calculations could be performed for all SSMA sections, i.e., a table could be provided to the engineer so that the k_ϕ or L_b to eliminate distortional buckling is known for each section.

For any of the sections considered in Table 1, the interplay between k_ϕ and L_b on strength can be demonstrated in a single design chart as shown for the 800S200-54 (50ksi) section in Table 2. Table 2 provides the nominal capacity for lateral-torsional buckling as a function of unbraced length along the horizontal dimension and the nominal capacity for distortional buckling as a function of rotational restraint (k_ϕ) along the vertical dimension. The shaded (highlighted) region of Table 2 indicates those combinations of k_ϕ and L_b for which distortional buckling will control.

Table 2 Example design chart for 800S200-54 (50ksi)[2]

Sect: 800S200-54 (50ksi)			M_n NOMINAL Table						
fy	50	ksi							
			Local and lateral-torsional per AISI 2004 (calc per CFS 5.02)						
			M_n	75.16	75.16	73.57	62.10	41.2	-	(kip-in)
Distortional buckling			ϕ	1.00	1.00	1.00	1.00	1.00	1.00
per C3.1.6(b) ϕ=1.00			ϕM_n	75.16	75.16	73.57	62.10	41.2	-
M_n	ϕM_n	k_ϕ	L	0	2	4	6	8	10	(ft)
62.41	62.41	0.000		62.41	62.41	62.41	62.10	41.19	-
63.66	63.66	0.025		63.66	63.66	63.66	62.10	41.19	-
64.85	64.85	0.050		64.85	64.85	64.85	62.10	41.19	-
65.99	65.99	0.075		65.99	65.99	65.99	62.10	41.19	-
67.08	67.08	0.10		67.08	67.08	67.08	62.10	41.19	-
69.12	69.12	0.15		69.12	69.12	69.12	62.10	41.19	-
71.00	71.00	0.20		71.00	71.00	71.00	62.10	41.19	-
72.74	72.74	0.25		72.74	72.74	72.74	62.10	41.19	-
74.35	74.35	0.3		74.35	74.35	73.57	62.10	41.19	-
77.23	77.23	0.4		75.16	75.16	73.57	62.10	41.19	-
79.73	79.73	0.5		75.16	75.16	73.57	62.10	41.19	-
81.91	81.91	0.6		75.16	75.16	73.57	62.10	41.19	-
82.15	82.15	0.7		75.16	75.16	73.57	62.10	41.19	-
82.15	82.15	0.8		75.16	75.16	73.57	62.10	41.19	-
82.15	82.15	0.9		75.16	75.16	73.57	62.10	41.19	-
82.15	82.15	1.0		75.16	75.16	73.57	62.10	41.19	-
(kip-in)		(kip/rad)							

DB controls: M_n for dist. buckling per C3.1.6(b) is less than M_n per NASpec (2004)

2.2 Discontinuity in ϕ (Ω) between local and distortional buckling

For distortional buckling the nominal strength has a maximum value of M_y and the design strength ϕM_y where ϕ=0.90. For local buckling the nominal strength has a maximum value of M_y and the design strength ϕM_y where ϕ=0.95. Thus, though the two limit states nominally converge to the same capacity, their design strength does not converge and a discontinuity exists because of ϕ.

Even for an infinitely stiff rotational restraint, k_ϕ, distortional buckling will control when the section is locally fully effective. The effective section modulus (accounting for local buckling), S_{eff}, must be at least $0.95S_g$ before local buckling may be the limit state in a fully braced member. Table 3 shows

---

[2] Similar to Table 1 these tables can be provided for all SSMA sections. The use of linear interpolation in these tables was found to provide satisfactory predictions of the limiting k_ϕ and L_b values reported in Table 1. Additional tables for other example sections were calculated and may be provided electronically upon request.

how the design chart is modified (from Table 2) if the design strength is considered for the comparison instead of the nominal strength. The k_ϕ required to eliminate distortional buckling in all cases is increased, and in some situations no such maximum k_ϕ to eliminate distortional buckling will even exist. The situation is similar in ASD with an Ω discontinuity replacing the ϕ discontinuity.

Table 3 Example design chart for 800S200-54 (50ksi) including resistance (ϕ) factors

Sect: 800S200-54 (50ksi)			ϕM_n Table							
fy	**50**	**ksi**								
			Local and lateral-torsional per AISI 2004 (calc per CFS 5.02)							
			M_n	75.16	75.16	73.57	62.10	41.2	-	(kip-in)
Distortional buckling			ϕ	0.95	0.95	0.90	0.90	0.90	-	
per C3.1.6(b) ϕ=0.90			ϕM_n	71.40	71.40	66.21	55.89	37.1	-	
M_n	ϕM_n	k_ϕ	L	**0**	**2**	**4**	**6**	**8**	**10**	**(ft)**
62.41	56.17	**0.000**		56.17	56.17	56.17	55.89	37.07	-	
63.66	57.29	**0.025**		57.29	57.29	57.29	55.89	37.07	-	
64.85	58.37	**0.050**		58.37	58.37	58.37	55.89	37.07	-	
65.99	59.39	**0.075**		59.39	59.39	59.39	55.89	37.07	-	
67.08	60.37	**0.10**		60.37	60.37	60.37	55.89	37.07	-	
69.12	62.21	**0.15**		62.21	62.21	62.21	55.89	37.07	-	
71.00	63.90	**0.20**		63.90	63.90	63.90	55.89	37.07	-	
72.74	65.47	**0.25**		65.47	65.47	65.47	55.89	37.07	-	
74.35	66.92	**0.3**		66.92	66.92	66.21	55.89	37.07	-	
77.23	69.51	**0.4**		69.51	69.51	66.21	55.89	37.07	-	
79.73	71.76	**0.5**		71.40	71.40	66.21	55.89	37.07	-	
81.91	73.72	**0.6**		71.40	71.40	66.21	55.89	37.07	-	
82.15	73.94	**0.7**		71.40	71.40	66.21	55.89	37.07	-	
82.15	73.94	**0.8**		71.40	71.40	66.21	55.89	37.07	-	
82.15	73.94	**0.9**		71.40	71.40	66.21	55.89	37.07	-	
82.15	73.94	**1.0**		71.40	71.40	66.21	55.89	37.07	-	
(kip-in)		**(kip/rad)**								

DB controls: ϕM_n for distortional buckling per C3.1.6(b) is less than ϕM_n per AISI 2004

The official justification for the discontinuity in the ϕ and Ω factors in C3.1.1 of the AISI-S100 (2007) between lateral-torsional buckling (ϕ=0.90) and local buckling of a laterally braced section (ϕ=0.95) are unknown to the authors. In fact, the Canadian ϕ values do not have this discontinuity.

The justification for the discontinuity would seem to be that fully laterally braced sections have higher reliability; indeed this holds a certain logic. If this is the case then the ϕ for distortional buckling of C3.1.6 should also be increased to 0.95 when the nominal capacity reaches M_y. Alternatively, ϕ should be set to 0.90 for all bending members – a number that is basically borne out by the statistics available to the authors.

It is the authors opinion that the most likely reason for the higher ϕ for the local buckling case is that such members which are fully effective and fully laterally braced often exhibit moderate inelastic reserve (i.e. $M_n > M_y$). Rather than modify ϕ, it would be more appropriate to use a uniform ϕ, and increase the applicability of the methods for inelastic reserve prediction in beams.

3   EXPERIMENTAL TESTING TO MEASURE k_ϕ (AISI TS-1-02)

To determine the rotational restraint k_ϕ in typical floor (and wall) systems, cantilever tests, based primarily on the existing AISI test standard AISI TS-1-02, were conducted.

3.1   Test setup

The basic test setup is illustrated in Figure 4 and Figure 5. Sheathing material (in our case always 54 in. wide[3]) is placed in a cantilever fashion with a joist attached a prescribed length, L, away from the clamped end. The side of the joist not attached to the sheathing has a load (displacement) applied which generates a moment (rotation) on the sheathing-joist connection. As the sheathing bends and the connection rotates, vertical Δ_v and horizontal displacement Δ_h, and the load, P, are recorded.
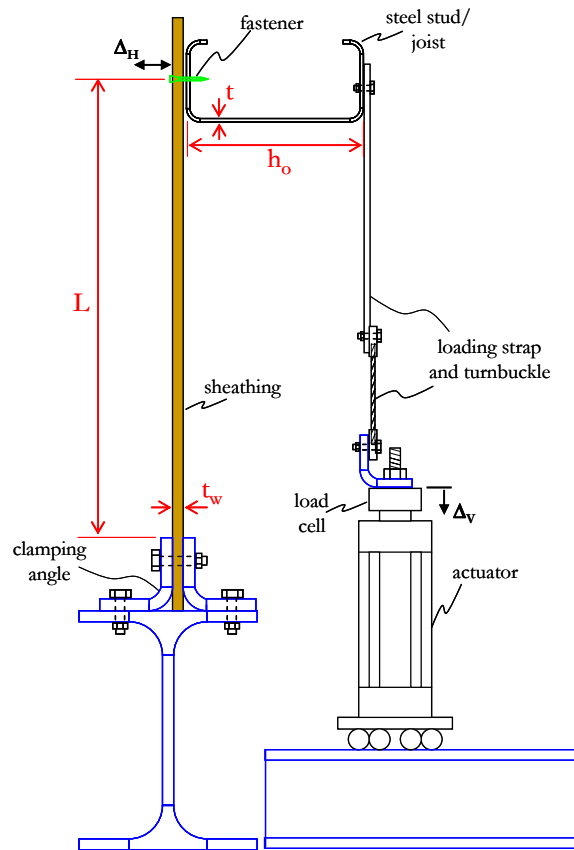
Figure 4 Basic test setup (line drawing)

The base of the sheathing is clamped between 6 x 4 x 5/16. in. angles, shown at the top of the blue testing frame in Figure 5(a) and (c) and in Figure 4. The angle called out as the "clamping angle" in Figure 4 has a slotted connection to the testing frame so that the legs of the angle can be brought flush with the sheathing. The clamping angles have pre-drilled holes spaced every 5 ¾ in. to through-fasten and clamp the sheathing with 5/8 in. diameter structural bolts. Once clamped in place, the base of the sheathing is fixed and aligned (all initial warp is removed at the base).

---

[3] Width of the test specimen in a cantilever test is not codified in AISI-TS-1-02. Selection of 54 in. for the width of the tests conducted here reflect (1) a width that insured at least 5 fasteners spaced at 12 in. o.c. were used thus providing a reasonable average connector response, (2) a width that was longer than any expected distortional buckling half-wavelength, even for the 12 in. deep members, and, (3) the width used in cantilever tests conducted in the metal building industry which were never less than 28 in. in the testing the author is aware of.

The load is applied by a 22kip MTS hydraulic actuator with 6 in. stroke. The base of the actuator is attached to a linear guide system (guide block with wheels that slides along a track) that allow the load to move as the specimen bends and helps keep the vertical load in alignment, Figure 5(a),(b). The top of the actuator has a load cell attached, Figure 5(b), and a 4 x 4 x 5/16 angle which provides the yoke for evenly pulling on the joist specimen, Figure 5(c). A strap and turnbuckle system is fastened between the loading yoke and the flange of the joist, Figure 5(c). The 1 ¼ in. wide by 0.031 in. thick high-carbon steel strap is fastened to the free flange of the joist with pre-drilled holes and ¼ in. cap screws with a lock washer and nut. The stainless steel eye and eye 5/16 in. turnbuckle is attached to the strap with ¼ in cap screws and to the loading angle, through pre-drilled holes with ¼ in. cap screws.

Horizontal displacement is measured by a pair of position transducers, Figure 5(d). These transducers are discussed in detail in Section 5.2.

(a) front view of testing rig, angles spaced with holes 6 in. o.c. are attached to specimen for fixed conditions

(b) hydraulic actuator on linear guide, load cell on top measures P, and internal LVDT measures Δ_v
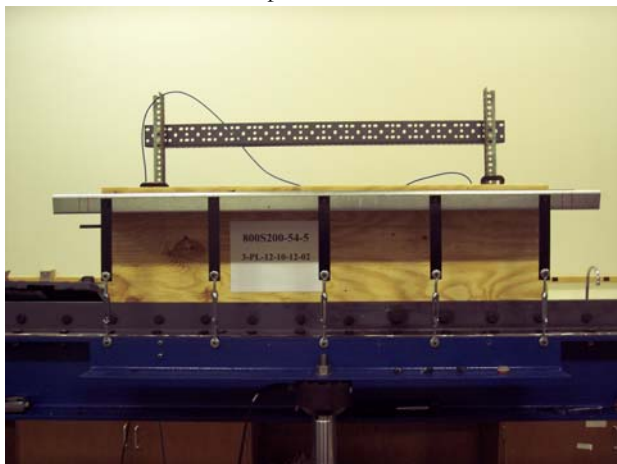
(c) testing rig with L=12 in. plywood specimen in place, actuator attached to angle which is attached to loading straps with turnbuckles and bolted to joist flange

(d) rear view of L=12 in. plywood panel, position transducers mounted to frame and attached to back of panel for measurement of Δ_{h1} and Δ_{h2}

Figure 5 Basic test setup (pictures)

3.2   Test specimens

A summary of the tests conducted and reported on herein is given in Table 4. The rows of Table 4 are organized by the joist, which uses standard SSMA nomenclature for the designators.

Table 4 Conducted rotational restraint tests

conducted tests											
Sheathing -->	Plywood					OSB		Gypsum			
Joist Spacing (L) -->	12"				24"	24"		12"		24"	
Fastener # -->	6		10		6	6	10	6	10	6	10
Fastener Spacing -->	6"	12"	6"	12"	12"	12"	12"	12"	12"	12"	12"
362S162-33		1						1			
362S162-68		1						1			
800S200-54	2	4		1	3	1	1	1	1	1	1
800S250-54		1		1							
800S200-97			1	4			1		2		
1200S200-54		2				1					
1200S200-97				2			1				

3.2.1   *Joists*

In the testing, joist depth was varied from 3 5/8 in. to 12 in. and designated joist thickness from 0.033 in. to 0.097 in. Typical tested joists, shown in the testing rig, are provided in Figure 6. Measured joist dimensions are given in Section 10 of this report. Joist thickness was verified against ordered thickness by measuring with the galvanized coating in place and assuming a nominal thickness for the coating. Nominal joist thickness was used for all calculations reported herein.

362S162-033 just under load

800S200-054 just prior to load

800S200-097 just prior to load

1200S200-054 just under load

Figure 6 Range of joists used for test specimens

3.2.2 *Sheathing*

Three sheathing types were investigated: 15/32 in. plywood, 7/16 in. OSB, and ½ in. gypsum board, as shown in Figure 7. All tests were conducted such that the strong axis for the material is perpendicular to the primary stress direction in the sheathing. This provides the most conservative orientation for the sheathing, but may lead to increased variability in the results – particularly for the plywood sheathed specimens.

15/32 in. plywood

7/16 in. OSB

1/2 in. gypsum board

7/16 in. OSB in testing rig

Figure 7 Range of sheathing types used

3.2.2.1 Initial warp in sheathing

The sheathing specimens were neither uniform in property nor in geometry; after assembly and installation in the testing rig the initial condition of the sheathing often included a warp, as shown in Figure 8. This warp causes difficulty with initial alignment of the loading and generally leads to difficulties in ensuring that the load in the specimens is equally distributed across the sheathing-to-joist fasteners. Measurement of the initial warp was made for each specimen. For the plywood specimens the average initial warp was 1/3 in., for the OSB 1/8 in., and for the gypsum board less than 1/32 in. The relatively large warp in the plywood leads to greater expected variability in the testing.

$$\text{warp} = \text{warp}_1 + \text{warp}_2$$

measured warp is the sum of two values shown, i.e., warp=warp₁+warp₂
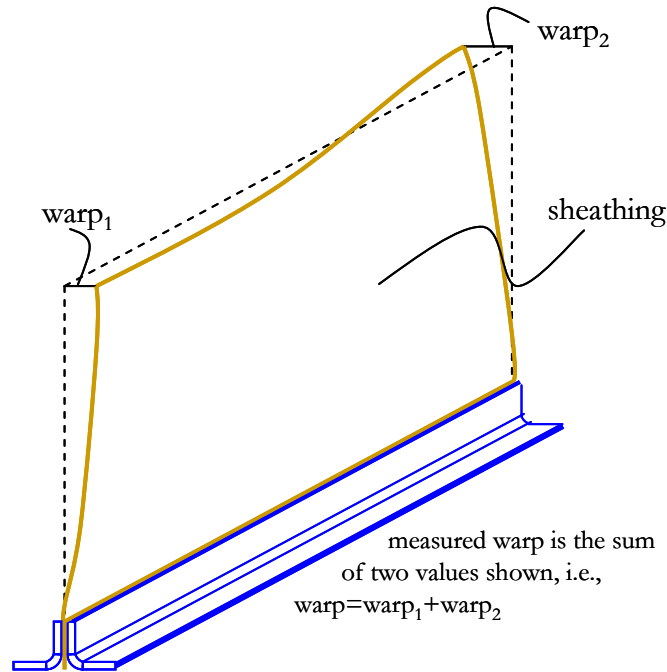
Figure 8 Initial warp in sheathing

3.2.2.2 Sheathing condition

For the plywood sheathing the initial condition of the external plies was recorded for each specimen. Cracks, large and small, and knots, large and small, were regularly observed in the specimens and on both the compression and tension side of the external plies. Nothing in the observation lead us to conclude that the plywood does not meet its rated standard, but given the large range of initial conditions for the plywood sheathing, significant variability in response is to be anticipated.

3.2.3   Joist Spacing / Cantilever length

Two cantilever lengths were investigated in the tests: 12 in. and 24 in. As shown in Figure 9 this corresponds to center-to-center joist spacing of 24 and 48 in. In the cantilever tests the length of the cantilever is measured from the tip of the base clamping angles to the centerline of the fasteners as illustrated in Figure 10.

(a)

w_j

$\tfrac{1}{2}\, w_j = L$

L

(b)

$$\text{test}: \quad k_{\phi w} = \frac{EI_w}{L}$$

floor

$$\text{interior}: \quad k_{\phi w} = 2\,\frac{EI_w}{\tfrac{1}{2}\, w_j} = 2\,\frac{EI_w}{L}$$

$$\text{exterior}: \quad k_{\phi w} = \frac{EI_w}{\tfrac{1}{2}\, w_j} = \frac{EI_w}{L}$$
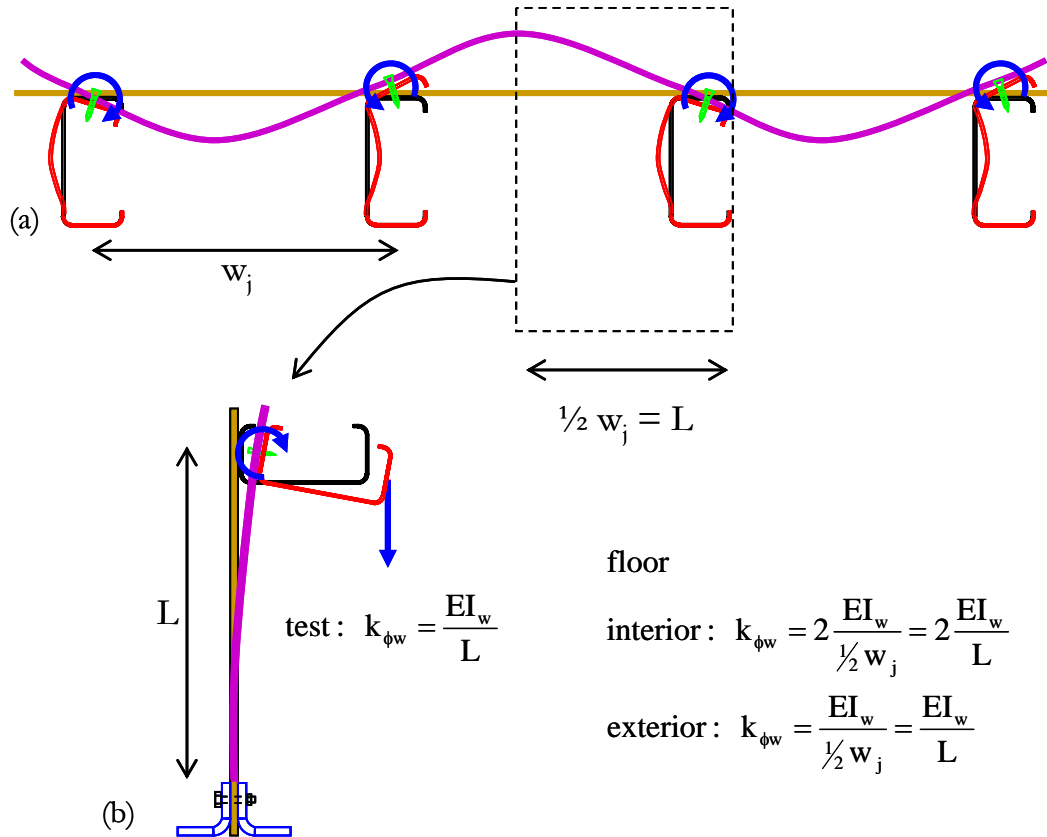
Figure 9 Relation between joist spacing and cantilever length in test (a) floor with joists in distortional buckling showing bending of sheathing, and (b) test showing bending of sheathing

Figure 10 Detail of test setup from behind, cantilever length is taken from the tip of the clamping angles to the fastener line (12 in. or 24 in. from the tip of the angles)

3.2.4   Fasteners

Two fasteners types were employed in the testing: #6 and #10 as shown in Figure 11. The #6 fastener is a Simpson Strong-Tie DWFSD114PS and the #10 fastener is a Simpson Strong-Tie FHSD1S1016 (which is not currently commercially available). The #6 fasteners were installed using Simpson Strong-Tie's QuikDrive system and the #10 fasteners with an industrial grade screw gun.

#10 and #6 screw, note drive type

#10 and #6 screw, note head geometry, potentially important for pull-through resistance

Figure 11 Fasteners

3.2.5   Fastener Spacing

Two fastener spacings were investigated, 6 in. and 12 in. on center, as illustrated in Figure 12.
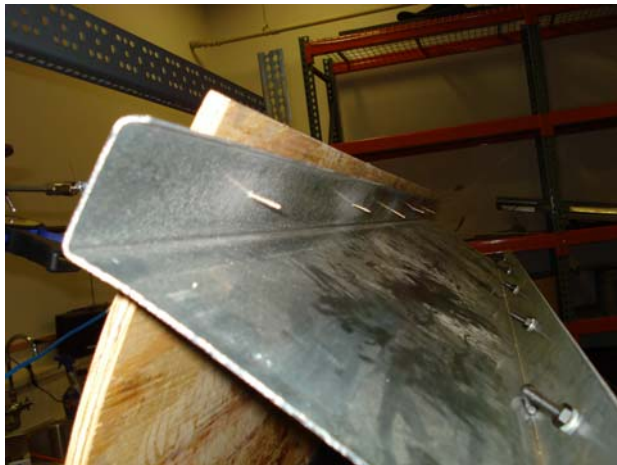
#6 @ 12 in. o.c. with 800S200-54 joist

#6 @ 6 in. o.c. with 800S200-54 joist

Figure 12 Fastener spacing

3.2.6   Specimen assembly

Assembly of the specimens was completed via the following steps. Holes were pre-drilled in the sheathing to match the clamping angles on the testing rig. Based on the clamping angle dimensions and the hole locations a fastener line was established by marking the sheathing either L = 12 in. or L = 24 in. above the tip of the clamping angle. Joists were rough cut (using a portable chop saw) to the appropriate length (54 in. for the tests conducted herein) and placed on the floor. The sheathing was placed on top of the joists and c-clamps were used to clamp the joist to the sheathing. Fasteners were installed by standing above the sheathing and drilling down through the sheathing and into the joist in a vertical fashion along the established fastener line similar to the method that would be used in typical floor installations.

3.2.6.1   Fastener alignment

The specimen assembly method was intended to ensure that the fasteners were aligned mid-width of the joist flange. However, due to warp in the sheathing, imperfections in the joists, and installation difficulties perfect alignment was not consistently achieved. For example, Figure 13(a) shows a typical specimen with misaligned fasteners. Statistics were collected by visual observation on the accuracy of the alignment, with screws misaligned by approximately ¼ in. or greater noted as being misaligned towards the web or towards the lip. These statistics are summarized in the histogram of Figure 13(b) which indicates the number of fasteners misaligned out of 5 (only the 12 in o.c. spacing is shown in the histogram). In some cases as many as 4 out of 5, or 5 out of 5, of the screws were misaligned. The most common situation was no misalignment, and generally the error is random with little bias towards the web or lip noticeable. Misalignment increases the variability of the test results, but we would not expect that field installations would be perfectly aligned either. As such, the misalignment in the tests is considered to be a reasonable approximation of expected misalignment in the field.
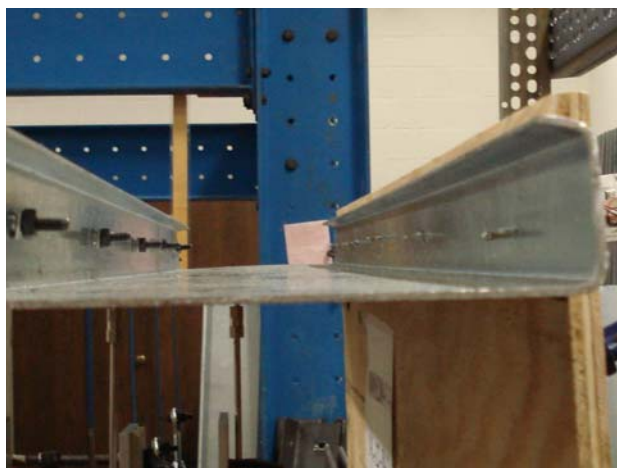
typical sheathing-joist fastener alignment,
2 out of 5 noted as mis-aligned for this specimen
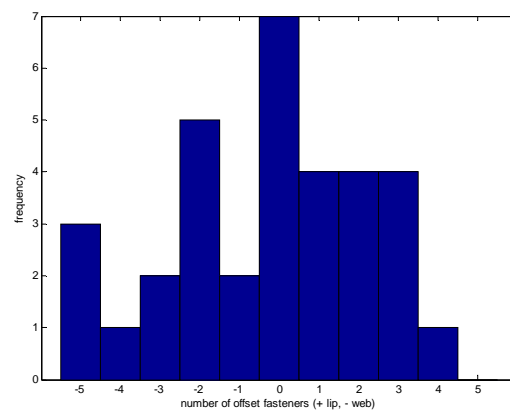
histogram indicating the frequency of fastener mis-
alignment towards the web or lip out of 5 total fasteners

Figure 13 Fastener alignment

3.2.6.2   Overdriven screws

Mildly (less than 10% penetration of the sheathing) overdriven screws were relatively common in the assembly of the specimens. Using a strict definition of overdriven screws, and considering any screw in which the screw face terminates below the face of the sheathing; 25% of the installed fasteners are found to be overdriven. Examples of properly and overdriven fasteners are provided in Figure 14.

It is not immediately clear as to what role the relatively high percentage of overdriven fasteners will have on the results. Pull-through capacity would be expected to reduce; but only the gypsum board sheathing is dominated by this mode of behavior. Loss in connection stiffness due to mildly overdriven screws is not known. However, like the initial warp of the sheathing, differences in the stiffness of the sheathing-to-joist connections through the fact that some are overdriven would make it difficult to ensure that all fasteners are evenly loaded; thus, the observed variability in testing is again potentially increased.
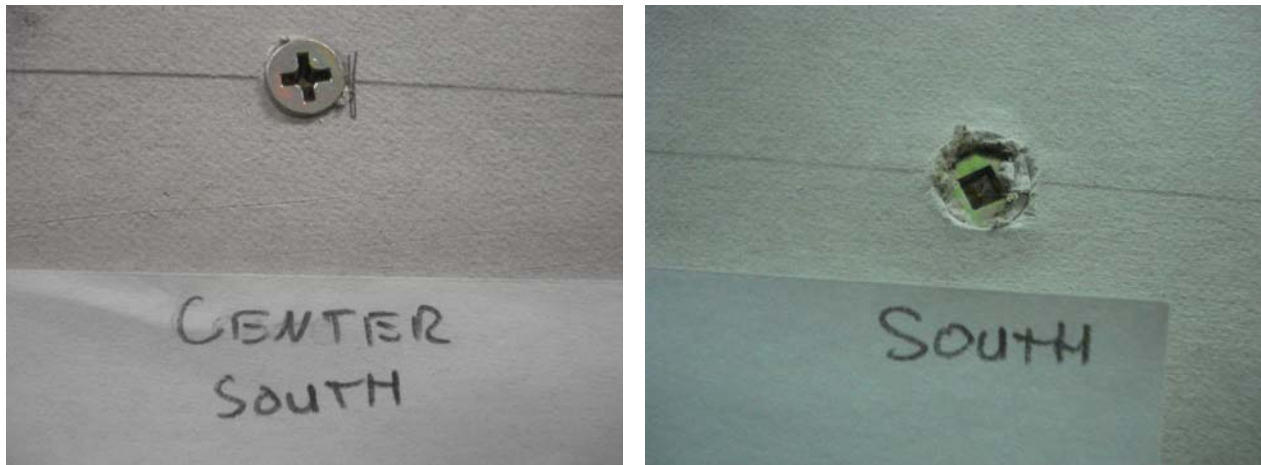
example of properly driven screw (in gypsum board)   example of overdriven screw (in gypsum board)

Figure 14 Overdriven screws

3.2.7   Alignment in testing apparatus

Placement of the specimen in the testing rig is straightforward due to the pre-drilled holes in the sheathing. After placing the sheathing in the clamping angles, the 5/8 in. diameter through bolts are tightened and the base of the sheathing becomes effectively fixed. Connection of the joist to the loading straps and the loading angle (yoke) is a more involved and subjective process. Holes are pre-drilled in the flanges and ¼ in. cap screws are through fastened and tightened with a lock washer and nut to the loading strap, these black loading straps have a turnbuckle which attaches to the loading angle, as shown in Figure 15. The turnbuckles allow initial misalignment between the loading angle and the joist to be accommodated. Each turnbuckle is tightened until the slack is removed from the straps in an iterative process. In addition, a carpenter's square and bubble level are used to ensure each strap is initially vertical and the loading angle is horizontal (not tilted). Additional adjustments of the turnbuckle are typically required to achieve a level system, finally resulting in a loading arrangement which initially begins with even distribution of forces in the fasteners. As discussed with regard to the initial warp of the sheathing, the loading angle may twist (see Figure 15) moderately under load to accommodate uneven bending of the sheathing – it is intended that accommodating the twist allows the load into the fasteners to remain as even as possible throughout the loading duration.
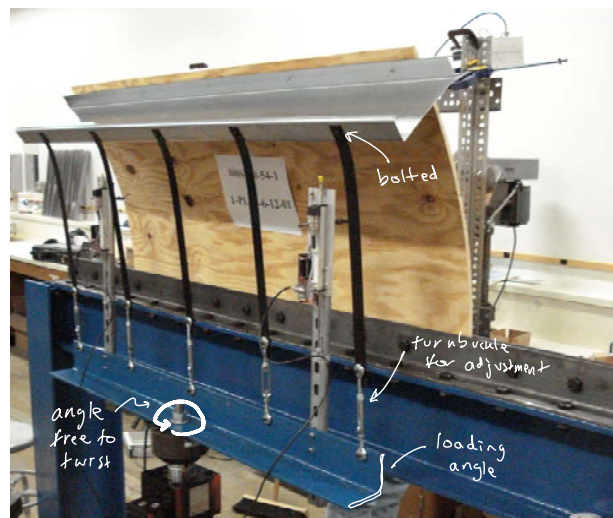
Figure 15 Plywood test under load with details of the loading system called out

3.2.8   Loading rate

Tests are conducted at a Δ_v rate of 0.0033 in./sec (0.2 in./min). Depending on the stiffness and the joist depth, this displacement rate correlates to different "rotation" rates. For the plywood and OSB tests all but one of each were conducted for 30 minutes, where 30 minutes is the time required for the actuator to reach its maximum stroke. Thus, we conclude that the plywood and OSB tests are "static" as intended. Though not dynamic, given the very brittle nature of the gypsum board tests, in some cases those tests, even at these slow displacement rates, failed in only a few minutes.

3.3 P-Δ to M-θ to k_ϕ

The basic test setup is shown in Figure 4. The essential data that is recorded is the load measured from the load cell at the end of the hydraulic actuator, P and the vertical displacement of the hydraulic actuator, Δ_v, measured from the internal actuator LVDT. The moment, per unit width, imposed on the connection is calculated as

$$M = (P/w)h_o$$

This definition for M is exact for the undeformed state, but becomes approximate for higher Δ_v. In the conducted tests the width 'w' is 54 in.

The rotation of the sheathing-connector-joist assembly may be calculated and broken into its component parts with various methods (discussed in Section 4.1), but the simplest method, lumping all deformations together, considers only Δ_v and h_o where

$$\theta_2 = \tan^{-1}(\Delta_v/h_o)$$

The subscript 2 on the rotation angle θ separates this definition from those used in Section 4.1.2. Based on these definitions for M and θ the rotational stiffness may now be defined as

$$k_{\phi 2} = M/\theta_2$$

where $k_{\phi 2}$ has units of (force•distance/length)/radian or simply force/radian.

Typical results for a plywood specimen are provided in Figure 16 and are broken into 4 subplots to illustrate the steps necessary to convert the gross test results from P-Δ to M-θ and finally k_ϕ. Figure 16(a) provides the raw P-Δ_v output from the test, sampled at a rate of 10 Hz, resulting in approximately 18,000 points per test. A 100 point moving average is passed over the data, the data is subsequently sampled down, and unloading is removed, resulting in the cleaned up P-Δ_v results shown in Figure 16(b). Using the formula above for conversion to M and θ_2 the results are converted from P-Δ_v to M-θ_2 in Figure 16(c).

The initial rotational restraint $k_{\phi 2}$ is found by linear regression on the M-θ_2 curve for M<0.4M_{peak}[4], where M_{peak} is the maximum recorded moment in the test. Note, M_{peak} is not the failure moment in all tests, instead M_{peak} is the moment at 6 in. of Δ_v displacement or the failure moment whichever is less[5]. (For the plywood tests failure did not occur in the tests, but for some OSB tests and all gypsum board tests large displacement could not be maintained without failure and thus M_{peak} is the failure moment.) In the example of Figure 16(c), typical for the plywood sheathed tests, the range of moment from 0 to 0.4M_{peak} covers θ_2 from 0 to 0.28 radians, or 16 degrees. For comparison, even far into formation of a distortional buckling collapse mechanism the rotation of a flange in distortional buckling is typically less than 16 degrees. Finally, in Figure 16(d) the change in $k_{\phi 2}$ as the test progresses past 0.4M_{peak} is examined. In this plot linear regression over the established range of θ_2 (in this case 0.28 radians) is continued for larger displacements to generate an approximate tangent stiffness value for $k_{\phi 2}$. Figure 16(d) indicates the loss in $k_{\phi 2}$ as rotations increase, in this case the degradation is only slight and the connection maintains nearly its entire stiffness even for extreme rotations, i.e. 30 degrees or more.

---

[4] 0.4M_{peak} was established by trial-and-error as an acceptable limit whereby the response remained linear.
[5] The 6 in. limit is a practical limit that reflects the maximum stroke of the hydraulic actuator; however at 6 in. of displacement the sheathing and connector are significantly deformed and response is well into the nonlinear range.
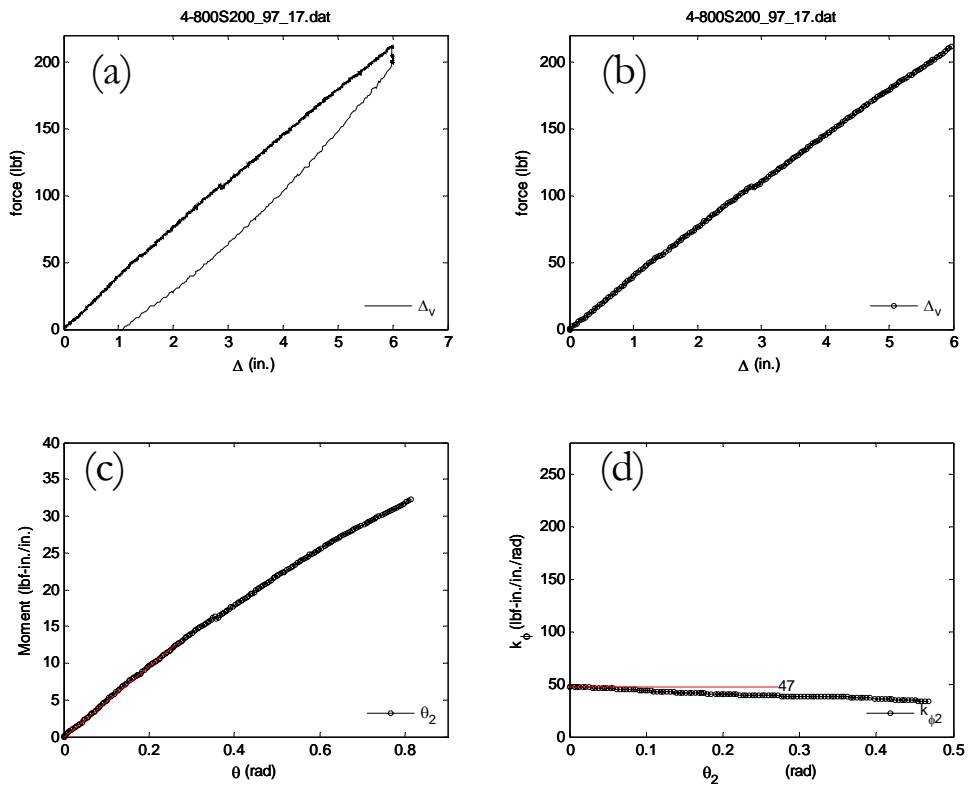
Figure 16 Typical experimental results for plywood specimen: 800S200-97 joist with plywood sheathing, L=12in., #10@6in. (test 18 completed on March 13 2007, file 4-800S200_97_17, designator 4-PL-12-10-6-01)

A complete set of figures, similar to Figure 16, for every conducted test, are provided in the test summary data sheets of Section 10.

3.4   Summary Results

The measured rotational restraint from the tests ($k_{\phi 2}$) is summarized in Table 5. In comparison to the desired rotational restraint to restrict distortional buckling (i.e., Table 1) the available rotational restraint is not great enough to categorically eliminate distortional buckling from consideration.

As discussed below (Section 3.4.3) the $k_{\phi 2}$ results for gypsum board are somewhat misleading as little moment or rotation can be sustained in these connections before failure.

As presented, the rotational restraint includes deformations from the sheathing, connector, joist, and loading apparatus. To provide a more general methodology for incorporating rotational restraint in design, these different components are considered in Section 4.1.

Table 5 Rotational restraint $k_{\phi 2}$ from tests

$k_{\phi 2}$ (lbf-in./in./rad)										
Sheathing -->	Plywood					OSB		Gypsum			
Joist Spacing (L) -->	12"				24"	24"		12"		24"	
Fastener # -->	6		10		6	6	10	6	10	6	10
Fastener Spacing -->	6"	12"	6"	12"	12"	12"	12"	12"	12"	12"	12"
362S162-33		40						75			
362S162-68		42						94			
800S200-54	41	34		33	18	57	44	76	60	53	58
800S250-54		53		43							
800S200-97			47	44			66		58		
1200S200-54		34				44					
1200S200-97				59			75				

(1) average values reported when multiple tests conducted

(2) re-tests of specimens not included in average value calculations (only original test)

3.4.1   *Plywood*

Response of the specimens with plywood sheathing are shown in Figure 17 and Figure 18. All but one of the specimens tested was able to undergo a full 6 in. of Δ_v actuator displacement prior to failure. The one specimen that did fail, shown in Figure 17(b) and Figure 18(a), fractured, initiating at a large knot in the plywood. In some cases, Figure 17(c) for example, large separation between the joist and sheathing was initiated at the larger rotations. In other cases, Figure 17(d) for example, little separation was observed.

(a) typical response of plywood sheathed joist shown for an 800S200-54 joist with plywood, L = 24 in., and #6 fasteners @ 12 in. (1-PL-24-6-12-01_A, 1-800S200_54_1A)

(b) failure in plywood initiating at a knot shown for 800S200-54 joist with plywood, L = 12 in., and #6 fasteners @ 12 in. (1-PL-12-6-12-03, 1-800S200_54_6(12))
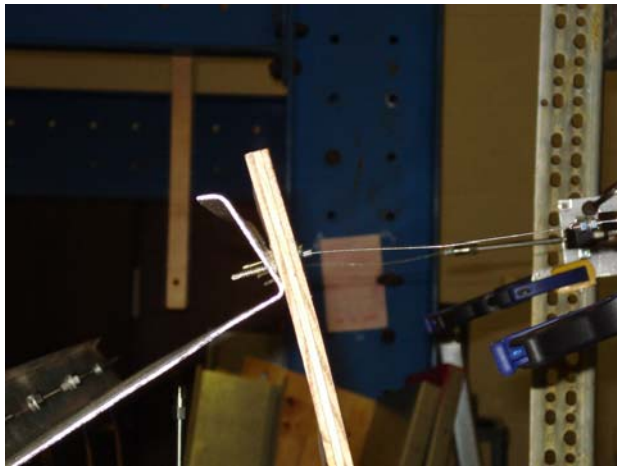
(c) separation between plywood sheathing and joist flange shown for 800S200-54 joist with plywood, L = 12 in., and #6 fasteners @ 12 in. (1-PL-12-6-12-02, 1-800S200_54_5(12))
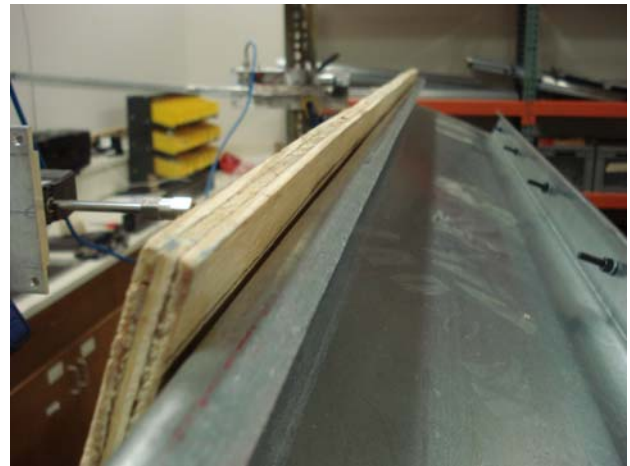
(d) separation between plywood sheathing and joist flange for 800S200-97 joist with plywood, L = 12 in., and #10 @ 12 in. fasteners (1-PL-12-10-12-03, 1-800S200_97_4B)

Figure 17 Response of plywood sheathed joists
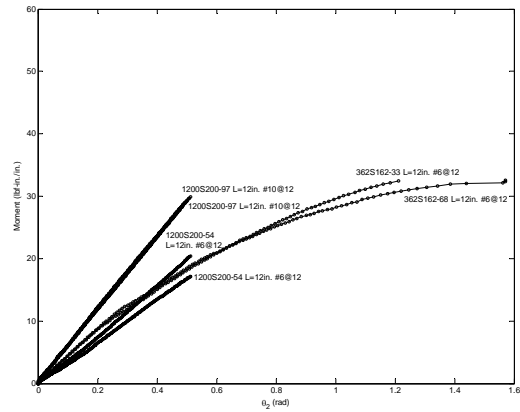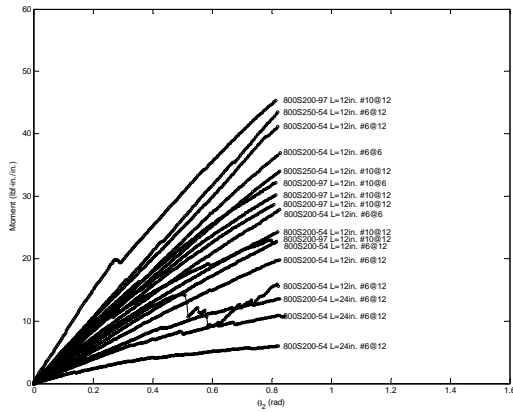
(a) M-θ response for all plywood sheathed tests with 8 in. deep joists

(b) M-θ response for plywood sheathed joists with 3.62 and 12 in. deep joists

Figure 18 M-θ response for plywood sheathed joists (a) 8 in. deep (b) 3.62 and 12 in. deep joists

Overall the M-θ response of the plywood specimens is highly variable (see Figure 18). Even for nominally identical specimens: 800S200-54 joists with #6 fasteners @ 12 in. on center, or 800S200-97 joists with #10s @ 12 in. o.c., significant variability is observed in the overall rotational response. The important role of the sheathing stiffness in determining the rotational response is highlighted directly by the specimens with 8 in. deep joists of Figure 18(a), the most flexible specimens are always when the plywood cantilever length, L, is 24 in., thus providing half the stiffness of the L = 12 in. specimens. Complete P-Δ, M-θ, and k_ϕ results for all specimens with plywood sheathing are provided in Section 10.

As the test progressed the rotational stiffness provided degrades. The resulting tangent rotational stiffness for the 8 in. deep steel joists with 12 in. plywood cantilever length are provided in Figure 19. With the exception of the single 800S200-054 specimen which fractured in the plywood, the 800S200-097 specimens experience much greater degradation in rotational stiffness as the test progressed than the 800S200-054 specimens. This issue is examined in greater detail in Section 4.
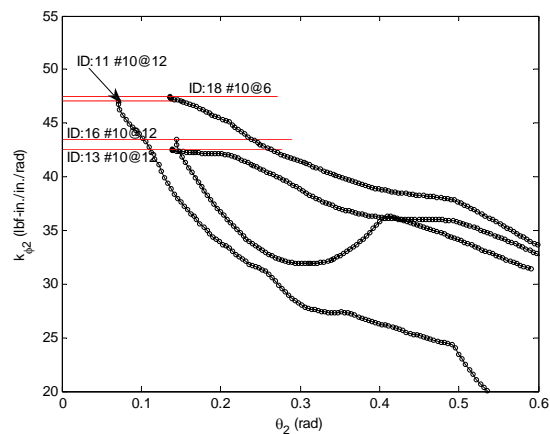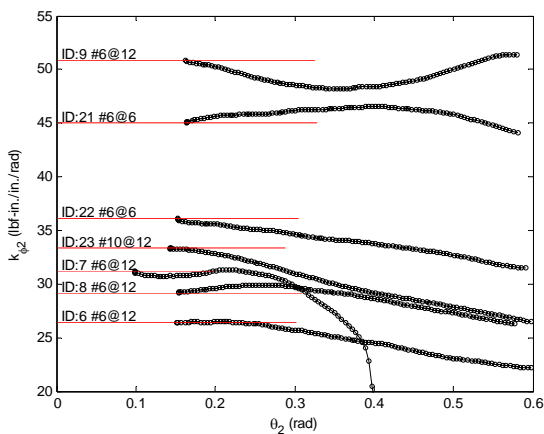
(a) 800S200-054 joists, plywood cantilever length L = 12 in., fastener details given on plot

(b) 800S200-097 joists, plywood cantilever lenegth L=12 in., fastener details given on plot

Figure 19 tangent rotational stiffness, $k_{\phi 2}$, for (a) 800S200-054 and (b) 800S200-07 joists

3.4.2 OSB

Response of the OSB sheathed specimens is summarized in Figure 20 and Figure 21. The OSB sheathing is stiffer than the plywood sheathing and testing was therefore conducted at the 24 in. cantilever length. One of the 5 OSB sheathed specimens (800S200-97 with #10 fasteners) failed in pull-through, as shown in Figure 20(b). However, the rotation at which this failure occurred (see Figure 21) was high, ~0.5 rad = 28.6 deg., and well beyond expected rotation demands. The other 097 specimen, a 1200S200-97 with #10 fasteners also appeared to be initiating a pull-through failure when the actuator stroke $\Delta_v = 6$ in. was maxed out. The 097 specimens (using #10 fasteners) have higher initial stiffness than the 054 specimens, but suffer greater and quicker degradation in that stiffness, as shown in Figure 21(b).
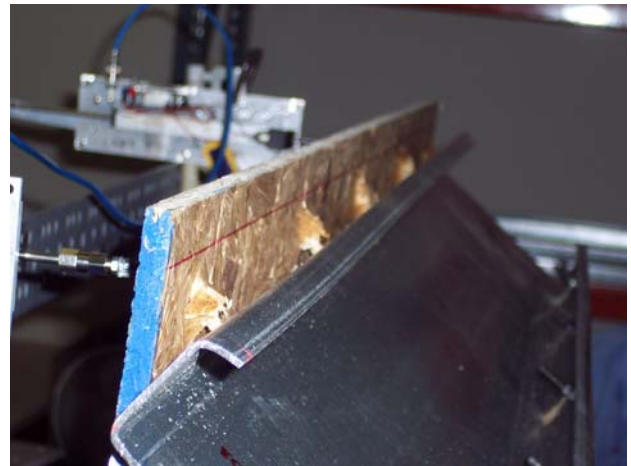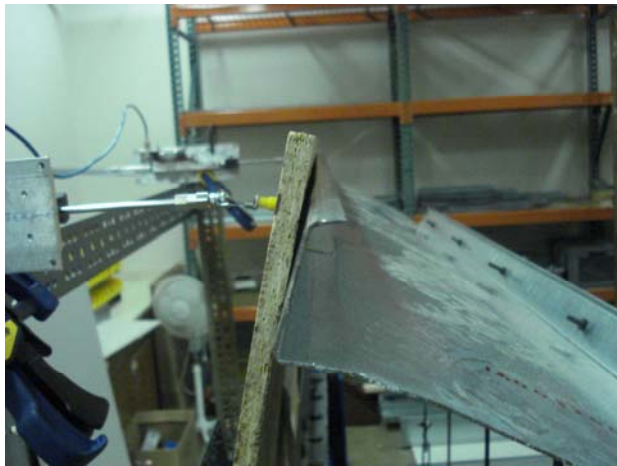
(a) sheathing-connector-joist response of OSB sheathed joist shown for an 1200S200-54 joist with OSB sheathing, L = 24 in, and #6 fasteners @ 12 in. (5-OSB-24-6-12-02, 5-1200S200_54_3)

(b) pull-through failure shown for an 800S200-97 joist with OSB sheathing, L = 24 in., with #10 fasteners @ 12 in. (5-OSB-24-10-12-01, 5-800S200_97_20)

Figure 20 Response of OSB sheathed joists
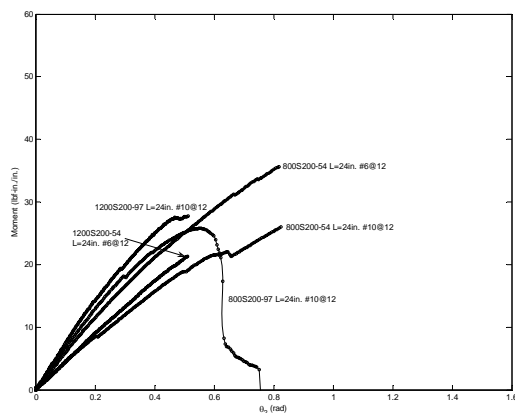
(a) M-θ_2 for OSB sheathed joists
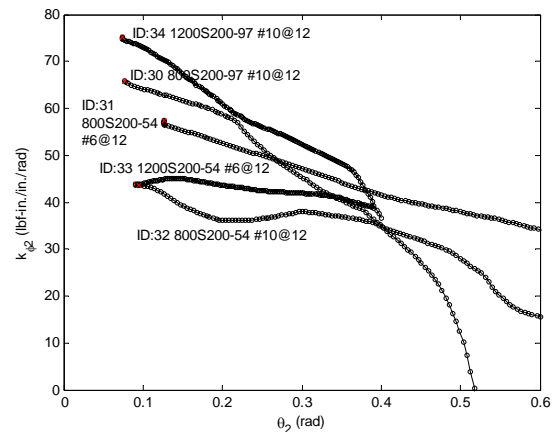
tangent $k_{\phi 2}$ for OSB sheathed joists

Figure 21 M-θ and tangent $k_{\phi 2}$ response for OSB sheathed joists

3.4.3   Gypsum

Response of the joists sheathed with gypsum board is provided in Figure 22 and Figure 23. All gypsum board tests failed by pull-through with little bending in the gypsum board observed, as shown in Figure 22. Though initial stiffness was somewhat similar, the total rotational capacity available in the gypsum board specimens was a fraction of that in the OSB or plywood sheathed specimens - Figure 23(a) plots the M-θ response to the same scale as that used for plywood (Figure 18) and OSB (Figure 21) and demonstrates the very small moment and rotation that can be developed before the pull-through causes loss of rotational capacity.

(a) large separation between joist and gypsum board with little bending in gypsum board shown for an 800S200-54 joist with gypsum board, L = 12 in., and #10 fasteners @ 12 in. (6-GYP-24-10-12-01, 6-800S200_54_33)

(b) pull-through failure and fracture of gypsum board shown for an 800S200-54 joist with gypsum board, L = 12 in., and #10 fasteners @ 12 in. (6-GYP-24-10-12-01, 6-800S200_54_33)

Figure 22 Response of gypsum board sheathed joists
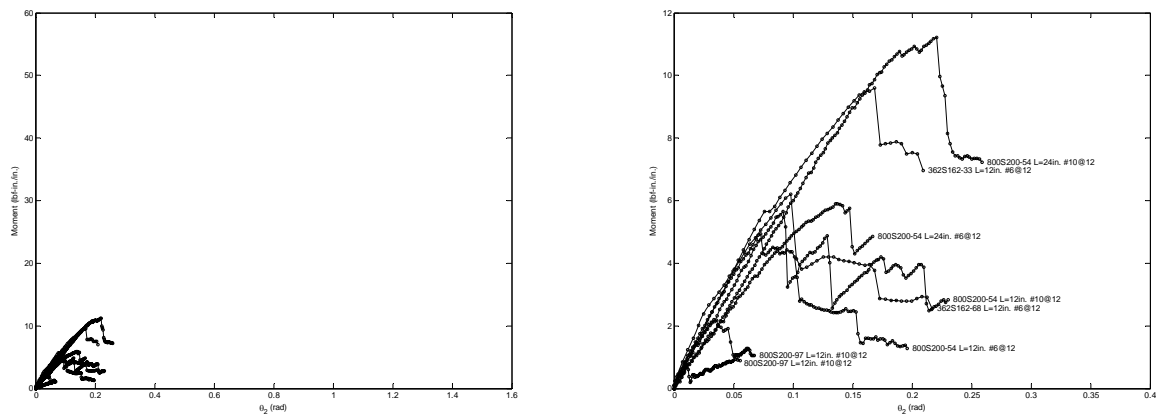
(a)   M-θ   response   plotted   to same scale as Figure 18 and Figure 21

(b) M-θ response plotted to smaller scale (0.1 rad = 5.7 deg.)

Figure 23 M-θ response for gypsum board sheathed joists

4 EXPERIMENTAL TESTING FOR COMPONENT STIFFNESS ($k_{\phi w}$, $k_{\phi c}$)

The standard AISI-TS-1-02 test procedure only provides a methodology for examination of the overall stiffness. While this is indeed the value needed in design it implies that an individual test would be needed for every sheathing-fastener-joist combination to be used in design. As an alternative, in this section modifications to the AISI-TS-1-02 test standard are considered whereby the stiffness is broken into two components; one due to the sheathing and another due to the connector.

4.1 Separating sheathing and connector

4.1.1 Simplified sheathing model

Using simple beam mechanics and assuming small angles and linear elastic deformation, we may arrive at a simple set of expressions for the behavior of the sheathing (wood). The cantilevered sheathing and the relevant variables are depicted in Figure 24.
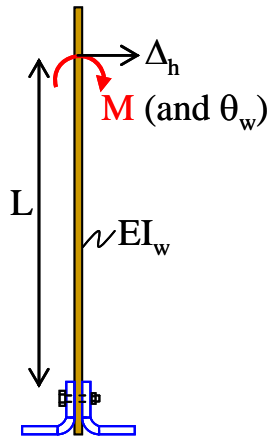
Figure 24 Analytical model for the sheathing

The lateral deflection at the point of moment application in the linear elastic range assuming standard beam theory assumptions for the sheathing deformation is

$$\Delta_h = \frac{ML^2}{2EI_w}$$

and the rotation at the point of moment application is

$$\theta_w (\text{at } \Delta_h) = \frac{ML}{EI_w}$$

Using the two preceding expressions, a relationship between rotation of the sheathing and the lateral deflection of the sheathing is determined:

$$\theta_w = \frac{2\Delta_h}{L}$$

Thus, the rotation of the wood may be determined from the lateral deformation of the wood, which is highly advantageous since the lateral deformation may be readily measured. Similarly, the rotational stiffness of the wood may be determined via:

$$k_{\phi w} = \frac{M}{\theta_w} = \frac{Ph_o}{2\Delta_h / L}$$

In addition, it is worth noting that the bending rigidity of the wood sheathing may be estimated using similar, simple, expressions:

$$EI_w = \frac{ML^2}{2\Delta_h} = \frac{Ph_o L^2}{2\Delta_h}$$

4.1.2   Rotation angles

The rotation of the assembly consists of rotation θ_w of the sheathing (wood), and rotation θ_c at the connector – in addition, since measurement is made at the free flange and not directly at the connection, rotation θ_s due to bending of the steel joist and rotation θ_L due to the loading apparatus (straps, turnbuckle. etc) also occur. Figure 25 depicts these component rotations along with overall definitions of the rotation, θ, θ_1, and θ_2 as shown.
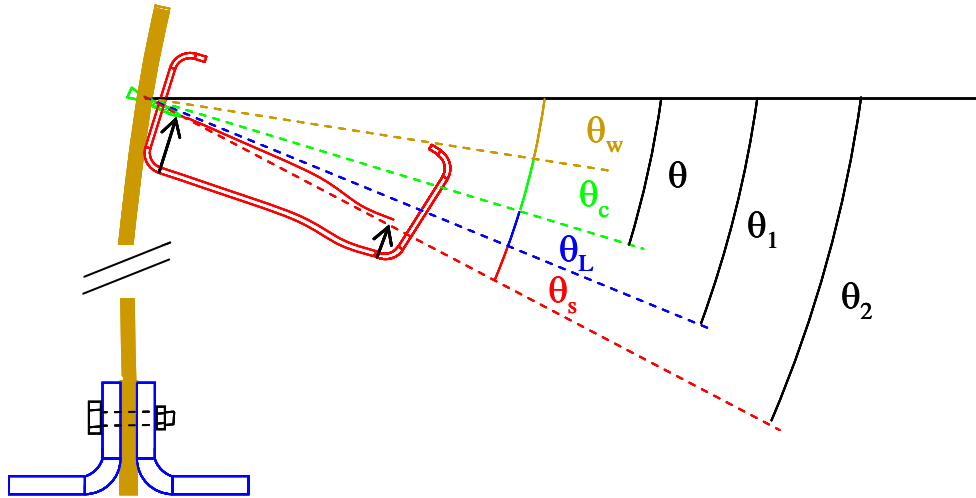
Figure 25 Breakdown of rotation at the joist-sheathing juncture

As discussed in the preceding section the rotation of the sheathing (wood) is known through an analytical approximation ($\theta_w = 2\Delta_h / L$, see Section 4.1.1). The total rotation can be determined from the measured vertical displacement (Δ_v, see Figure 4) as:

$$\theta_2 = \tan^{-1}\left(\frac{\Delta_v}{h_o}\right)$$

If we approximate the bending of the joist as cantilever bending of the joist web, via

$$\Delta_s \approx \frac{Ph_o^3}{3E_s I_s}$$

where I_s is the moment of inertia of the web of the joist, then

$$\theta_1 = \tan^{-1}\left(\frac{\Delta_v - \Delta_s}{h_o}\right)$$

If we approximate the deformations due to the loading apparatus as axial deformations in the strap:

$$\Delta_L \approx \frac{(P/5)L_L}{E_s A_L}$$

where P is divided by 5 because there are 5 straps, L_L is the length of the strap, E_s is the elastic modulus of steel, and A_L is the cross-sectional area of the straps, then the rotation θ, is

$$\theta = \tan^{-1}\left(\frac{\Delta_v - \Delta_s - \Delta_L}{h_o}\right)$$

Rotation θ_2 is the simplest and most direct measurement of the total rotation; however θ_2 includes all sources of deformation: sheathing, connector, joist bending, and loading apparatus. If we lump connector, joist bending, and loading apparatus rotations all into the connector rotations we arrive at the simplest definition for the connector rotation:

$$\theta_{c2} = \theta_2 - \theta_w$$

Using the approximations for θ_s and θ_L as given above we may also arrive at approximations for the connector rotation which attempt to isolate joist bending (θ_{c1}) and both joist bending and the loading apparatus deformations (θ_c), i.e.:

$$\theta_{c1} = \theta_1 - \theta_w$$
$$\theta_c = \theta_2 - \theta_w$$

4.1.3   Stiffness definitions

The possible stiffness definitions follow directly from the defined angles, where

overall rotational stiffness:

$$k_{\phi2} = M/\theta_2$$
$$k_{\phi1} = M/\theta_1$$
$$k_\phi = M/\theta$$

wood rotational stiffness:

$$k_{\phi w} = M/\theta_w$$

connector rotational stiffness

$$k_{\phi c2} = M/\theta_{c2} \text{ where } \theta_{c2} = \theta_2 - \theta_w$$
$$k_{\phi c1} = M/\theta_{c1} \text{ where } \theta_{c1} = \theta_1 - \theta_w$$
$$k_{\phi c} = M/\theta_c \text{ where } \theta_c = \theta - \theta_w$$

Based on these models the rotational restraint of the joist may be envisioned as a simple spring in series model (Figure 26). The spring in series model provides alternative definitions for the connector stiffness based on the overall and wood stiffness. These alternative definitions are equivalent, as shown below:
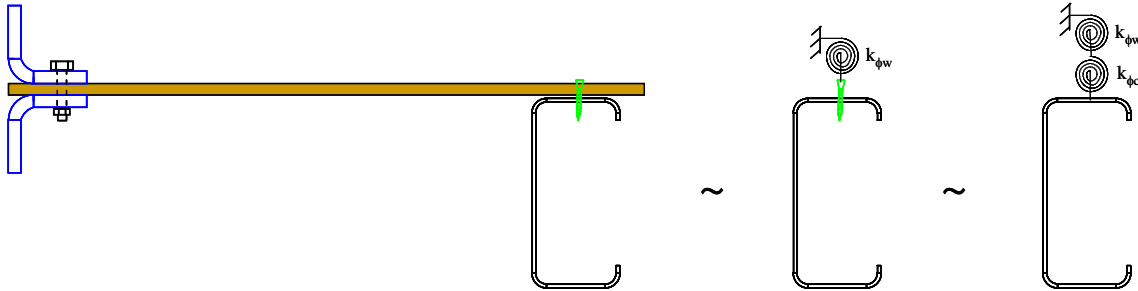
Figure 26 Illustration of rotational springs for sheathing and fastener

Consider the total rotation is idealized as the sum of the two component rotations

$$\theta = \theta_c + \theta_w$$

springs in series model   moment-rotation model

$$\frac{M}{k_\phi} = \frac{M}{k_{\phi c}} + \frac{M}{k_{\phi w}} \qquad \text{or} \qquad \theta = \frac{M}{k_{\phi c}} + \theta_w$$

$$k_{\phi c} = \frac{1}{\dfrac{1}{k_\phi} - \dfrac{1}{k_{\phi w}}} \qquad \text{or} \qquad k_{\phi c} = \frac{M}{\theta - \theta_w}$$

As described in Section 3.3 the initial rotational restraint $k_{\phi 2}$ is found by linear regression on the M-θ_2 curve for $M < 0.4 M_{peak}$, where M_{peak} is the maximum recorded moment in the test. Note, M_{peak} is not the failure moment in all tests, instead M_{peak} is the moment at 6 in. of Δ_v displacement or the failure moment, whichever is less. (For the plywood tests failure did not occur in the tests, but for some OSB tests and all gypsum board tests large displacement could not be maintained without failure and thus M_{peak} is the failure moment.)

All other rotational stiffness values are found in a similar fashion, first the rotation angles $(\theta, \theta_w, \theta_c)$ are defined and then linear regression is performed on the data for $M < 0.4 M_{peak}$. Based on an examination of the results, discussed further in Section 4.3, it was determined that the simplest definitions of the rotation angles, θ_2, θ_w, θ_{c2} are the most consistent; thus, all of the information provided herein are based on these definitions.

4.1.4   *Example k_ϕ to $k_{\phi w}$ and $k_{\phi c}$*
Using the methodology of Sections 4.1.1 to 4.1.3 the example of an 800S200-097 joist with plywood sheathing, L = 12 in., and #10 fasteners at 6 in. on center (of Section 3.3 Figure 16) is updated and decomposed into response for the connector (subscript 'c2'), sheathing (subscript 'w', denoting "wood"), and the total response (subscript '2') as shown in Figure 27.

Figure 27(a) provides the raw P-Δ response, both for the actuator displacement (Δ_v) and for the horizontal displacement of the sheathing-joist assembly (Δ_h). Δ_h is measured by position transducers at either end of the specimen (Δ_{h1} and Δ_{h2}) as shown in Figure 5(b). As described in Section 3.3 the data is post-processed and provided in its final form in Figure 27(b); the small separation between Δ_{h1} and Δ_{h2} represents a 'warp' (or twist) in the response. Nonsymmetric response was common in the plywood specimens which were all initially warped to varying degree, thus increasing the variability of response in the plywood specimens.

Conversion to M-θ response following Sections 4.1.1 to 4.1.3 is provided in Figure 27(c). Figure 27(c) demonstrates that the flexibility of the overall system (M-θ_2) is largely a function of the flexibility of the plywood itself, as the M-θ_w curve is quite close to the M-θ_2 response. This behavior is typical for the plywood specimens, and even more pronounced in the L = 24 in. plywood specimens. Linear regression to determine the overall ($k_{\phi2}$), sheathing ($k_{\phi w}$), and connector ($k_{\phi c2}$) stiffness is performed for the range of θ with M<0.4M_{peak}, designated by the straight lines in Figure 27(c). The degradation of the overall, sheathing, and connector response using a moving window regression analysis is provided in Figure 27(d). In the example, connection stiffness degrades in a more pronounced fashion than sheathing (plywood) stiffness.

A complete set of figures, similar to Figure 27, for every conducted test are provided in the test summary data sheets of Section 10.
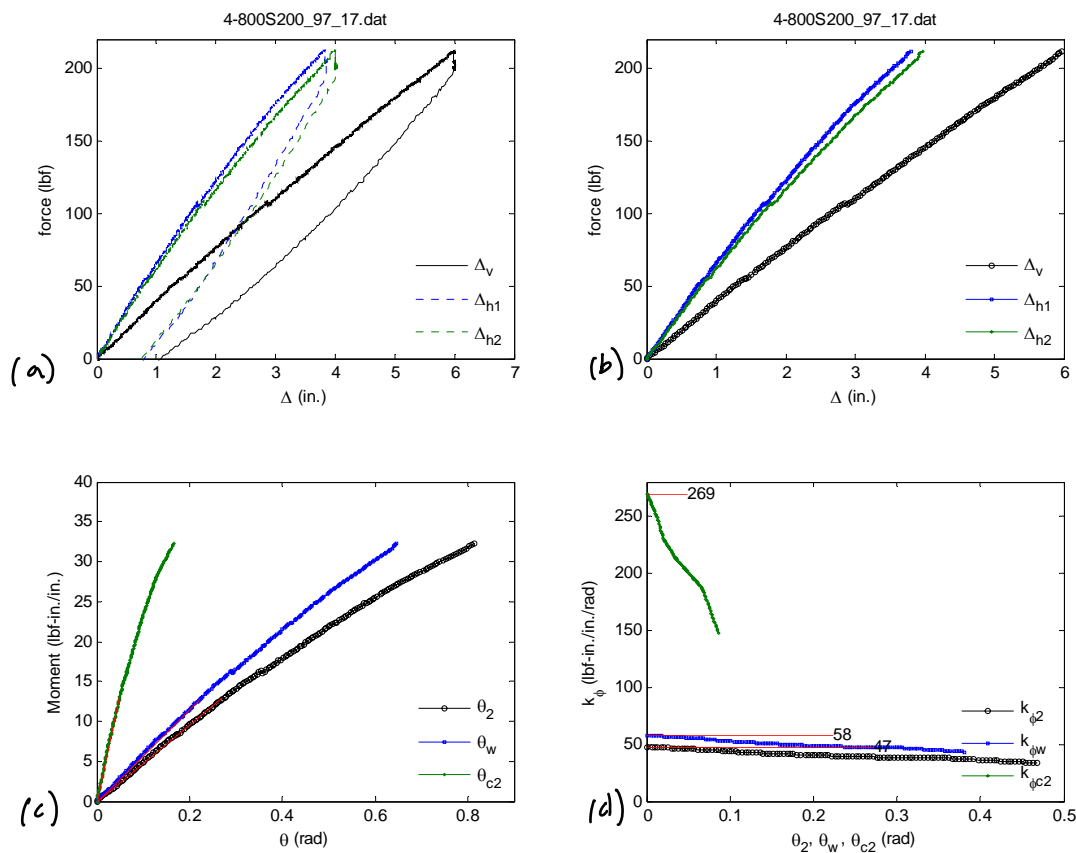
Figure 27 Typical experimental results for plywood specimen: 800S200-97 joist with plywood sheathing, L=12in., #10@6in. (test 18 completed on March 13 2007, file 4-800S200_97_17, designator 4-PL-12-10-6-01,) – revised from Figure 16 which only shows global response

4.2   Component stiffness results

The average component stiffness results from the testing are summarized in Table 6. The subsequent sections presented here break down this table and provide supplementary moment-rotation curves and degradation in rotational stiffness curves to explain and compare the details of this table.

Table 6 Average overall and component stiffness results

(a) overall average stiffness results

$k_{\phi 2}$ (lbf-in./in./rad)											
Sheathing -->	Plywood					OSB		Gypsum			
Cantilever (L) -->	12"				24"	24"		12"		24"	
Fastener # -->	6		10		6	6	10	6	10	6	10
Fastener Spacing -->	6"	12"	6"	12"	12"	12"	12"	12"	12"	12"	12"
362S162-33		40						75			
362S162-68		42						94			
800S200-54	41	34		33	18	57	44	76	60	53	58
800S250-54		53		43							
800S200-97			47	44			66		58		
1200S200-54		34				44					
1200S200-97				59			75				

(b) sheathing average stiffness results

$k_{\phi w}$ (lbf-in./in./rad)											
Sheathing -->	Plywood					OSB		Gypsum			
Cantilever (L) -->	12"				24"	24"		12"		24"	
Fastener # -->	6		10		6	6	10	6	10	6	10
Fastener Spacing -->	6"	12"	6"	12"	12"	12"	12"	12"	12"	12"	12"
362S162-33		78						295			
362S162-68		72						300			
800S200-54	63	56		51	21	117	101	295	285	128	138
800S250-54		98		66							
800S200-97			58	59			112		378		
1200S200-54		60				89					
1200S200-97				82			122				

(c) connection average stiffness results

$k_{\phi c2}$ (lbf-in./in./rad)											
Sheathing -->	Plywood					OSB		Gypsum			
Cantilever (L) -->	12"				24"	24"		12"		24"	
Fastener # -->	6		10		6	6	10	6	10	6	10
Fastener Spacing -->	6"	12"	6"	12"	12"	12"	12"	12"	12"	12"	12"
362S162-33		81						100			
362S162-68		102						137			
800S200-54	116	109		97	137	113	77	103	77	91	99
800S250-54		116		124							
800S200-97			269	167			159		144		
1200S200-54		78				85					
1200S200-97				215			195				

4.2.1 Plywood

4.2.1.1 Plywood variability much greater than connector variability

Large variability in the response is observed for the plywood sheathed specimens, even when the specimens are nominally identical. For example, Figure 28 provides the M-θ results for the first three tests conducted. The tests employed 800S200-54 joists connected to plywood sheathing on an L = 24 in. cantilever with #6 fasteners at 12 in. on center. Use of horizontal measurements (Δ_h) to isolate the contribution from the sheathing demonstrates that nearly all of the observed rotation (θ_2) is coming from the sheathing (θ_w). In addition, while large variability is observed in the sheathing M-θ_w response, little variability is observed in the connection (M-θ_{c2}) response. This result suggests that for plywood sheathing the variability in overall response (stiffness) is more likely to be a function of the variability of the plywood stiffness as opposed to the connection stiffness.
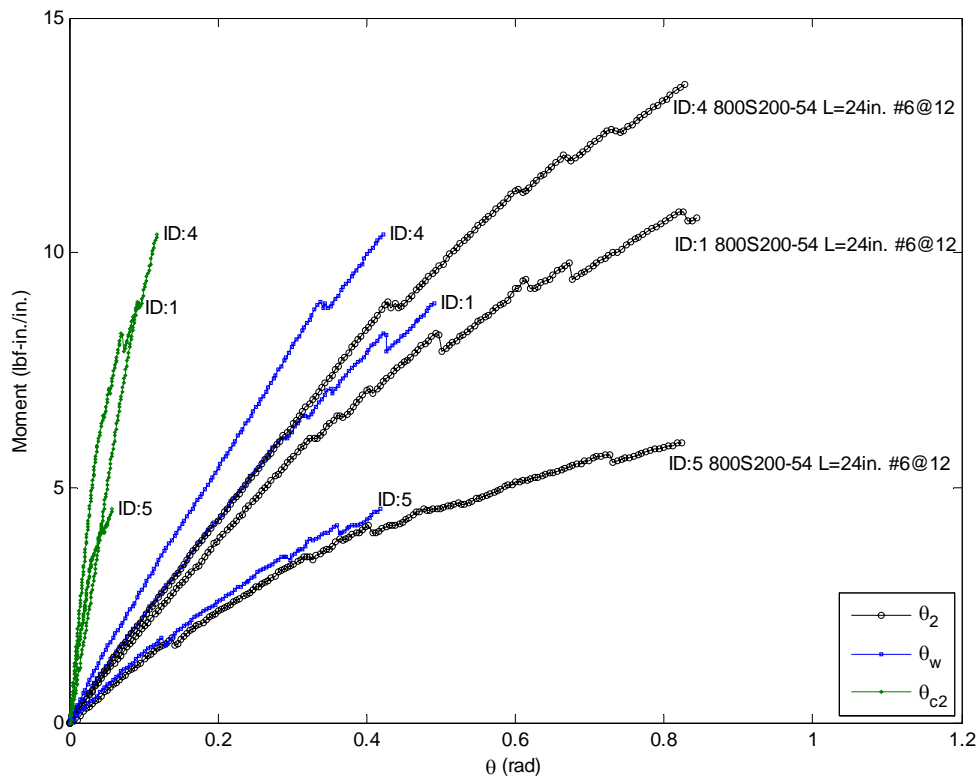
Figure 28 M-θ response for plywood sheathed joists with L = 24 in. cantilever

Due to the small moments developed and the fact that the bulk of the flexibility was derived from the sheathing it was decided to use a shorter cantilever length (L = 12 in.) for the additional plywood tests. This shorter length (L = 12 in.) doubles the rotational stiffness of the sheathing and allows the system to develop higher moments and greater rotations (θ_{c2}) in the connection. The results of these L = 12 in. tests for 800S200-054 and 800S200-097 joists are summarized in Figure 29 and Figure 30. The significant variability in plywood stiffness remains the over-riding factor in the response of the plywood sheathed specimens of Figure 29 and Figure 30. Connection stiffness is less variable than the plywood stiffness, and this is broken down further in the subsequent sections.
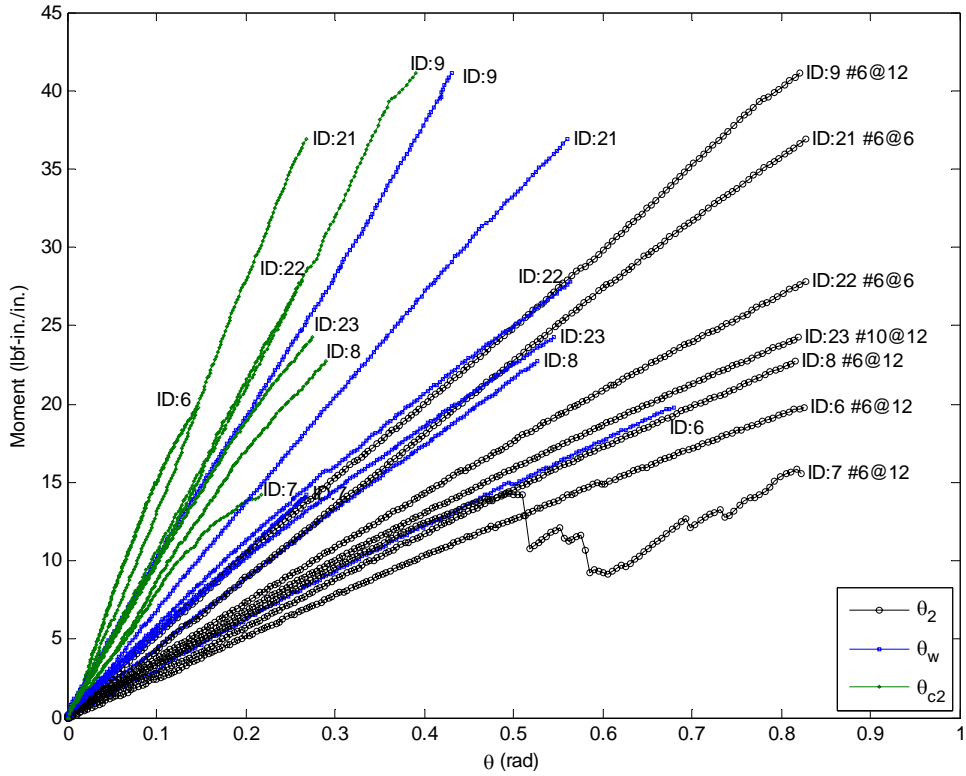
Figure 29 M-θ response for plywood sheathed joists with L = 12 in. cantilever, all 800S200-054 joists shown
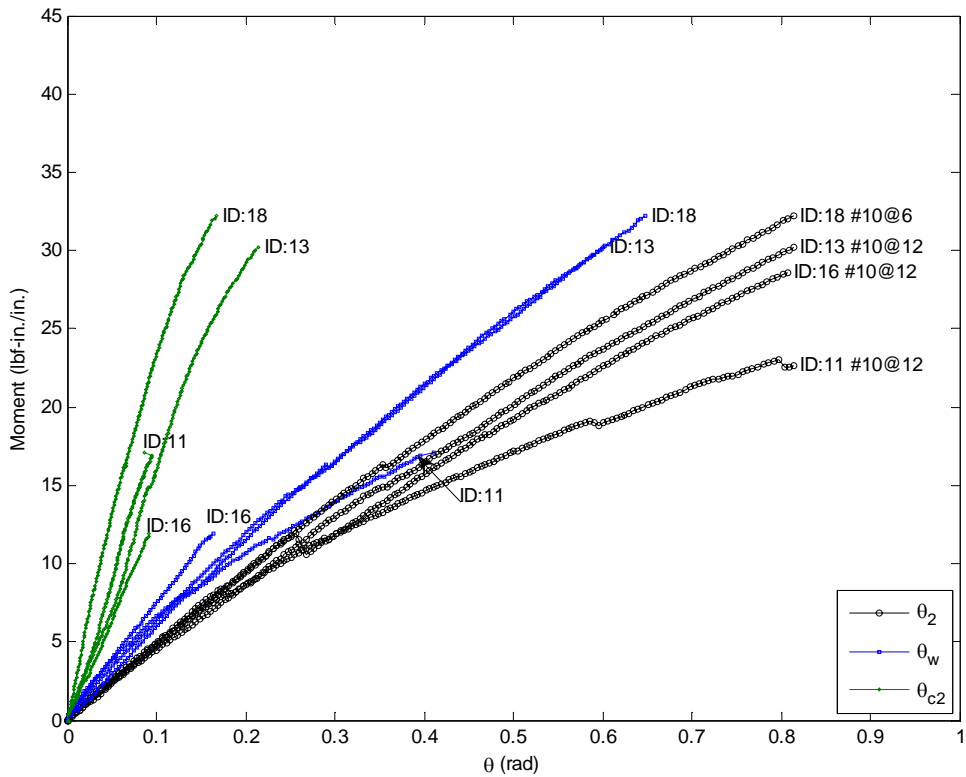
Figure 30 M-θ response for plywood sheathed joists with L = 12 in. cantilever, all 800S200-097 joists shown

The success of the decomposition of the results into sheathing response and connector response is partially reflected in Figure 31. In Figure 31 the connector M-θ_{c2} response is shown for nominally identical 800S200-054 joists with #6 @ 12 in. o.c. fasteners, but with the sheathing stiffness doubled by changing the plywood cantilever length, L, from 24 in. down to 12 in. Although variability is relatively high, even with a doubling of the sheathing stiffness, the response (slope) is largely the same for all these tests (see Table 6 as well). The connector response with the stiffer (L=12 in.) sheathing is smoother, reflecting a better balance in these experiments between connector and sheathing response – as opposed to the L=24 in. tests which were nearly dominated by sheathing response, thus leaving the connector response to be determined from only small differences in the data. The L=12 in. cantilever length was subsequently used for all plywood tests.
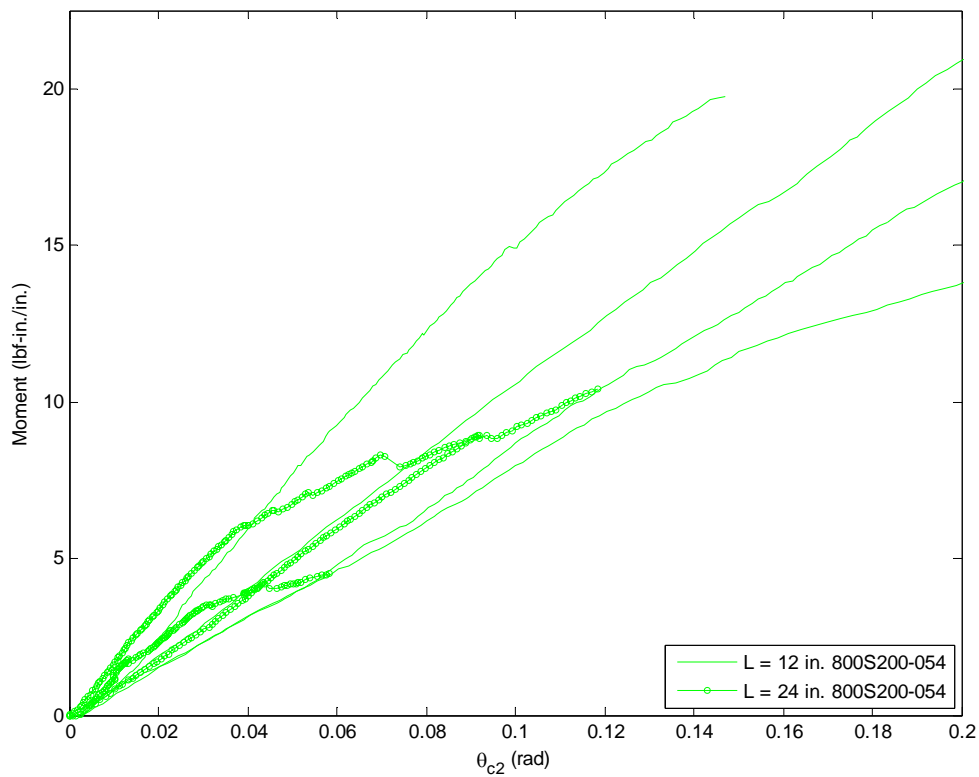
**Figure 31 Influence of cantilever length, L, on connector stiffness
for 800S200-54 joists with plywood and #6 fasteners @ 12 in. o.c.**

4.2.1.3   Thicker joists with bigger fasteners give stiffer results, but bigger fasteners in smaller joists don't

The connection stiffness is dependent on the joist thickness most prominently and fastener spacing and fastener size to a lesser extent. A series of 800S200 joists with plywood sheathing at L=12 in. were examined at different thickness and fastener details as summarized in Figure 32 and Table 6. The thicker (097) joists paired with the larger (#10) fasteners give the greatest stiffness. However, use of a larger fastener, e.g., a #10, in a thinner (054) joist does not appreciably increase the stiffness. Decreasing the fastener spacing from 12 in. o.c. to 6 in. o.c. provides only a modest increase in stiffness.
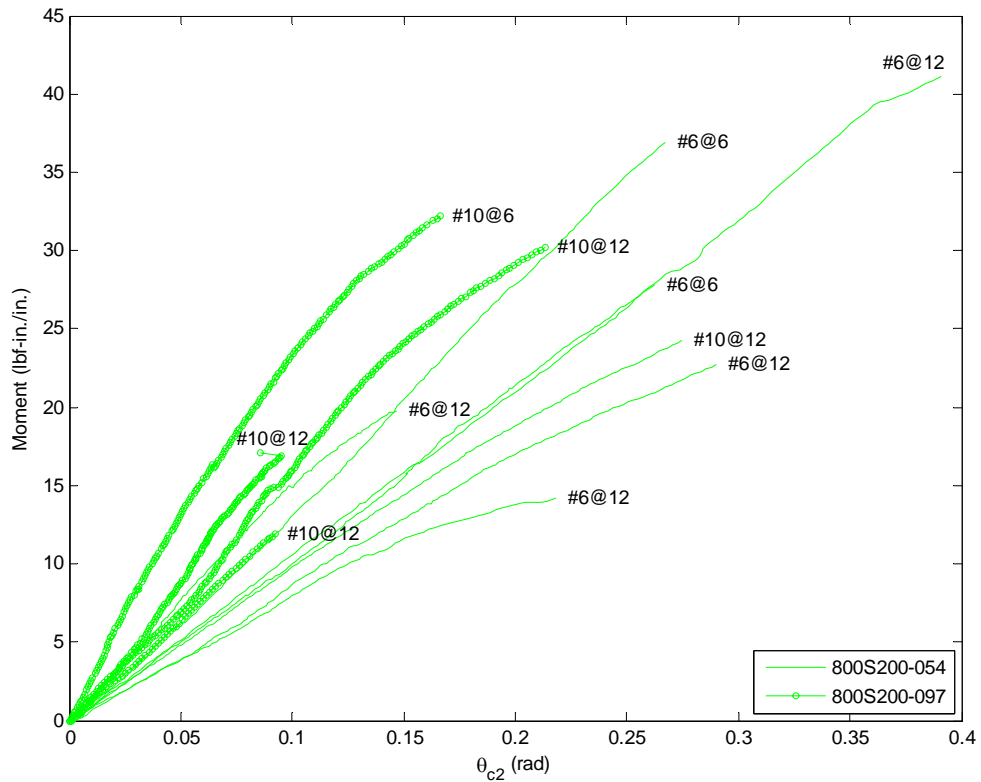
**Figure 32 Influence of joist thickness on connector stiffness for
800S200 joists with plywood and varied fastener details**

4.2.1.4   Flange width increases connection stiffness marginally, but not as much as one might expect

As the flange width increases it seems reasonable to assume the connection rotational stiffness increases in kind. In particular, supporting such a notion is a reasonable model for the connection stiffness in which one assumes that the rotational stiffness is derived from bearing at the edge of the joist and a linear spring to account for the pull-out stiffness of the fastener, as shown in Figure 33b. The moment derived in such a simple model is

$$M = k\Delta b_o / 2$$

recognizing that the axial pull-out is a function of the rotation, via

$$\Delta = \theta_c h_o$$

then the moment M is

$$M = k\theta_c h_o b_o / 2$$

The moment in the rotational spring model (Figure 33c) assumes

$$M = k_{\phi c}\theta_c$$

Equating these moments and solving for the rotational stiffness in terms of the pull-out stiffness:

$$k_{\phi c} = \tfrac{1}{2} k h_o b_o$$

Thus, this model suggests that if you double the flange width the measured rotational stiffness $(k_{\phi c})$ should double, i.e., the measured connection rotational stiffness is linear in changes with b_o (and h_o).

Thus, the $k_{\phi c2}$ for a 2.5 in. flange compared to a 2 in. flange would be expected to be 2.5/2.0 or 25% greater. However, examination of Figure 34 and Table 6 indicates a much smaller increase in the stiffness as flange width increases. Direct comparison of the 800S200-54 with the 800S250-54 with L=12 in plywood and #6@12 in. o.c. shows an increase of 6% (from 109 to 116 lbf-in./in./rad). Given the small sample size this increase is essentially inside the variability of the reading. As a result, flange width does not appear to be an influential means for understanding the response, at least in this range of widths. Further, the pull-out stiffness model, though mechanically attractive, appears to miss fundamental deformations that are largely independent of flange width.
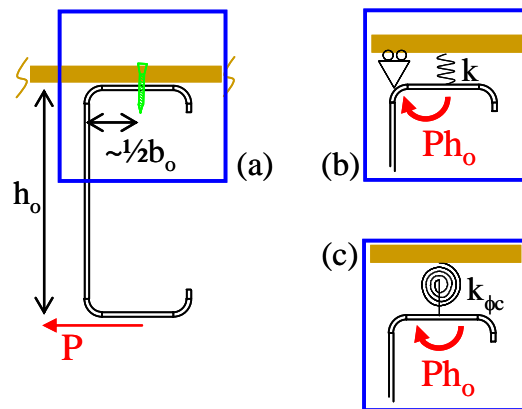
Figure 33 Fastener stiffness (a) joist-fastener-sheathing schematic (b) postulated bearing with pull-out stiffness model (c) rotational spring model
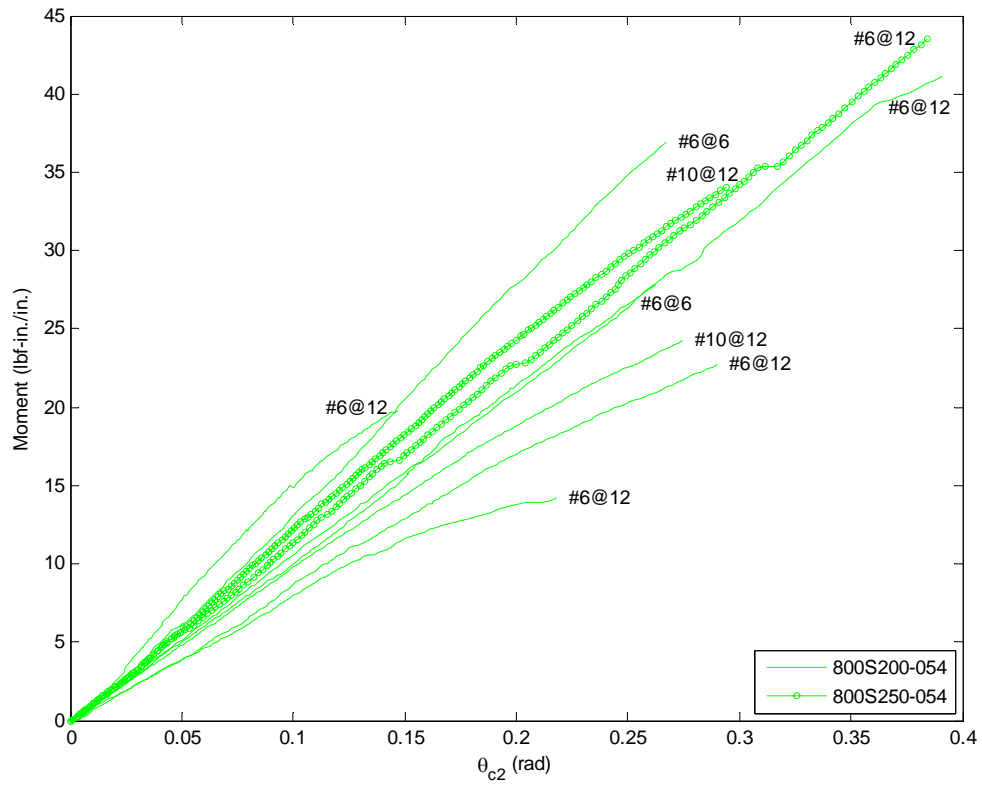
**Figure 34 Influence of flange width on connector stiffness
for 800S200-54 and 800S250-54 joists sheathed with plywood of L = 12in. and fastener details as given**

4.2.1.5   Joist depth is not an influential variable for connector stiffness

The joist depth impacts the moment and rotations developed at a given actuator displacement, Δ_v, as shown in comparison between Figure 18(b) and Figure 18(a). Further, joist depth directly determines the shear to moment ratio on the fastener itself (Figure 35) with higher joist depths carrying more moment. As summarized in Table 6 and depicted below in Figure 36 through Figure 38 the impact of joist depth on observed connection stiffness is small.
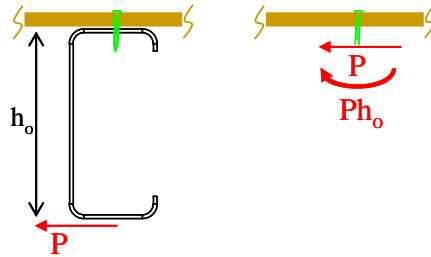
Figure 35 Fastener forces as a function of joist depth

For 8 in. and 12 in. deep joists with 0.054 in. thickness the connections in the 12 in. deep joists are slightly less stiff than in the 8 in. joists; as depicted in Figure 36; however for 0.097 in. thickness the connections in the 12 in. deep joists are slightly more stiff than their 8 in. counterparts (see Figure 37). Further, for 3.62 in. deep joists compared with 8 in. deep joists, the joist thickness is clearly more influential than the joist depth, as shown in Figure 38. Taken in total, the response with respect to joist depth is within the observed variability and joist depth is not found to be an influential variable for determining connection stiffness.
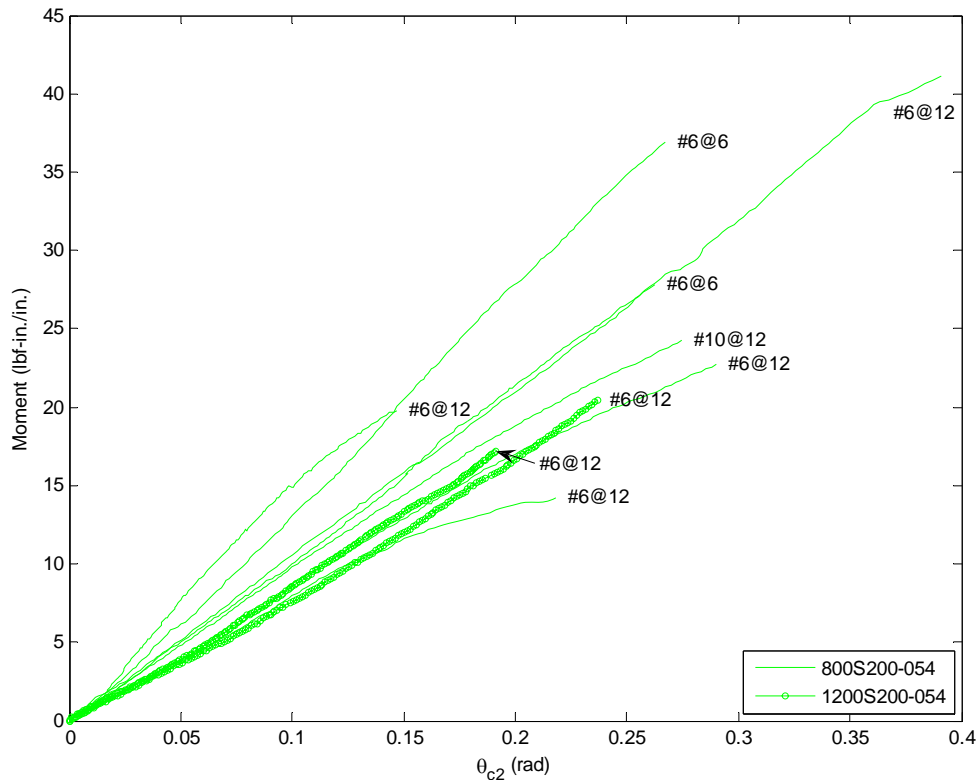
Figure 36 Influence of joist depth on connector response for
800S200-054 and 1200S200-054 joists
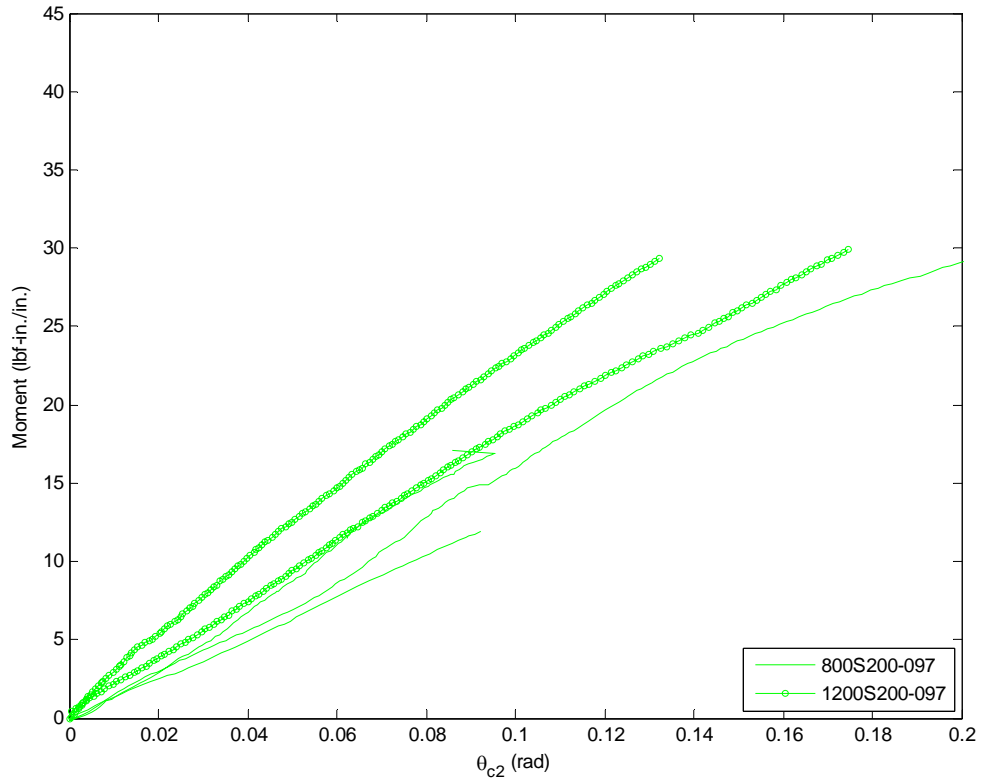
Figure 37 Influence of joist depth on connector response for 800S200-097 and 1200S200-097 joists
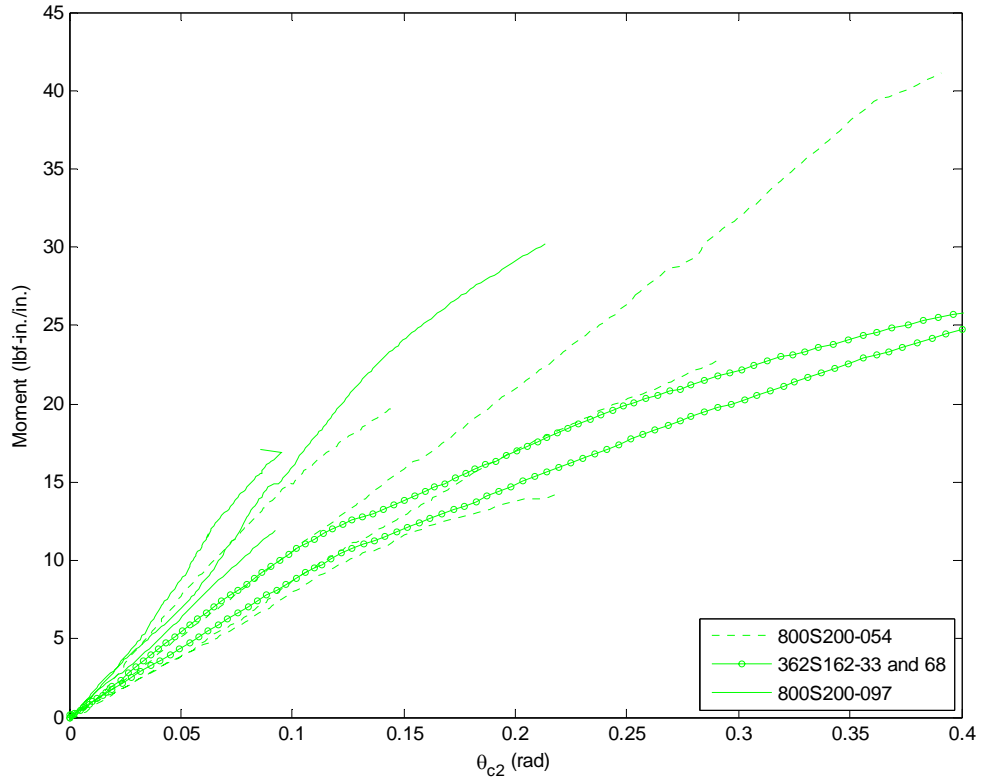
Figure 38 Influence of joist depth vs. joist thickness on connector response for 800S200 and 326S162 plywood sheathed joists

4.2.1.6   Degradation in stiffness in plywood, sheathing or fastener?

The tangent stiffness of the sheathing and the tangent stiffness of the connector was determined in order to examine whether or not the loss in stiffness during the testing occurs primarily in the sheathing (plywood) or the connectors. Results for the 8 in. deep joists are summarized in Figure 39. For the plywood specimens, in all but one case, significant loss in stiffness is not observed; as a result it is inconclusive as to whether or not the sheathing or connector is degrading more quickly. At large displacement (rotations) audible cracking and deformations were observed. Whether these were primarily due to the large rotation of the sheathing, or the local deformations at the fastener locations is inconclusive; both appear to degrade modestly in most tests as shown in Figure 39. Based on these observations it would appear that the use of the initial stiffness, as determined herein, is a reasonable measure of the overall stiffness for the plywood sheathed specimens.
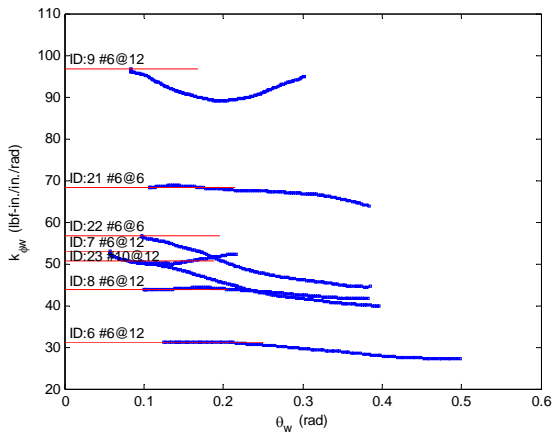
(a) sheathing stiffness, tangent k_{ϕ_w} (b) connector stiffness, tangent $k_{\phi_{c2}}$
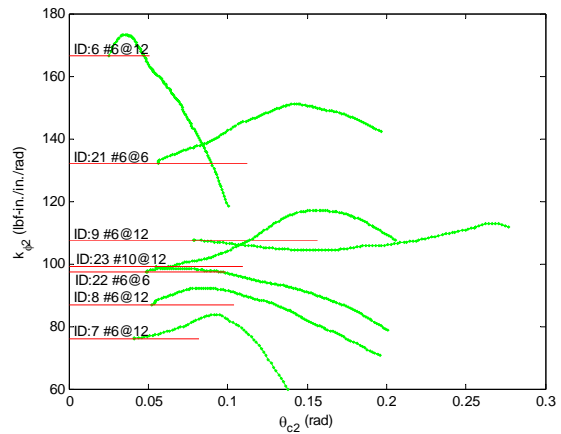
plywood (L=12 in.) with 800S200-054 joists
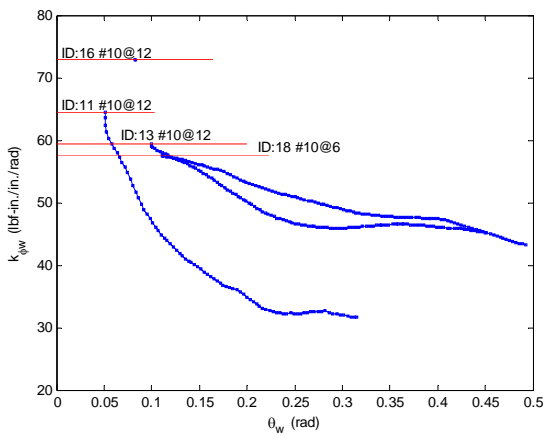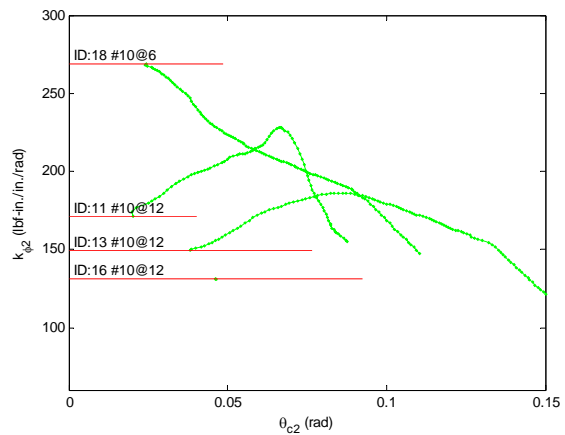
(c) sheathing stiffness, tangent k_{ϕ_w} (d) connector stiffness, tangent $k_{\phi_{c2}}$

plywood (L=12 in.) with 800S200-097 joists

Figure 39 Tangent stiffness of plywood and connector for (a) 800S200-054 joists and (b) 800S200-097 joists sheathed with plywood

4.2.2 OSB

4.2.2.1 *OSB stiffness is not variable, connections in OSB are*

In sharp contrast to the plywood sheathed specimens, the variability in the response of OSB sheathed specimens (which is less than in the plywood, but still significant) is primarily derived from the connections, not the bending stiffness of the OSB. As shown in Figure 40 the M-θ_w response for the OSB is largely the same, but the connection response is more variable. In addition, the choice of the L=24 in. cantilever for testing appears appropriate as a good balance between the sheathing stiffness and connection stiffness is established in these tests. Given the reliability of the OSB stiffness it may be appropriate to use a shorter cantilever length for future tests, thereby focusing more exclusively on the connection stiffness.
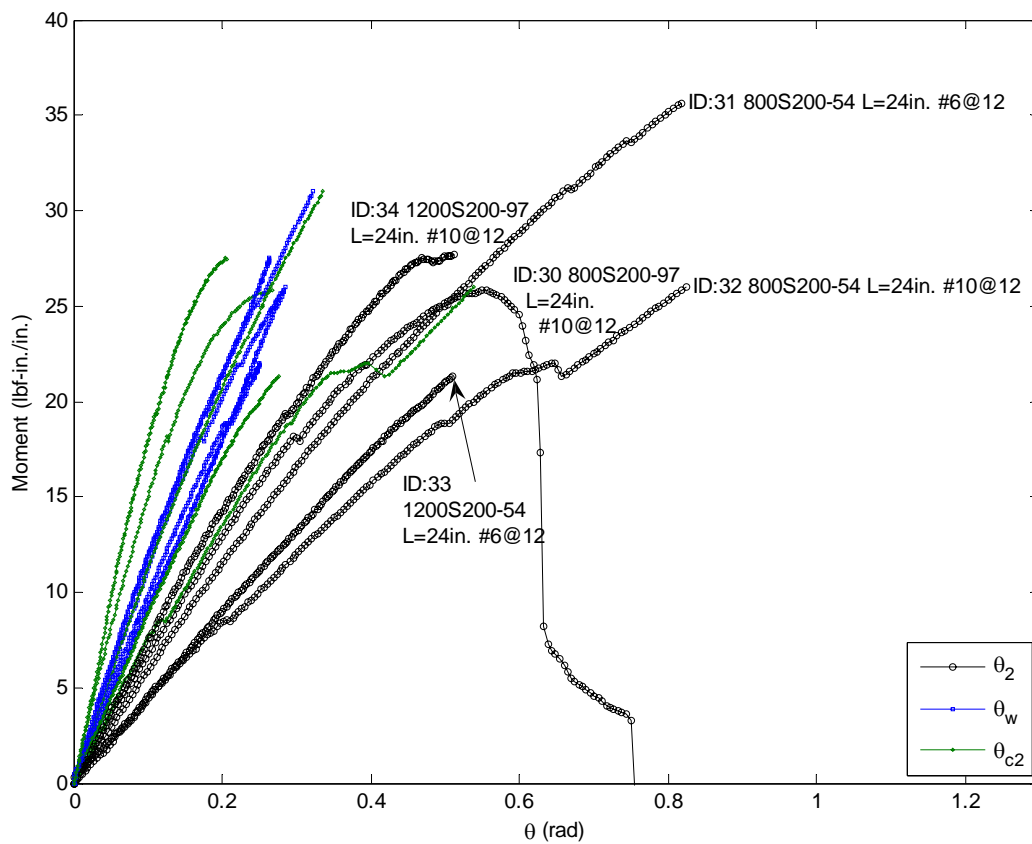
Figure 40 M-θ response for OSB sheathed tests

4.2.2.2   Thicker joists with bigger fasteners have greater stiffness in OSB

As Figure 41 shows, the thicker joists (097) with the larger fasteners (#10) have higher initial stiffness than thinner joists (054) with smaller fasteners (#6). Joist thickness is more influential than fastener details for initial stiffness, but fastener detail (#6 vs. #10) is more influential for connection strength, and loss of stiffness – as all of the specimens with #10 fasteners experience some significant loss in stiffness during the testing. The OSB specimens appear to be potentially sensitive to pull-out failures and the head (see Figure 11) is slightly different for the #10 fasteners, perhaps leading to a smaller pullout resistance/stiffness for that case.
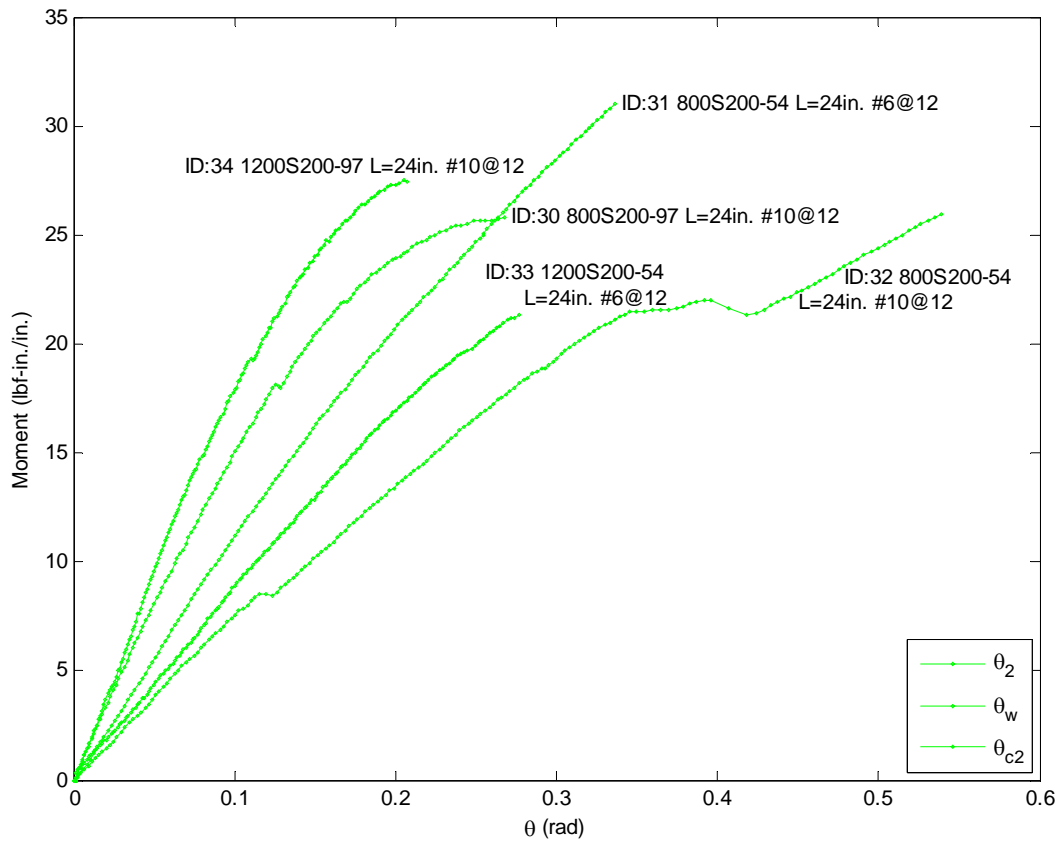
Figure 41 Connection response in OSB sheathed specimens

4.2.2.3   Degradation in OSB sheathed joists happens at connection and the mighty fall the fastest

The tangent stiffness of the OSB sheathing and connector are provided in Figure 42(a) and (b). The degradation in stiffness in the OSB sheathed tests is most pronounced in the connection, and much less so in the overall bending stiffness of the OSB. Further, the stiffest connections (in the thickest members) suffer the most precipitous loss in stiffness (see Figure 42(b)). For plywood it was concluded that the initial stiffness provided a robust measure of the provided stiffness, for OSB it appears that for higher thickness and larger fasteners, strength limits or rotation limits may be prudent for use in design.
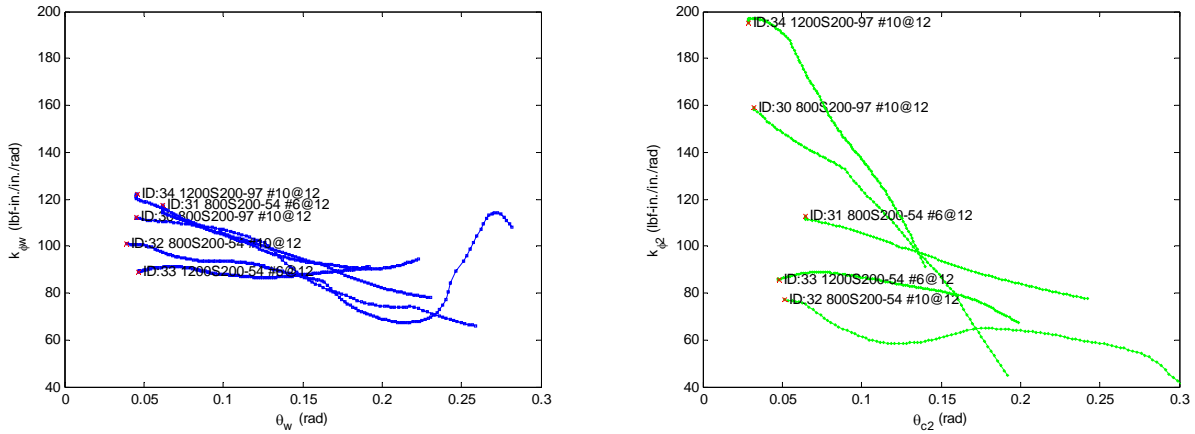
(a) OSB sheathing stiffness, tangent k_{ϕ_w} (b) connector stiffness, tangent $k_{\phi_{c2}}$

OSB (L=24 in.)

Figure 42 Tangent stiffness of OSB sheathing and connector

4.2.3   Gypsum

4.2.3.1   Gypsum stiffness is not variable, the strength of connections in gypsum are

The tests with gypsum sheathing exhibit little variability in the stiffness response, but large variability in the strength response, as shown in Figure 43. The thicker studs (and larger fasteners) generally generate lower strength results. The small forces and rotations that developed are the most important observation in the tests with gypsum sheathing.
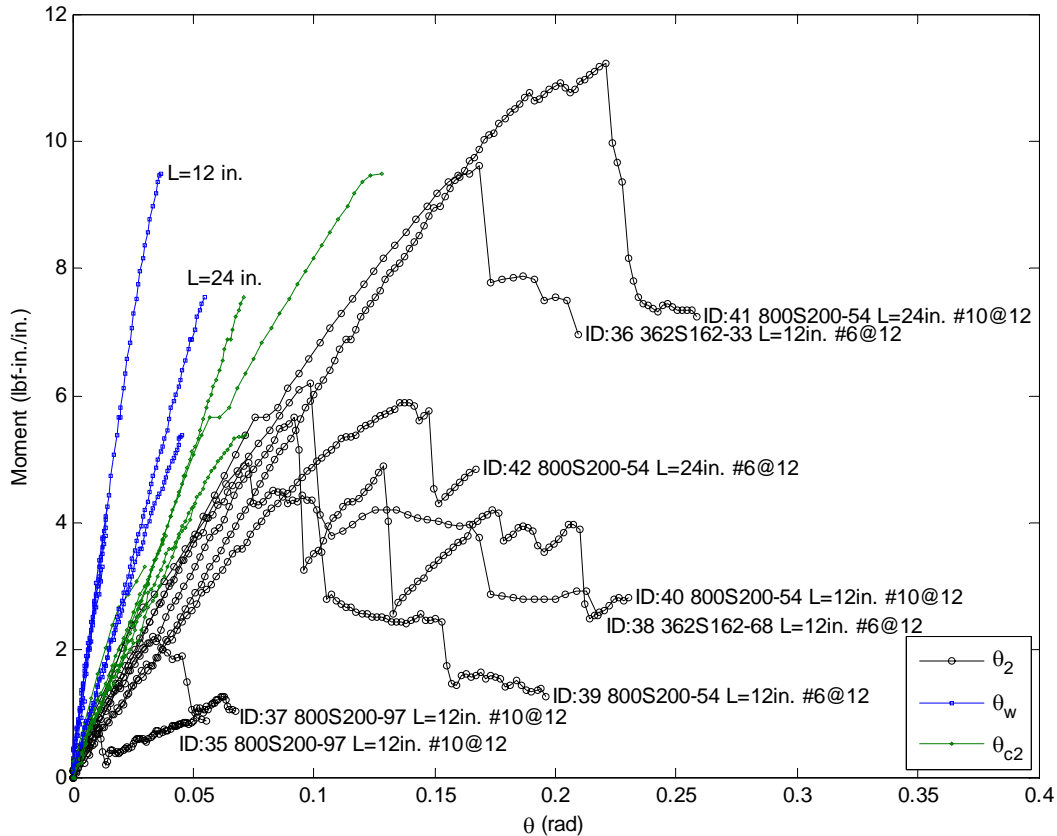
Figure 43 M-θ response for gypsum sheathed specimens

4.2.3.2   Connection stiffness in gypsum is not variable, connection strength is

Initial stiffness of the connections ($k_{\phi c2}$) is largely the same for all of the specimens tested with gypsum sheathing, see Figure 44. In fact, the stiffness is not dissimilar from that observed in plywood or OSB (see Table 6), but the variability in the strength (rotation) at failure is high enough to make the results questionable for use in design. While this stiffness may be available in pristine gypsum, or under lightly loaded service conditions, what would happen at ultimate load if a bending member was counting on this rotational stiffness to restrain distortional buckling? It seems clear that some measure of strength (rotation) criteria is needed along with the stiffness, perhaps even a rudimentary pull-through calculation. Tangent stiffness calculations of the connection were impossible to reliably conduct given the sudden nature and low load (and rotation) levels in the tests. Needless to say, degradation in the stiffness of the connection is essentially absolute – as this is a brittle failure.
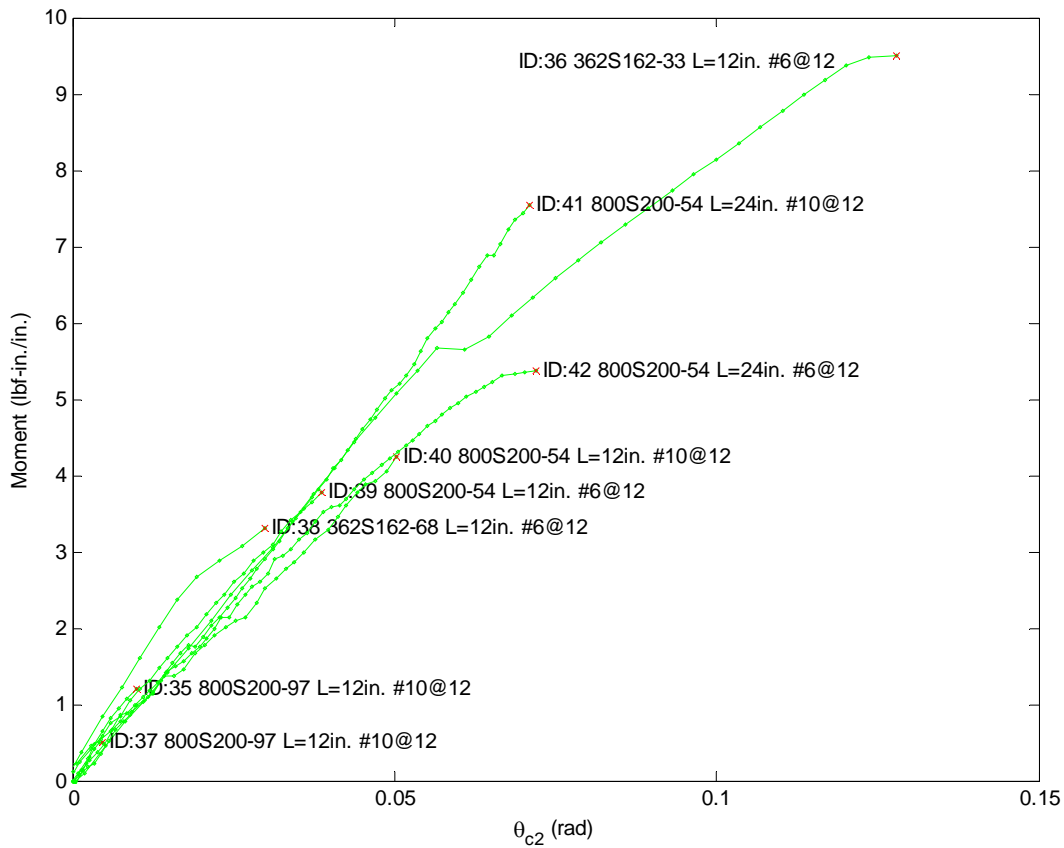
Figure 44 M-θ_{c2} response of connections with gypsum sheathing

4.3   Impact of rotation angle definitions on component stiffness

Throughout the analysis presented herein the simplest rotation angle, θ_2, has been employed for the determination of total stiffness ($k_{\phi 2}$) and connection stiffness ($k_{\phi c2}$). The θ_2 angle, as described in Section 4.1.2, includes all load apparatus deformations and joist bending. Defining the connection rotation θ_{c2} as $\theta_2 - \theta_w$ therefore implies all these additional deformations are lumped in with the connector rotation. This is a conservative approximation, but given the difference between the deformations in the distortional buckling mode and the test (see Figure 45) it would be ideal to separate these deformations and isolate the connection stiffness. This turns out to be a difficult task.

<div align="center">

(a) estimated cross-section deformations   (b) deformations in distortional bucking
in an AISI TS-1-02 test   as predicted from a finite strip model
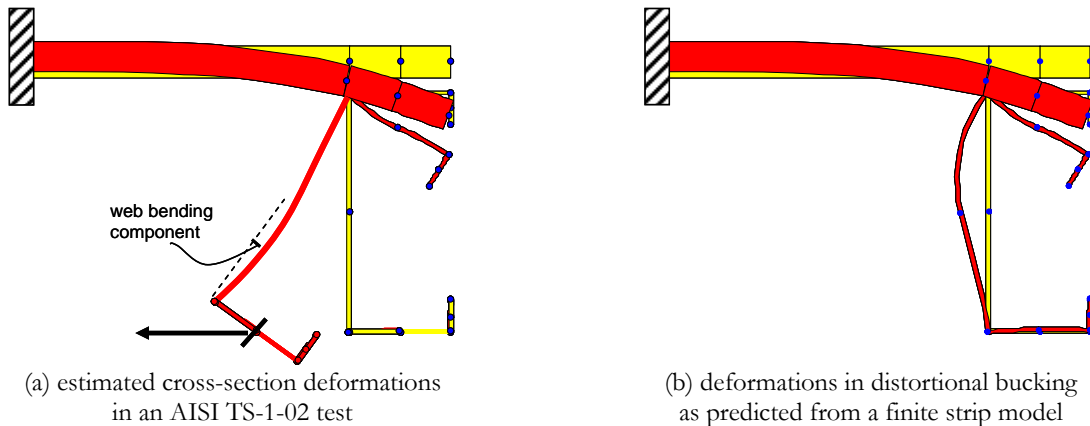
Figure 45 Cross-section deformations in an AISI TS-1-02 test compared with distortional buckling

</div>

Two aspects of the total rotation θ_2 are isolated in Section 4.1.2 for possible removal: rotation due to the loading, θ_L, and rotation due to joist bending, θ_s. Δ_L, which results in θ_L, is the estimated vertical displacement due to the loading straps. The analytical model employed for Δ_L is simply the PL/EA deformation of the straps themselves. This deformation is so small that its inclusion is found to be unnecessary; changes in the stiffness prediction are less than 1%. This does not necessarily imply that deformations due to the loading apparatus are inconsequential, but rather analytical approximation of connector slip, the small bending that occurs in the straps, etc. are all more involved and not considered here.

Δ_s, which results in θ_s, is the estimated vertical displacement due to bending of the joist. If we follow the analytical approximation in Section 4.1.2 ($\Delta_s = Ph_o^3/(3E_sI_s)$) we may remove this component of deformation and re-examine the connection stiffness. This is performed for the 8 in. and 12 in. deep 0.054 in. thick joists first presented in Figure 36, but now re-examined with connection rotation θ_c defined as $\theta_c = \theta_2 - \theta_L - \theta_s$, as given in Figure 46. With this "correction" the 12 in. deep joists appear to be stiffer than the 8 in. deep joists (where before in Figure 36, using θ_{c2}, they were approximately the same stiffness) – but the results are nonsensical for higher deformations, indicating the connectors stiffen at higher rotation; this conclusion is clearly at odds with the observed performance. The simple analytical expression employed for the joist bending assumes that plate bending drives the deformation but based on the results shown here, this is not an accurate model. The actual joist bending is far less as both direct torsional resistance and minor axis bending of the joist get engaged to resist the load. As a result, the analytical model for Δ_s is not employed in the conclusions of this report, and the much simpler θ_{c2} definition is instead employed.
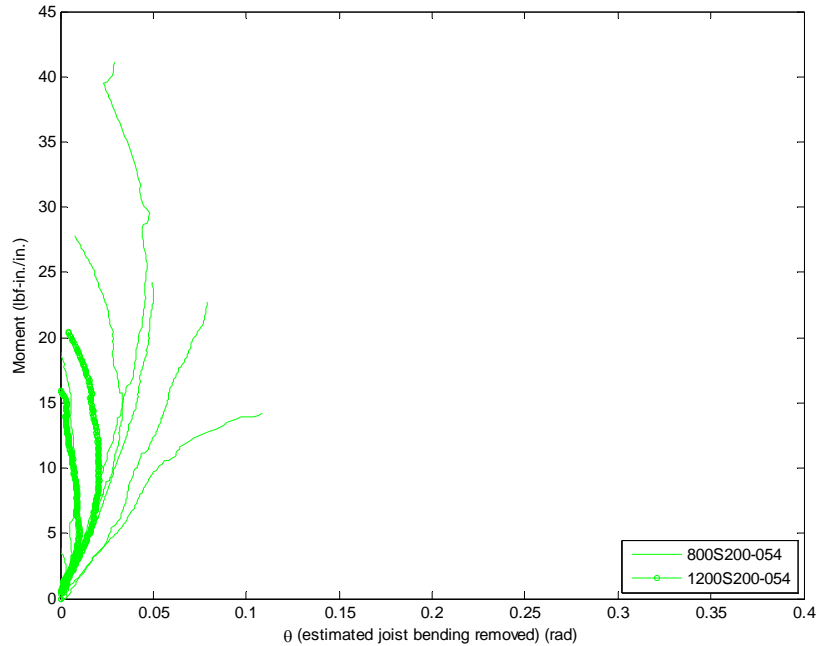
Figure 46 Influence of joist depth on connector response accounting for web bending for 800S200-054 and 1200S200-054 joists

Rather than use analytical approximations for the loading apparatus deformations and the joist bending deformations these two displacements could be directly measured. Using an extensometer or other fine position transducer, the rotation at the flange-to-sheathing connection could be measured, potentially leading to a more accurate approximation of the connection stiffness. Indeed these ideas were partially investigated in this work, but ultimately found to be more trouble than they were worth. Such local measurements have their own difficulties when compared to Δ_v and Δ_h as measured here which are well-behaving global displacements representing average response of the entire assembly.

One additional note on connection rotation definitions: the use of θ_w is strictly only valid for small rotation angles; however, for the plywood specimens in particular, relatively large rotation angles are investigated. In addition, in the deformed state the loading on the sheathing includes not only the bending moment and axial load, but shear and additional P-Δ moments as illustrated in Figure 47. Further, the forces on the sheathing and fastener also could consider large deformations as illustrated in Figure 47. However, since initial stiffness and not ultimate strength is the focus of this work, the small angle assumptions used herein are believed to be reasonable and consistent.
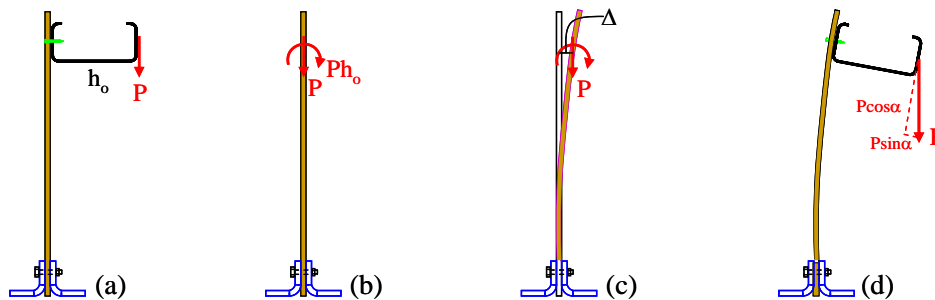
Figure 47 Large deformation effects in cantilever test (a) test (b) sheathing with forces (c) P-Δ moment (d) load direction

5 DISCUSSION OF EXPERIMENTAL TESTING

5.1 Variability and repeatability of testing

A small number of tests, as summarized in Table 7, were repeated to investigate the variability and repeatability of the cantilever tests conducted herein. The results indicate that the experimental methodology provides an accurate means of assessing the stiffness and that observed variability across testing is largely a function of inherent variability in the specimens due to sheathing stiffness and fastener location as opposed to variability in the testing method due in particular to alignment of the loading straps and tightening of the turnbuckles.

Tests 1, 2 and 3, summarized in Table 7, provide the repeatability of a test conducted in series with the same test setup. These three tests were conducted in sequence, each displaced to a full Δ_v of 6 in. The results show that in this case the connection stiffness degrades from Test 1 (172 lbf/rad) to Test 3 (111 lbf/rad), while the plywood stiffness remains largely the same. Behavior is well controlled and the decrease in the stiffness is well explained by the loss in connection stiffness.

The remaining tests in Table 7 represent a series of re-tests that were conducted several weeks after the initial tests. These tests were conducted to confirm the initial findings and to provide wood and connection stiffness values for two tests that had used an overly stiff spring within the horizontal displacement measurements (see notes 2 and 3 in the table.). These tests provided consistently the same performance as the initial testing with a slight degradation in overall stiffness due to damage that occurred in the initial testing.

Table 7 Summary of tests where re-testing was conducted to examine variability

ID (#)	Test Date	Joist	Trial	Sheathing Type	L (in.)	Fastener #	s (in.)	$k_{\phi 2}$	$k_{\phi w}$	$k_{\phi c2}$
1	1.19	800S200-54	A	Ply	24	6	12	19	21	172
2	1.19		B					18	20	142
3	1.19		C					16	19	111
9	2.16	800S200-54	A	Ply	12	6	12	51	97	107
10	3.12		B					46	91	95
11	2.09	800S200-97	A	Ply	12	10	12	47	65	171
12	3.12		B					44	53	252[(1)]
14	2.22	800S200-97	A	Ply	12	10	12	53[(2)]		
15	3.12		B					48	63	201
16	2.22	800S200-97	A	Ply	12	10	12	35[(3)]		
17	3.12		B					37	49	145

(1) test #11 showed an increase in connector stiffness above 171 during testing indicating some initial accomodation in the loading apparatus during that testing (strap and turnbuckle deformations are lumped with connector deformations in the $k_{\phi c2}$ definition) initial stiffness in test #12 is equal to the peak stiffness in test 11.

(2) this test used a spring loaded instrument for measuring the horizontal displacement that was overly stiff, stiffness $k_{\phi 2}$ was measured at 0.3 radians after this instrument was removed.

(3) similar to note 2, this is one of two tests that used an overly stiff spring loaded transducer for measuring horizontal displacement, $k_{\phi 2}$ was thuse determined after 0.28 radians when the overly stiff instrument was removed from the rig.

5.2 Difficulties with instrumentation scheme for horizontal measurement

Horizontal displacements of the sheathing were measured by a pair of position transducers. A number of difficulties were encountered for the experimental setup with these transducers.

5.2.1 *horizontal measurement excitation voltage*

As shown in Figure 48(a) the excitation voltage initially employed was a 9V battery. This transducer was originally used as part of a field instrumentation scheme where this convenience was needed. The accuracy (calibration) of the position transducer is linearly proportional to the supplied voltage, if the voltage supplied is too low and the calibration for the higher (expected) voltage is employed the instrument will read smaller displacements than actual. In this test setup this means a draining battery under-predicts the sheathing displacement which has the effect of predicting greater deformations in the connection. Note that overall stiffness (k_{ϕ_2}) is not affected since it is measured directly from the LVDT in the actuator. The end result is that a small bias for higher k_{ϕ_w} and lower $k_{\phi_{c2}}$ is introduced due to the use of the 9V batteries. In some cases, when it was identified after the test that a battery for one of the transducers had gone bad this data was removed from consideration – this can be observed in the test data sheets of Section 10, where only Δ_{h1} or Δ_{h2} is kept – but not both. A directly supplied voltage is now used for these position transducers.

5.2.2 *horizontal measurement spring restraint*

The position transducer for horizontal measurement consists of a central piston which is free to move. One end of this piston was attached to the sheathing, and a number of different attachment methods were considered before this detail was finalized. The basic transducer to sheathing attachment is shown in Figure 48(b),(d),(f). Initially a long wire was used to attach the transducer to the sheathing, but this was felt to introduce some uncertainty, particularly in panels that exhibited twist during deformation. To remedy this a spring was added to the transducer so that it would have a small resistance and measure both positive and negative movements; however, this spring (Figure 48(c)) was initially too stiff. The final detail consisted of a spring-loaded transducer using a flexible spring that did not influence the measured results; and a magnetic attachment of the piston end to a fastener, as illustrated in Figure 48(e) and (f).
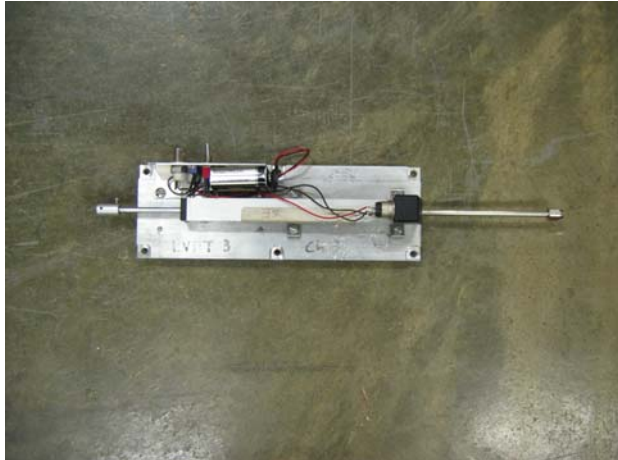
(a) position transducer used for measuring horizontal displacement, note 9V battery used for excitation
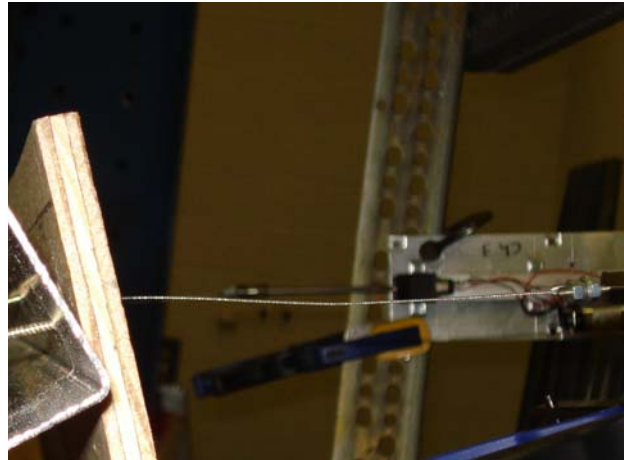
(b) initial transducer to sheathing attachment using long flexible wire

(c) stiff spring added to transducer, spring found to be overly stiff and was used on only two tests, see Table 7
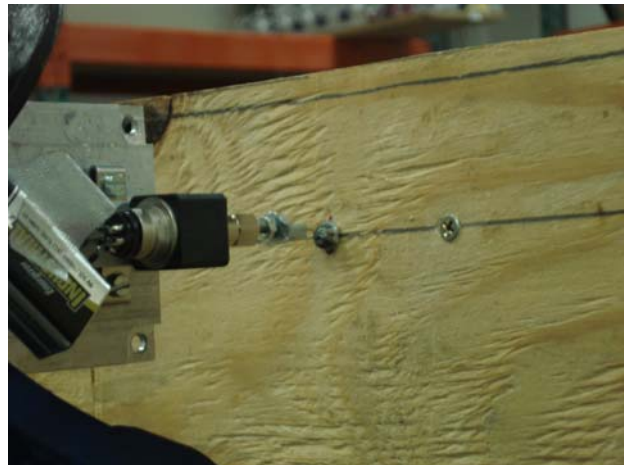
(d) modified transducer to sheathing connection using short wire
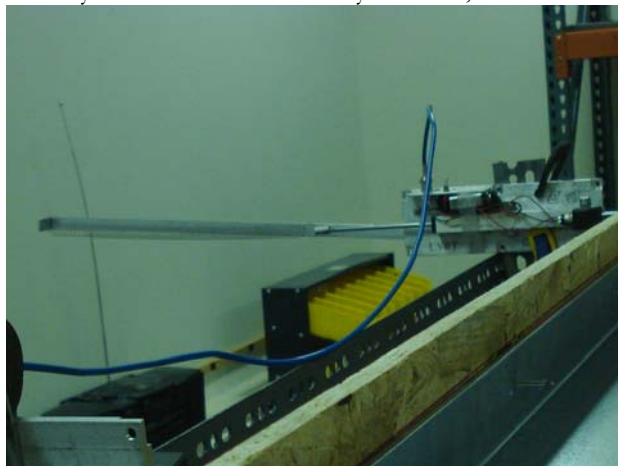
(e) flexible spring added to transducer to provide accurate positive and negative measurments

(f) final transducer to sheathing connection using short wire and magnet connection to a fastener

Figure 48 Position transducers for horizontal measurement

5.3 Limitation of applied rotation versus sine wave rotation

The applied rotation in the cantilever test is uniform; however the applied rotation in distortional buckling is over a discrete length (the distortional buckling half-wavelength) and is a maximum at center of that length and decreasing to the ends of the length. Thus, the uniform rotation applied in the test is more critical (more demanding) than the rotational stiffness required in distortional buckling. As a result the actual k_ϕ is greater than the k_ϕ measured in these tests. Research to quantify and rectify this difference, most likely with a simple adjustment to the uniform test results, is a possible subject for future research.

6   DEVELOPMENT OF COMPONENT STIFFNESS MODEL FOR DESIGN ($k_{\phi w}$, $k_{\phi c}$)

6.1   Springs in series model

The decomposition provided in Section 4.1 leads directly to a simple rotational springs in series model for the prediction of the rotation stiffness. The total rotation (θ_2) may be defined in terms of the sheathing (wood) rotation (θ_w) and the connector rotation (θ_{c2}) simply as:

$$\theta_2 = \theta_w + \theta_{c2}$$

Introducing the rotational stiffness definitions and recognizing that the springs are in series and thus experience the full moment, M:

$$M/k_{\phi 2} = M/k_{\phi w} + M/k_{\phi c2}$$

$$k_{\phi 2} = (1/k_{\phi w} + 1/k_{\phi c2})^{-1}$$

6.2   Sheathing

The sheathing stiffness may be taken as

$$k_{\phi w} = EI_w/L$$

where:

$k_{\phi w}$ = sheathing rotational stiffness per unit width
EI_w = bending rigidity per unit width, i.e. $E_w t_w^3/12$
　　　E_w = modulus of elasticity (for the loading direction) of the sheathing
　　　t_w = thickness of the sheathing
L = cantilever length, see Section 3.2.3 for relation to joist spacing

EI_w: Using the derivation of Section 4.1.1, the material stiffness (E_w) or bending rigidity (EI_w) may be back-calculated for the conducted tests. This information is provided in Table 8. Table 8(b) provides the bending rigidity in units of lbf-in.^{2}/ft of panel width, which though relatively speaking is an awkward set of units, appears to be standard in industry literature.

Comparison of the experimentally determined bending rigidity with values available from industry (Table 9) is favorable. The measured plywood bending rigidity is slightly higher (11%) than tabled values and the gypsum bending rigidity is within the range of reported values. The measured OSB rigidity is higher than the tabled values, and in fact is more similar to 32/16 span rated OSB than a 24/16 span rating; but given the wide range of reported stiffness values the results are deemed acceptable.

Based on the comparison of results between Table 8 and Table 9 it is deemed reasonable to estimate the bending rigidity for the rotational stiffness component for the sheathing from available literature. Please note, it is common in wood standards (e.g. NDS) to defer to manufacturer data on mechanical properties; thus, the use of APA and Gypsum association values is believed to be consistent with practice in timber design. Suggested values are provided, for convenience in Table 10 (tables remain copyright of APA and GA respectively).

Table 8 Sheathing material stiffness determined from testing
(a) direct experimental data

	E_w (psi)				
	mean	C.O.V.	n	min	max
Plywood*	96149	0.31	27	48125.9	154540
OSB*	342515	0.12	5	281361	386042
Gypsum	307427	0.06	7	277283	325909

*stress perpindicular to strength axis

(b) averaged and converted to EI_w in industry standard units

	EI_w (lbf-in.^{2}/ft of panel width)				
	mean	C.O.V.	n	min	max
Plywood*	9000	0.3	27	4000	14000
OSB*	31000	0.1	5	26000	35000
Gypsum	41000	0.1	7	37000	43000

*stress perpindicular to strength axis

Table 9 Sheathing material stiffness available from standards

	EI_w (lbf-in.^{2}/ft of panel width)	
	mean	source
32/16 Plywood*	8100	APA, Panel Design Spec. (2004)
24/16 OSB*	16000	APA, Panel Design Spec. (2004)
32/16 OSB*	25000	APA, Panel Design Spec. (2004)
Gypsum (min)	18000	Gypsum Assoc, GA-235-01, (2001)
Gypsum (max)	48000	Gypsum Assoc, GA-235-01, (2001)

*stress perpindicular to strength axis

Table 10 Sheathing bending rigidity from standards
(a) Plywood and OSB bending rigidity per APA, Panel Design Spec. (2004)

RATED PANELS DESIGN CAPACITIES

Span Rating	Stress Parallel to Strength Axis				Stress Perpendicular to Strength Axis			
	Plywood			OSB	Plywood			OSB
	3-ply	4-ply	5-ply		3-ply	4-ply	5-ply	
PANEL BENDING STIFFNESS, EI (lb-in.^{2}/ft of panel width)								
24/0	66,000	66,000	66,000	60,000	3,600	7,900	11,000	11,000
24/16	86,000	86,000	86,000	78,000	5,200	11,500	16,000	16,000
32/16	125,000	125,000	125,000	115,000	8,100	18,000	25,000	25,000
40/20	250,000	250,000	250,000	225,000	18,000	39,500	56,000	56,000
48/24	440,000	440,000	440,000	400,000	29,500	65,000	91,500	91,500
16oc	165,000	165,000	165,000	150,000	11,000	24,000	34,000	34,000
20oc	230,000	230,000	230,000	210,000	13,000	28,500	40,500	40,500
24oc	330,000	330,000	330,000	300,000	26,000	57,000	80,500	80,500
32oc	715,000	715,000	715,000	650,000	75,000	165,000	235,000	235,000
48oc	1,265,000	1,265,000	1,265,000	1,150,000	160,000	350,000	495,000	495,000

(b) Gypsum board bending rigidity (modified to APA units) Gypsum Assoc., GA-235-01 (2001)

Effective Stiffness (EI)*		
(typical range)		
Board Thickness (in.)	lbf in^2/ft of width	N•mm^2/mm of width
1/2	18,000 to 48,000	220,000 to 580,000
5/8	36,000 to 96,000	440,000 to 1,160,000
* EI is dependent on board density, relative humidity, type of board, paper type, direction of board during testing and the amount of handling prior to measurement. In general the value of EI follows the following relationships: Type X Gypsum Board > Regular Gypsum Board Denser Gypsum Board > Less Dense Gypsum Board Machine Direction > Cross Direction Low Relative Humidity > High Relative Humidity		

6.3 Connection

The average measured connection stiffness is summarized in Table 11(a), as originally provided in Table 6. Based on the discussions of Section 4.2 we may begin to compile and simplify the results. First, if we assume connection stiffness is independent of flange width and joist depth, then the connection stiffness becomes a function of joist thickness and sheathing and fastener details as shown in Table 11(b). Further, if we embrace the component stiffness model which concludes that cantilever length is only relevant to the sheathing, and we focus only on those fastener details deemed practical, i.e. #6 @ 12 in. for the thinner joists and #10 @ 12 in. for the 0.097 in. thick joists then we may simplify the results further, as shown in Table 11(c).

Table 11 Connection stiffness

(a) average connection stiffness as originally provided in Table 6

$k_{\phi c2}$ (lbf-in./in./rad)											
Sheathing -->	Plywood					OSB		Gypsum			
Cantilever (L) -->	12"				24"	24"		12"		24"	
Fastener # -->	6		10		6	6	10	6	10	6	10
Fastener Spacing -->	6"	12"	6"	12"	12"	12"	12"	12"	12"	12"	12"
362S162-33		81						100			
362S162-68		102						137			
800S200-54	116	109		97	137	113	77	103	77	91	99
800S250-54		116		124							
800S200-97			269	167			159		144		
1200S200-54		78				85					
1200S200-97				215			195				

(b) assume connection stiffness is independent of flange width and joist web depth

$k_{\phi c2}$ (lbf-in./in./rad)											
Sheathing -->	Plywood					OSB		Gypsum			
Cantilever (L) -->	12"				24"	24"		12"		24"	
Fastener # -->	6		10		6	6	10	6	10	6	10
Fastener Spacing -->	6"	12"	6"	12"	12"	12"	12"	12"	12"	12"	12"
0.033		81						100			
0.054	116	101		111	137	99	77	103	77	91	99
0.068		102						137			
0.097			269	183			177		144		

(c) assume connection stiffness is independent of sheathing cantilever length and focus only on 12 in. fastener spacing as the most practical for implementation

$k_{\phi c2}$ (lbf-in./in./rad)						
Sheathing -->	Plywood		OSB		Gypsum	
Fastener # -->	6	10	6	10	6	10
Fastener Spacing -->	12	12	12	12	12	12
0.033	81				100	
0.054	112	111	99	77	97	88
0.068	102				137	
0.097		183		177		144

C.O.V. of $k_{\phi c2}$ (lbf-in./in./rad)						
Sheathing -->	Plywood		OSB		Gypsum	
Fastener # -->	6	10	6	10	6	10
Fastener Spacing -->	12	12	12	12	12	12
0.033	*				*	
0.054	0.32	0.17	0.19	*	0.09	0.18
0.068	*				*	
0.097		0.21		0.15		0.06

(blank) no tests   (*) insufficient tests for statistic

(d) assume connection stiffness is independent of sheathing material

$k_{\phi c2}$ (lbf-in./in./rad)			
joist thickness	mean	C.O.V.	n
0.033	91	0.15	2
0.054	105	0.27	19
0.068	119	0.20	2
0.097	174	0.19	10

* 12 in. o.c. fastener spacing

Table 11(c) represents a reasonable means for establishing connection stiffness based on the available data; however, we may note that sheathing material does not have a strong influence on

average connection stiffness (it does show some impact on measured variability). If we ignore the sheathing material altogether (note its influence is still partially captured through the sheathing component of the stiffness model), then we arrive at Table 11(d) which presents the connection stiffness in the simplest possible means, a function of joist thickness given 12 in. o.c. fastener spacing is employed.

Based on the results of Table 11(d) a simple empirical expression for the connection rotation stiffness was determined.

$$k_{\phi c2} = 0.00035Et^2 + 75$$

where:

$k_{\phi w}$ = sheathing rotational stiffness in units of lbf-in./in. width / radian
E = 29,500,000 psi, modulus of steel
t = nominal joist thickness in in.

This expression has no mechanical basis, and is merely a mathematical convenience. To date, the simple dimensionally consistent mechanical models that have been investigated lead to poor correlations with the data; thus the above has been developed. Comparison of the above expression with the available data is shown in Figure 49. The prediction equation matches the mean data reasonably well, however scatter is large both at a given thickness and across different sheathing materials. Either Table 11(d) or the empirical expression is recommended for use.
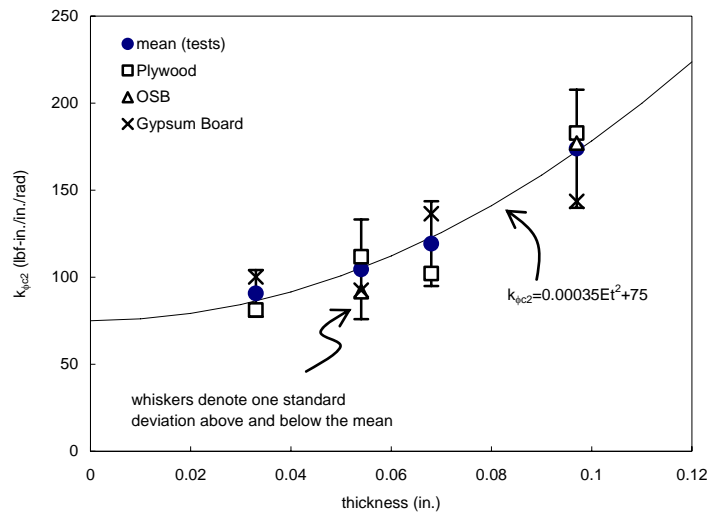
Figure 49 Connection rotational stiffness as a function of joist thickness

6.4 Comparison of recommended design models with conducted tests

The test-to-predicted ratios for various design model options for predicting the rotational stiffness of sheathing-connector-joist assemblies are summarized in Table 12. In all cases the total rotational stiffness is predicted by

$$k_{\phi2\text{-predicted}} = (1/k_{\phi w} + 1/k_{\phi c2})^{-1}$$

with

$k_{\phi w} = EI_w/L$
L = tested cantilever length, and
EI_w as given in Table 12 under the $k_{\phi w}$ column

and

$k_{\phi c2}$ = connection rotational stiffness as given in Table 12

Use of average tested values for the sheathing material leads to relatively high standard deviations for the plywood, but given the variability of plywood this would seem acceptable. Simplification of the connection stiffness to values based on the thickness of the joist increases the variability of the predictive method for OSB and gypsum, but leaves the average test-to-predicted values within acceptable ranges. Use of the empirical expression for $k_{\phi c2}$ is statistically equivalent to using the average tabled values for connection stiffness. Use of design values for the sheathing bending rigidity (i.e., based on APA or GA tables) introduces conservatism and increases variability of the predictive method.

Table 12 Test-to-predicted ratio for total rotational stiffness $k_{\phi2}$

$k_{\phi w}$	$k_{\phi c2}$	plywood		OSB		gypsum board	
		ave.	st. dev.	ave.	st. dev.	ave.	st. dev.
average of tested values per material (Table 8)	tested values	0.97	0.21	1.00	0.06	1.00	0.02
average of tested values per material (Table 8)	thickness only (Table 11d)	0.98	0.22	0.97	0.14	0.92	0.16
average of tested values per material (Table 8)	empirical equation	0.98	0.22	0.97	0.14	0.92	0.16
industry tabled values (Table 9/ Table 10, min values used)	empirical equation	1.03	0.23	1.47	0.26	1.30	0.21

6.5   Strength and stiffness requirement?

This report focuses on the rotational restraint (stiffness) provided by sheathing and connectors to stabilize the compression flange against distortional buckling. As such, the developed rotational stiffness is essentially the brace stiffness provided to the flange. As developed in AISI-S100 C3.1.6(b) the distortional bucking provisions are directly a function of this bracing stiffness. If the brace is stiff enough then, at least with respect to distortional buckling, the member may be able to develop its full capacity up to first yield. Unlike traditional bracing provisions even for smaller amounts of provided brace stiffness increased capacity is realized.

What is not checked in AISI-S100 C3.1.6(b) is whether or not the brace is strong enough – i.e., regardless of its stiffness can it develop and deliver the needed forces? As the tests conducted in gypsum board and reported herein show; stiffness may be available but strength perhaps not. This issue deserves further study, as the forces developed in restrained distortional buckling are not well understood.

Failures in the tests conducted herein are attributed to (1) weak plywood that fractured at a knot in one specimen (2) screw pull-through of one OSB specimen (3) screw pull-through of all gypsum board specimens. Failures (1) and (2) in plywood and OSB were rare and occurred at large levels of rotation, well beyond that which could be reasonably expected; this is not so for (3). If expected rotations could be determined or estimated, these rotations combined with the known stiffness could be used to determine demand forces for the sheathing and the fasteners; these could then be checked in a traditional fashion.

In the interim, in lieu of these more involved calculations and additional research, and reflecting on the experimental observations of this report, it is recommended that predicted rotational stiffness for plywood and OSB be employed without a strength check; however, given the variable and small strength available in gypsum board, rotational stiffness in gypsum board should be used only for serviceability calculations, and assumed to be zero for any ultimate strength calculation.

6.6   Reliability of k_ϕ calculation

What should be done to account for the variability in the connection stiffness prediction? Should a designer be provided with a reduced stiffness, i.e., ϕk_ϕ or k_ϕ/Ω? The difficulty in answering this question is that k_ϕ is not a direct measure of the member capacity, as, for example, M_n is, and thus cannot be compared using the reliability methodology of Chapter F of AISI-S100. Rather, k_ϕ is one of many inputs that go into producing the capacity. In some cases k_ϕ may have no impact on the result; in other cases it may be a significant contributor to the strength. Further, k_ϕ derives its strength from a system external to the member itself (the sheathing); such a situation is not directly envisioned in the traditional member-based reliability calculations used in codes. The problem, in many ways, is one of system reliability instead of component reliability.

Ideally, tests would be performed with k_ϕ as another one of the input variables, similar to the geometry and material parameters and the bending strength would be determined. Standard reliability methods of Chapter F of AISI-S100 could then be used to determine the reliability of strength predictions that include k_ϕ. Such testing is possible, but is currently unavailable, and given the expense is unlikely to be available in the near future.

Reliability has been applied in bracing provisions in design. In the hot-rolled steel AISC Specification (AISC 2005) the stability bracing provisions provide a required brace stiffness (the demand, not the capacity) calculated as $(1/\phi)\beta$ or $\Omega\beta$, where β is the nominal brace stiffness and

ϕ=0.75, Ω=2.0. However, the provisions say nothing about how to prove that a given brace has the required stiffness (only what it should be) and indeed reliability provisions for stiffness do not commonly exist. So, the designer is left, presumably, to his or her own judgment. The situation here is somewhat different – but the fact remains that a consistent reliability methodology applied to stiffness, as opposed to strength, does not exist in current design specifications.

At this point one is left with few avenues without additional research. Without additional testing what is needed is to examine the sensitivity of the bending strength prediction to k_ϕ; it is not linear. As discussed above, in some cases k_ϕ may have no impact on the result; in other cases it may be a significant contributor to the strength. If we (very) conservatively assume k_ϕ variability has a direct impact on the strength variability then we may compare the variability without calculation. The variability of the AISI-S100 calculation for test-to-predicted ratio of the bending capacity, based on its coefficient of variation (C.O.V. = standard deviation/mean) is near 0.10 (Schafer 2007).

reliability of connection stiffness
$k_\phi = (1/k_{\phi_w} + 1/k_{\phi_{c2}})^{-1}$

$\quad k_{\phi_w} = N(\mu_w, \sigma_w)$

$\quad k_{\phi_c} = N(\mu_c, \sigma_c)$

$\quad\quad$ N=normal distribution

$\quad\quad$ μ=mean, σ=st. dev.

$\quad r = \mu_c/\mu_w$

$\quad (C.O.V.)_w = \sigma_w/\mu_w$ 0.3 plywood, 0.1 OSB typ.

$\quad (C.O.V.)_c = \sigma_c/\mu_c$ 0.2 is typical

$\quad \mu_w = \overline{k}_{\phi_w}$

$\quad$ so $\sigma_w = 0.3\overline{k}_{\phi_w}$ (plywood) or $0.1\overline{k}_{\phi_w}$ (OSB)

$\quad \mu_c = r\overline{k}_{\phi_w}$

$\quad$ so $\sigma_c = 0.2r\overline{k}_{\phi_w}$

Assuming r is in the range of 1 to 4 what is expected C.O.V. of k_ϕ?
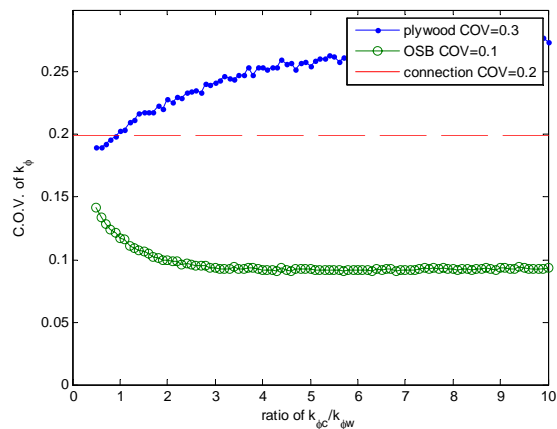
conclusion? C.O.V. of k_ϕ depends on the ratio of the stiffnesses (r), but is bounded by the weaker component – if this is the wood then C.O.V. for k_ϕ in plywood is ~ 0.3 and for k_ϕ in OSB is ~ 0.1

Figure 50 Simulation to examine C.O.V of k_ϕ based on component stiffnesses

Table 6(c) summarizes the relevant statistics for the connection stiffness variability and Table 8 for the sheathing stiffness variability. Assuming average values are used in design, the C.O.V. is the most important statistic for reliability consideration. Connection rotational stiffness in plywood using only the thickness of the joist as a design variable has a coefficient of variation between 0.2 and 0.3, in OSB (with limited tests) between 0.15 and 0.2, and in gypsum board with limited tests as high a 0.2. For purposes of preliminary calculation we assume a C.O.V of 0.2. For the sheathing C.O.V. in plywood is 0.3 and in OSB and gypsum 0.1. Figure 50 provides the results of a simulation to determine the C.O.V. of k_ϕ based on the C.O.V. of k_{ϕ_c} and k_{ϕ_w}. – for practical situations with $k_{\phi_c} > k_{\phi_w}$ the C.O.V. of k_{ϕ_w} is the most relevant. Hence expected C.O.V. for plywood sheathed connections is near 0.3 and for OSB sheathed connections 0.1.

Ultimately, without hard statistics or a testing program it is impossible to definitively conclude how reliability should figure into the connection stiffness, variability in the stiffness is high, but not

uniquely so. In the case of plywood sheathed specimens the variability is greater than in typical cold-formed steel design; however, the variability is from the plywood not the connection. Design values for plywood stiffness (from APA) appear suitably conservative. Use of these values is consistent with practice in other materials, and for now seems rational. In the case of OSB sheathed specimens, in the small number of samples conducted the variability of the stiffness is on par with variability in member strength determination; thus no reduction would seem appropriate. For gypsum board, connection strength, not stiffness limits the applicability. In the absence of further research it is recommended to use average connection $k_{\phi c2}$ values combined with industry standard sheathing $k_{\phi w}$ values.

7   CONCLUSIONS

A series of cantilever tests on joist-sheathing assemblies were conducted to determine the rotational restraint that sheathing provides to the compression flange of a floor joist in bending. This rotational restraint, which is characterized by the stiffness k_ϕ, can partially or fully retard distortional buckling. Distortional buckling is a mode of instability in which the flange undergoes rotation about the flange/web juncture of a member and the web locally bends. This mode of buckling has recently been recognized as a separate strength limit state in the North American Specification and design rules for its prediction adopted. The cantilever tests reported on herein cover joist thicknesses from 0.033 in. to 0.097 in., joist depths from 3.62 to 12 in., flange widths from 1.62 to 2.50 in., fasteners from #6 to #10, and plywood, OSB, and gypsum board sheathing. A total of 36 independent tests (and 6 re-tests) were conducted. The results of the tests are summarized in Table 5.

In this report a new method is proposed and validated for extending the cantilever tests such that the rotations associated with the sheathing and those associated with the connection may be decomposed, as given in Table 6. This decomposition allows for a separate examination of sheathing and connector performance and leads to a new proposed design method for determination of rotational stiffness, which is developed in Section 6, and summarized in Section 13.

Sheathing performance: the sheathing rotational stiffness (k_{ϕ_w}) is derived from simple cantilever bending under a concentrated moment. Measured bending rigidity is consistent with or slightly stiffer than industry provided (APA, Gyspum Assoc.) bending rigidity values. Plywood sheathing is able to undergo large rotations without significant degradation in stiffness, though in one case a fracture did occur at large rotation. Plywood stiffness is however a highly variable property, a coefficient of variation of 0.3 was observed in the testing here. OSB sheathing is more prone to connection damage as a result of fastener pull-through than plywood, however since the OSB is stiffer the forces developed at a given rotation are higher than in plywood. One of five OSB sheathed specimens tested failed in pull-through, but this failure occurred at large rotation. OSB stiffness is reasonably consistent and well behaved in the small sample of tests conducted here. Gypsum board sheathing provides a consistent stiffness, but all specimens tested failed at very low rotations and forces due to pull-through of the fasteners. Based on these tests, gypsum board is not a viable material for providing ultimate strength resistance, but may be adequate for serviceability calculations.

Connection/fastener performance: the connection rotational stiffness (k_{ϕ_c}) is derived from bearing between the joist flange and sheathing combined with tension at the fastener location, with additional bending and shear at the fastener location, and bending in the joist. Despite this relatively complex mechanism, one variable, the joist thickness, is by far the most influential in determining connection rotational stiffness. The role of (a) joist depth, (b) joist flange width, (c) fastener size, (d) fastener spacing, and (e) sheathing type were all investigated herein, but joist thickness remains the most influential variable. Joist depth (a) influences the forces developed, but does not strongly influence the stiffness. Joist flange width (b) should have a significant role to play based on simple theoretical models, but wider flange width only provides minimal improvements in stiffness. Fastener size (c) should be appropriate for the joist thickness, but use of larger fasteners in thinner materials, e.g., a #10 fastener in 0.054 in. thick material does not provide significant increases in stiffness. Fastener spacing (d) examined herein largely focused on fasteners spaced at 12 in. on center; closer fastener spacing was associated with increases in stiffness. Tighter fastener spacing is one means of increasing the connection rotational stiffness for a given joist, but additional work would be needed to quantify this effect. Sheathing type (e) is shown to have only a marginal impact

on the connection stiffness, but of course it has an enormous impact on the sheathing stiffness and the overall stiffness realized. All of the sheathing types investigated were of approximately the same thickness and further examination of the role of sheathing type on connection stiffness is likely warranted.

New design method: a design method is proposed for adoption that characterizes the available rotational stiffness as two rotational springs in series, i.e.: $k_\phi = (1/k_{\phi_w} + 1/k_{\phi_c})^{-1}$ where k_{ϕ_w} is the sheathing (wood) rotational stiffness, estimated as EI_w/L where EI_w is the bending rigidity of the sheathing (industry standard (APA, Gypsum Assoc.) tables may be used) and L is ½ the joist spacing; k_{ϕ_c} is the connection rotational stiffness, estimated as a function of the joist thickness based on the experimental results herein and assuming fastener spacing of at least 12 in. o.c. to the sheathing. Section 13 of this report provides the complete methodology for determining k_ϕ in draft specification form.

Future work: A number of additional tests and research could be performed to improve upon the design methods and findings presented herein.

Additional testing
- Additional tests at 0.033 in. thickness joists or thinner are needed. Similarly, tests at thicknesses greater than 0.097 in. are needed if such thicknesses are used in practice.
- A series of tests focused on fastener spacing, particularly tighter than 12 in. o.c., as this is one of the few influential variables under designer control, is needed. Preliminary results showed the benefits of tighter fastener spacing, but more work is required.
- A series of tests focused on fastener location are needed to account for the practical situation of joists which have two pieces of sheathing attached to the same flange in the location of a sheathing joint. Thus the sheathing-to-joist connection has two rows of fasteners, one for each piece of sheathing to connect to the flange.

Additional modeling and/or analytical studies
- Additional study on the nonlinear effects (P-Δ) from the applied forces in the test as discussed in Section 4.3 is needed.
- Additional study on isolating the joist bending component from the connection stiffness, either by an improved analytical model or direct measurement of the connection rotation, as discussed in Section 4.3 is needed.
- Analytical study of the impact of the distortional buckling half-wavelength, and sine wave deformations vs. uniform deformations, as discussed in Section 5.3 is needed.

Additional studies to improve design method
- A design methodology that incorporates strength, likely through (a) determining a rotation demand then (b) determining the forces developed in such a demand and finally (c) checking those forces against pull-through failure is needed. Analytical work is needed to determine the rotation demand in distortional buckling.
- Further consideration of reliability as discussed in Section 6.6 is needed.

Dissemination needs
- Design aids and technical notes associated with the application of the findings presented herein are needed.

While the above represents a significant amount of additional work, the findings presented herein provide support for a workable design method that immediately allows floors and other framing systems to benefit from the rotational restraint provided by sheathing to stabilize the compression flange of members in bending.

8 ACKNOWLEDGMENTS

9 REFERENCES

AISC (2005) Specification for Structural Steel Buildings, American Institute of Steel Construction, Chiicago, IL.

AISI (2002) "Rotational-Lateral Stiffness Test Method for Beam-to-Panel Assemblies" AISI TS-1-02, AISI Cold-Formed Steel Design Manual, 2002 Edition

AISI-COS (2006) Committee/Subcommittee Ballot: CS04-227B, C3.1.6 Distortional Buckling Strength [Resistance], Approved March 14, 2006, American Iron and Steel Institute – Committee on Specificaitons for the Design of Cold-Formed Steel Structural Members.

AISI-S100 (2007) North American Specification for the Design of Cold-Formed Steel Structural Members. AISI-S100-07. American Iron and Steel Institute, Washington, D.C.

APA (2004) Panel Design Specification, APA – The Engineered Wood Association.

GA (2001) Gypsum Board Typical Mechanical and Physical Properties, Gypsum Association, Washington, D.C., GA-235-01.

Hausler, R.W., Pabera, R.F. (1973). "Connection strength in thin metal roof structures." Second Specialty Conference on Cold-Formed Steel Structures. University of Missouri-Rolla. St Louis, Missouri.

LaBoube, R.A. (1986). "Roof Panel to Purlin Connections: Rotational Restraint Factor", Proceedings of the IABSE Colloquium on Thin–Walled Metal Structures in Buildings, Stockholm, Sweden.

MRI (1981). "Determination of Rotational Restraint Factor 'F' for Panel to Purlin Connection Rigidity". Observer's Report: MRI Project No. 7105-G. Midwest Research Institute, Kansas City, Missouri. Conducted for Metal Building Manufacturers Association.

AISI-S100 (2007). North American Specification for the Design of Cold-Formed Steel Structural Members. American Iron and Steel Institute, Washington, D.C.

NDS (2005) National Design Specification for Wood Construction, American Wood Council.

Schafer, B.W. (2007) "Review: The Direct Strength Method of cold-formed steel member design." Elsevier, *Journal of Constructional Steel Research.* (to be published 2007)

SFA (2000) Low-rise residential construction details, Steel Framing Alliance, Washington, D.C.

Yu, C. (2005). "Distortional Buckling of Cold-Formed Steel Members in Bending", PhD Thesis, Johns Hopkins University, Baltimore, MD.

Yu, C., Schafer, B.W. (2003). "Local Buckling Tests on Cold-Formed Steel Beams." ASCE, Journal of Structural Engineering. 129 (12) 1596-1606.

Yu, C., Schafer, B.W. (2006). "Distortional buckling tests on cold-formed steel beams." ASCE, Journal of Structural Engineering. 132 (4) 515-528.

10   TEST SUMMARY DATA SHEETS

This section provides a group summary and individual results for the testing conducted herein. The group summary on the following page lists the relevant statistics for each test, including in column 8, the ID number for the test. The following pages provide summary information and comments, along with pictures of the testing and figures showing the raw results and post-processed results for each test. the summary pages are ordered by figure number, i.e., Figure 10.1, 10.2, etc. The Figure number is the same as the ID number, i.e, Figure 10.1 is ID 1, figure 10.2 is ID 2, etc.

Table 10.1 Summary data sheet for all testing
(individual summary pages are by ID order, column 8 of the table below)

.dat file	w (in.)	L (in.)	ho (in.)	t (in.)	E (psi)	tw (in.)	ID (#)	Dvread (#)	h1read (#)	h2read (#)	npt (#)	Assembly ID	Test Date	Test Series	Joist	ID	Trial	bo	ho	t	Type	L	#	s	$k_{\phi 2}$	$k_{\phi 1}$	k_ϕ	$k_{\phi w}$	$k_{\phi c2}$	$k_{\phi c1}$	$k_{\phi c}$
1-800S200_54_1A	54	24	8	0.054	29500000	0.45	1	0	0	0	100	1-PL-24-6-12-01_A	1.19	1	800S200-54	1	A	2	8	0.054	PL	24	6	12	19	19	22	21	172	172	235
1-800S200_54_1B	54	24	8	0.054	29500000	0.45	2	0	0	0	100	1-PL-24-6-12-01_B	1.19	1	800S200-54	1	B	2	8	0.054	PL	24	6	12	18	18	20	20	142	142	320
1-800S200_54_1C	54	24	8	0.054	29500000	0.45	3	0	0	0	100	1-PL-24-6-12-01_C	1.19	1	800S200-54	1	C	2	8	0.054	PL	24	6	12	16	16	18	19	111	111	305
1-800S200_54_2	54	24	8.12	0.054	29500000	0.45	4	0	0	0	100	1-PL-24-6-12-02	1.22	1	800S200-54	2	A	2	8	0.054	PL	24	6	12	21	21	25	27	101	101	341
1-800S200_54_3	54	24	8.11	0.054	29500000	0.45	5	0	0	0	100	1-PL-24-6-12-03	1.19	1	800S200-54	3	A	2	8	0.054	PL	24	6	12	14	14	15	15	137	137	329
1-800S200_54_4(12)	54	12	8.13	0.054	29500000	0.45	6	0	0	0	100	1-PL-12-6-12-01	2.05	1m/2	800S200-54	4	A	2	8	0.054	PL	12	6	12	26	26	33	31	166	167	-440
1-800S200_54_6(12)	54	12	8.13	0.054	29500000	0.45	7	0	0	0	100	1-PL-12-6-12-03	2.16	1m/2	800S200-54	6	A	2	8	0.054	PL	12	6	12	31	31	40	53	76	76	177
1-800S200_54_5(12)	54	12	8.16	0.054	29500000	0.45	8	0	0	0	100	1-PL-12-6-12-02	2.06	1m/2	800S200-54	9	A	2	8	0.054	PL	12	6	12	29	29	38	44	87	87	302
2-800S200_54_11(12)	54	12	8.15	0.054	29500000	0.45	9	0	0	0	100	2-PL-12-6-12-01	2.16	2	800S200-54	11	A	2	8	0.054	PL	12	6	12	51	51	80	97	107	107	604
2-800S200_54_11B	54	12	8.15	0.054	29500000	0.45	10	0	0	0	100	x	3.12	2	800S200-54	11	B	2	8	0.054	PL	12	6	12	46	47	75	91	95	96	545
1-800S200_97_1(12)	54	12	8.21	0.097	29500000	0.45	11	0	0	0	100	1-PL-12-10-12-01	2.09	1m/2	800S200-97	1	A	2	8	0.097	PL	12	10	12	47	47	49	65	171	172	237
1-800S200_97_1B	54	12	8.21	0.097	29500000	0.45	12	0	0	0	100	x	3.12	1	800S200-97	1	B	2	8	0.097	PL	12	10	12	44	44	46	53	252	252	356
1-800S200_97_2(12)	54	12	8.221	0.097	29500000	0.45	13	0	0	0	100	1-PL-12-10-12-02	2.12	1m/2	800S200-97	3	A	2	8	0.097	PL	12	10	12	43	43	45	59	149	150	204
1-800S200_97_3(12)	54	12	8.225	0.097	29500000	0.45	14	0	0	0	100	1-PL-12-10-12-03	2.22	1m/2	800S200-97	4	A	2	8	0.097	PL	12	10	12	53	53	57				
1-800S200_97_4B	54	12	8.225	0.097	29500000	0.45	15	0	0	0	100	x	3.12	1	800S200-97	4	B	2	8	0.097	PL	12	10	12	48	48	51	63	201	202	277
2-800S200_97_15(12)	54	12	8.23	0.097	29500000	0.45	16	0	0	0	100	2-PL-12-10-12-02	2.22	2	800S200-97	15	A	2	8	0.097	PL	12	10	12	35	35	38				
2-800S200_97_15B	54	12	8.23	0.097	29500000	0.45	17	0	0	0	100	x	3.12	2	800S200-97	15	B	2	8	0.097	PL	12	10	12	37	37	39	49	145	145	179
4-800S200_97_17	54	12	8.22	0.097	29500000	0.45	18	0	0	0	100	4-PL-12-10-6-01	3.13	4	800S200-97	17	A	2	8	0.097	PL	12	10	6	47	47	50	58	269	268	372
3-800S250_54_01	54	12	8.13	0.054	29500000	0.45	19	0	0	0	100	3-PL-12-6-12-01	3.13	3	800S250-54	1	A	2.5	8	0.054	PL	12	10	12	43	43	63	66	124	124	-740
3-800S250_54_02	54	12	8.15	0.054	29500000	0.45	20	0	0	0	100	3-PL-12-6-12-01	3.13	3	800S250-54	2	A	2.5	8	0.054	PL	12	6	12	53	53	88	98	116	116	644
4-800S200_54_7	54	12	8.11	0.054	29500000	0.45	21	0	0	0	100	4-PL-12-6-6-01	3.14	4	800S200-54	7	A	2	8	0.054	PL	12	6	6	45	45	70	68	132	132	-496
4-800S200_54_10	54	12	8.12	0.054	29500000	0.45	22	0	-1	0	100	4-PL-12-6-6-02	3.16	4	800S200-54	10	A	2	8	0.054	PL	12	6	6	36	36	48	57	99	99	354
3-800S200_54_05	54	12	8.19	0.054	29500000	0.45	23	0	0	0	100	3-PL-12-10-12-02	3.20	3	800S200-54	5	A	2	8	0.054	PL	12	10	12	33	33	43	51	97	97	454
7-1200S200_97_02	54	12	12.2	0.097	29500000	0.45	24	0	0	0	100	7-PL-12-10-12-01	3.21	7	1200S200-97	2	A	2	12	0.097	PL	12	10	12	58	58	65	84	183	183	286
7-1200S200_54_01	54	12	12.14	0.054	29500000	0.45	25	0	0	0	100	7-PL-12-6-12-01	3.22	7	1200S200-54	1	A	2	12	0.054	PL	12	6	12	31	31	52	51	81	81	-458
7-1200S200_54_02	54	12	12.16	0.054	29500000	0.45	26	0	0	0	100	7-PL-12-6-12-01	3.22	7	1200S200-54	2	A	2	12	0.054	PL	12	6	12	36	36	67	70	75	75	330
7-1200S200_97_01	54	12	12.17	0.097	29500000	0.45	27	0	-1	0	100	7-PL-12-10-12-02	3.26	7	1200S200-97	1	A	2	12	0.097	PL	12	10	12	60	60	68	80	248	248	421
8-362S162_33_01	54	12	3.782	0.033	29500000	0.45	28	11000	11000	-1	100	8-PL-12-6-12-01	3.27	8	362S162-33	1	A	1.62	3.62	0.033	PL	12	6	12	40	40	71	78	81	80	-706
8-362S162_68_01	54	12	3.836	0.068	29500000	0.45	29	12000	10000	-1	100	8-PL-12-6-12-01	3.28	8	362S162-68	1	A	1.62	3.62	0.068	PL	12	6	12	42	42	45	72	102	101	113
5-800S200_97_20	54	24	8.207	0.097	29500000	0.45	30	0	-1	0	100	5-OSB-24-10-12-01	4.02	5	800S200-97	20	A	2	8	0.097	OSB	24	10	12	66	66	71	112	159	158	191
5-800S200_54_32	54	24	8.18	0.054	29500000	0.45	31	0	-1	0	100	5-OSB-24-6-12-01	4.03	5	800S200-54	32	A	2	8	0.054	OSB	24	6	12	57	57	88	117	113	112	374
5-800S200_54_31	54	24	8.11	0.054	29500000	0.45	32	0	-1	0	100	5-OSB-24-10-12-02	4.03	5	800S200-54	31	A	2	8	0.054	OSB	24	10	12	44	44	57	101	77	77	127
5-1200S200_54_3	54	24	12.15	0.054	29500000	0.45	33	0	-1	0	100	5-OSB-24-6-12-02	4.03	5	1200S200-54	3	A	2	12	0.054	OSB	24	6	12	44	44	82	89	85	86	727
5-1200S200_97_03	54	24	12.17	0.097	29500000	0.45	34	0	0	-1	100	5-OSB-24-10-12-02	4.04	5	1200S200-97	3	A	2	12	0.097	OSB	24	10	12	75	75	86	122	195	195	295
6-800S200_97_21	54	12	8.196	0.097	29500000	0.51	35	1500	-1	500	50	6-GYP-12-10-12-01	4.04	6	800S200-97	21	A	2	8	0.097	GYP	12	10	12	94	92	104	274	138	141	170
8-362S162_33_02	54	12	3.8	0.033	29500000	0.51	36	2500	2000	-1	50	8-GYP-12-6-12-01	4.05	8	362S162-33	2	A	1.62	3.62	0.033	GYP	12	6	12	75	75	244	295	100	101	-296
8-800S200_97_16	54	12	8.208	0.097	29500000	0.51	37	1800	300	-1	20	8-GYP-12-10-12-02	4.05	6	800S200-97	16	A	2	8	0.097	GYP	12	10	12	68	57	59	481	149	141	169
8-362S162_68_02	54	12	3.821	0.068	29500000	0.51	38	3000	-1	1000	50	8-GYP-12-6-12-02	4.05	8	362S162-68	2	A	1.62	3.62	0.068	GYP	12	6	12	94	93	107	300	137	136	170
6-800S200_54_30	54	12	8.16	0.054	29500000	0.51	39	5000	-1	1500	50	6-GYP-12-6-12-01	4.05	6	800S200-54	30	A	2	8	0.054	GYP	12	6	12	76	76	143	295	103	103	297
6-800S200_54_34	54	12	8.12	0.054	29500000	0.51	40	6000	2000	-1	50	6-GYP-12-10-12-01	4.06	6	800S200-54	34	A	2	8	0.054	GYP	12	10	12	60	60	108	285	77	76	177
6-800S200_54_33	54	24	8.13	0.054	29500000	0.51	41	6400	3200	-1	50	6-GYP-24-10-12-01	4.06	6	800S200-54	33	A	2	8	0.054	GYP	24	10	12	58	58	106	138	99	100	416
6-800S200_54_35	54	24	8.16	0.054	29500000	0.51	42	4200	-1	3000	50	6-GYP-24-6-12-01	4.06	6	800S200-54	35	A	2	8	0.054	GYP	24	6	12	53	53	83	128	91	91	204

Test Date: 1/19/07 Initials: ETD,YG,RHS   *Notes*:
Joist ID: 800S200-54   First test conducted
Assembly ID: 1-PL-24-6-12-01_A   1 of 5 screws offset near lip.
Sheathing: Plywood, L = 24 in.
Fastener: #6 @ 12 in.
datafile: 1-800S200_54_1A
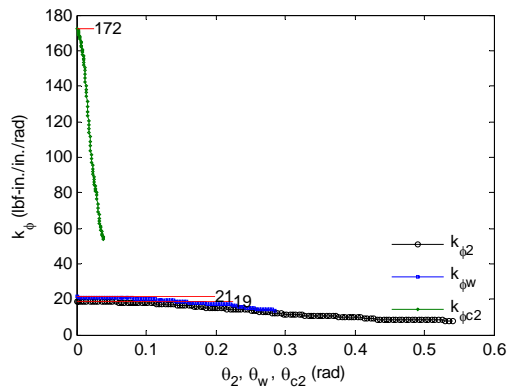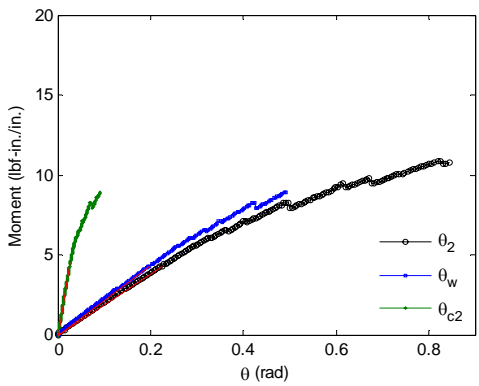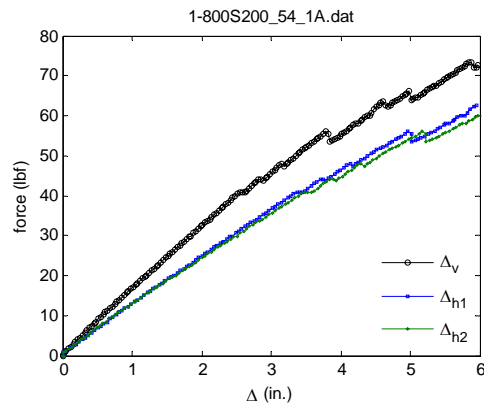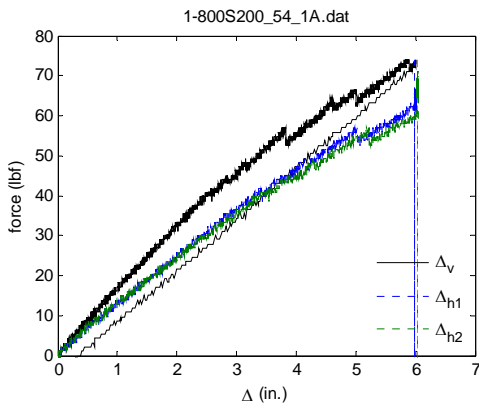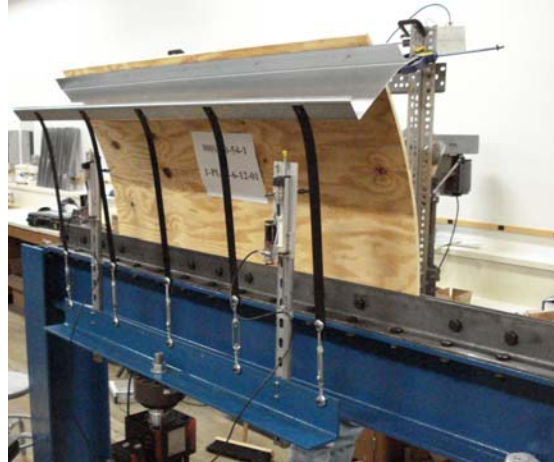
Figure 10.1

Test Date: 1/19/07 Initials: ETD,YG,RHS   *Notes*:
Joist ID: 800S200-54   Immediate re-test of 1-PL-24-6-12-01
Assembly ID: 1-PL-24-6-12-01_B
Sheathing: Plywood, L=24 in.
Fastener: #6 @ 12 in.
datafile: 1-800S200_54_1B
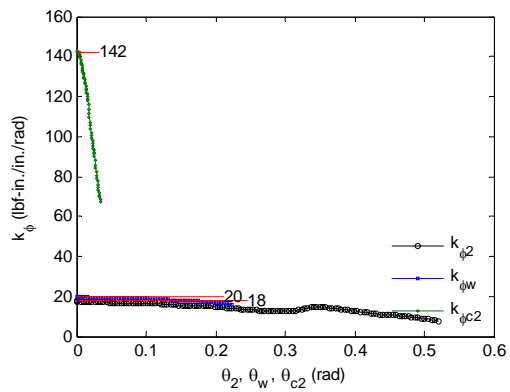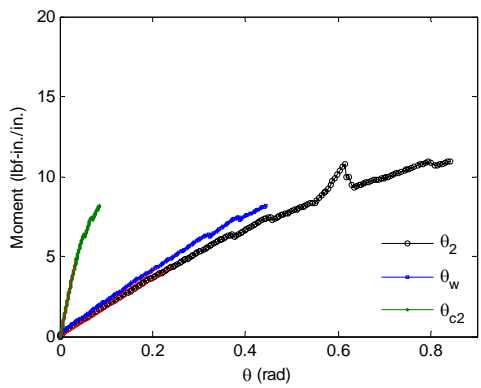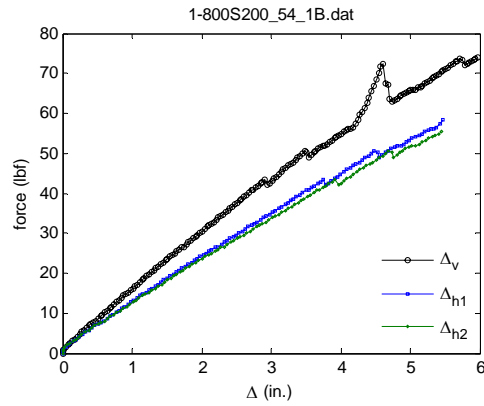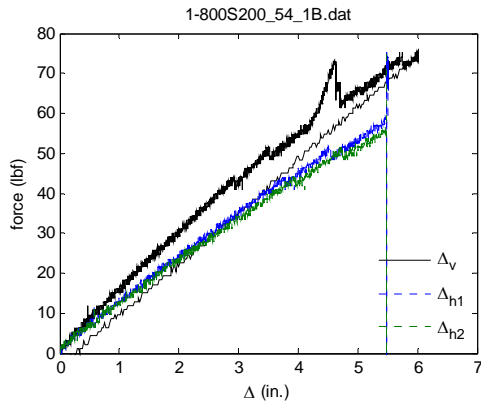
Figure 10.2

Test Date: 1/19/07 Initials: ETD,YG,RHS *Notes*:
Joist ID: 800S200-54 Immediate re-test of 1-PL-24-6-12-01_B
Assembly ID: 1-PL-24-6-12-01_C
Sheathing: Plywood, L = 24 in.
Fastener: #6 @ 12 in.
datafile: 1-800S200_54_1C
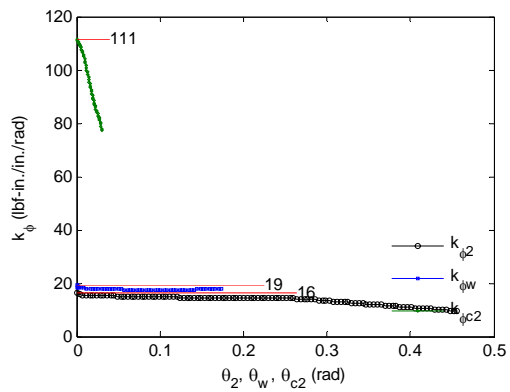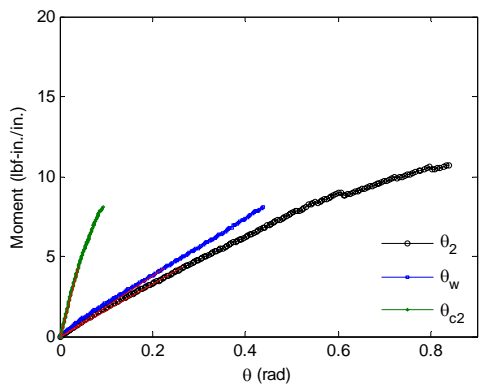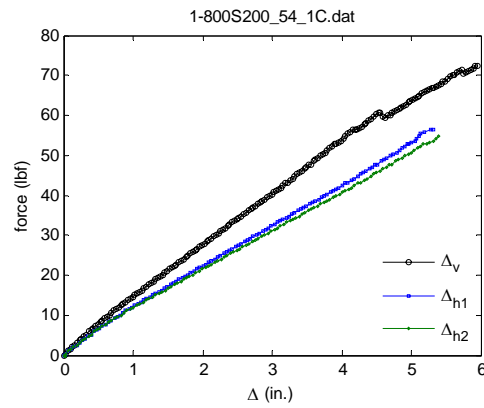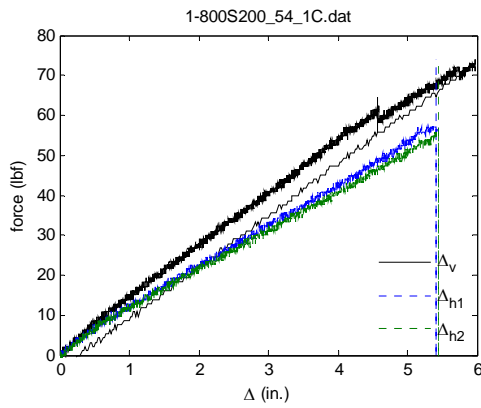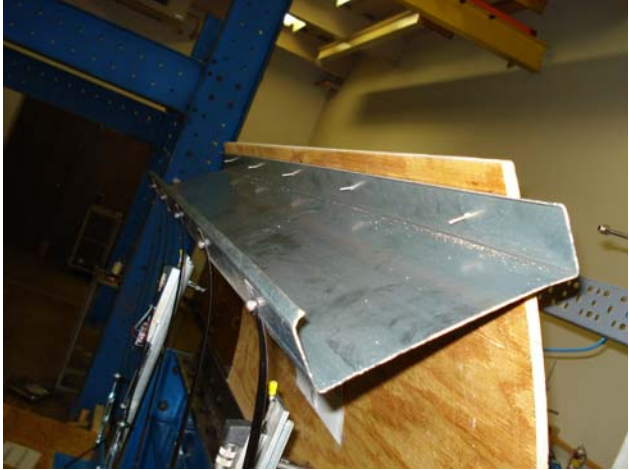
Figure 10.3

Test Date: 1/22/07 Initials: ETD,YG,RHS   *Notes*:
Joist ID: 800S200-54   4 of 5 screws offset near lip.
Assembly ID: 1-PL-24-6-12-02   Initial warp was .25".
Sheathing: Plywood, L = 24 in.
Fastener: #6 @ 12 in.
datafile: 1-800S200_54_2

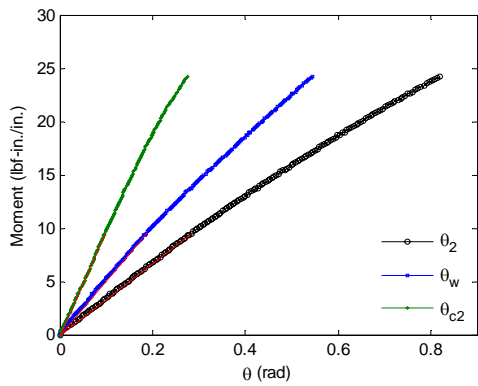Figure 10.4

Test Date: 1/19/07 Initials: ETD,YG,RHS
Joist ID: 800S200-54
Assembly ID: 1-PL-24-6-12-03
Sheathing: Plywood, L = 24 in.
Fastener: #6 @ 12 in.
datafile: 1-800S200_54_3

Notes:
3 of 5 screws offset near lip.
Initial cracks on compression side observed.
Initial warp was 1.375".
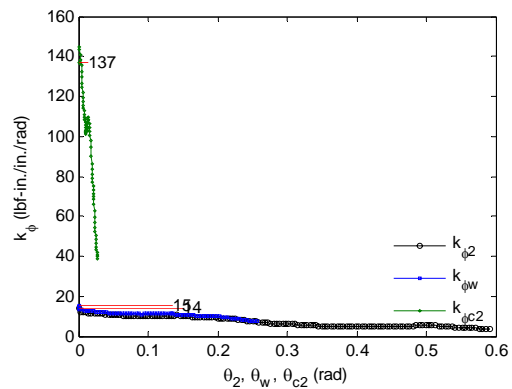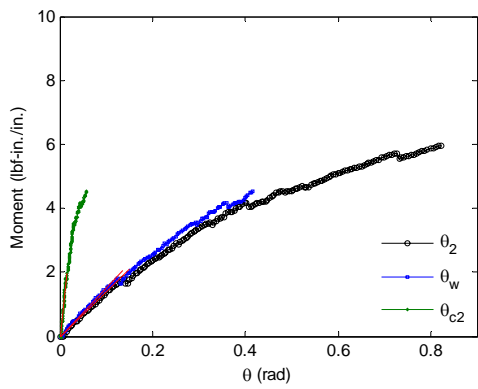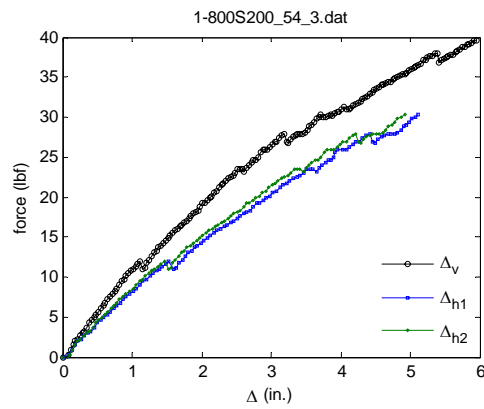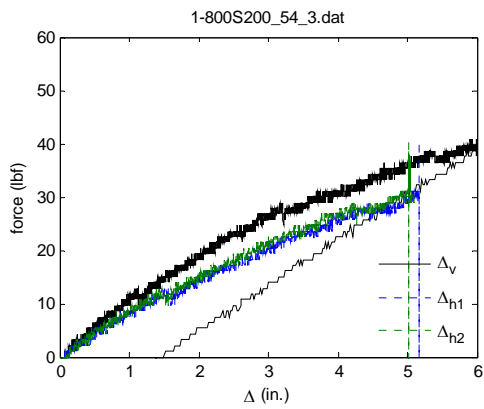
Figure 10.5

Test Date: 2/5/07 Initials: ETD,YG,RHS
Joist ID: 800S200-54
Assembly ID: 1-PL-12-6-12-01
Sheathing: Plywood, L = 12 in.
Fastener: #6 @ 12 in.
datafile: 1-800S200_54_4(12)

Notes:
Initial warp was .125".
1 of 5 screws offset near web.
Small crack on compression side observed.
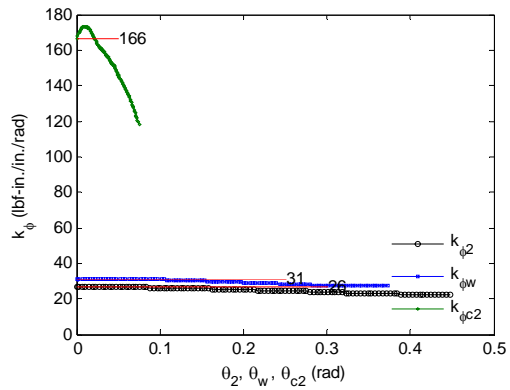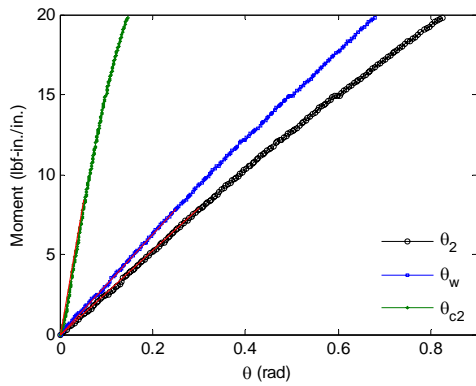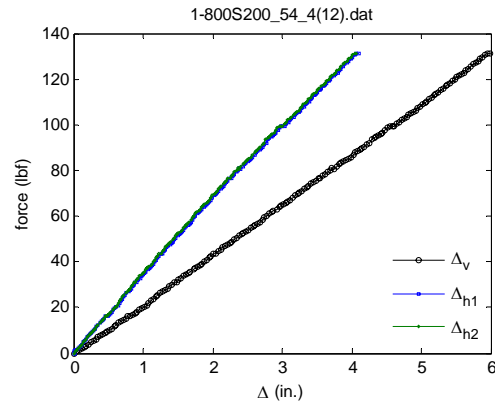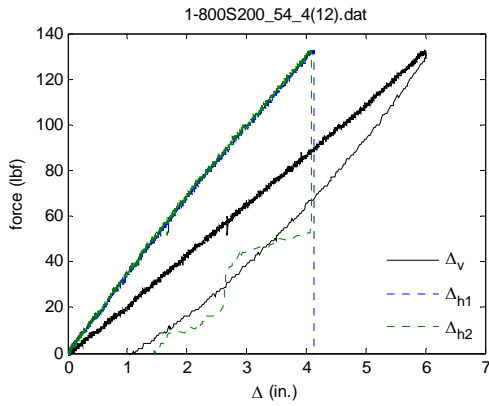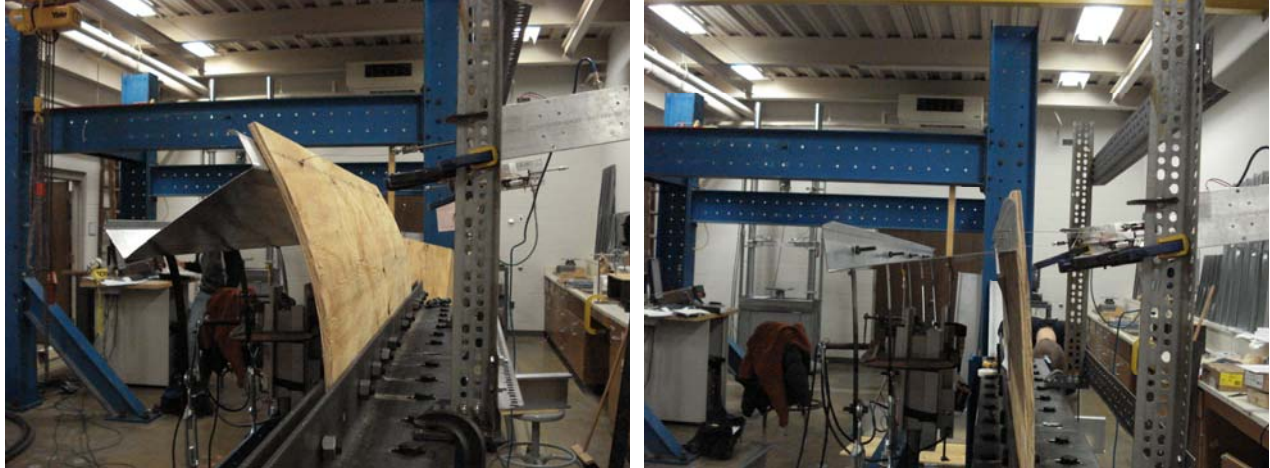
Figure 10.6

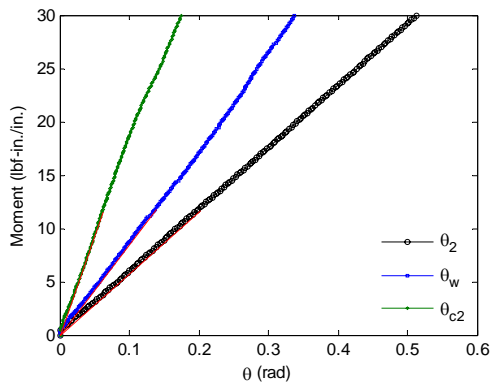Test Date: 2/16/07 Initials: ETD,YG,RHS   *Notes*:
Joist ID: 800S200-54   Initial warp was .25".
Assembly ID: 1-PL-12-6-12-03   5 of 5 screws offset near web
Sheathing: Plywood, L = 12 in.   5 of 5 screws moderately over driven.
Fastener: #6 @ 12 in.   Crack on compression side observed.
datafile: 1-800S200_54_6(12)
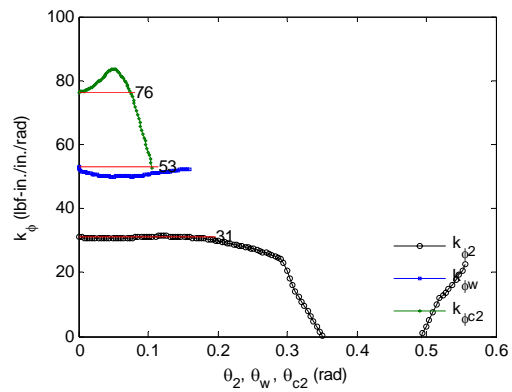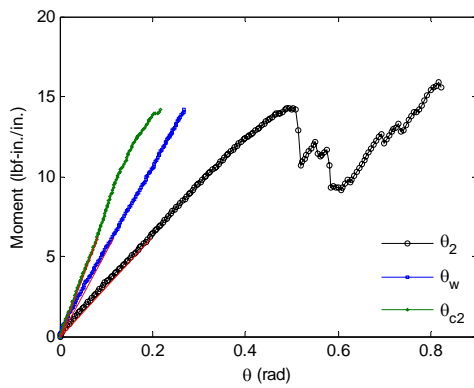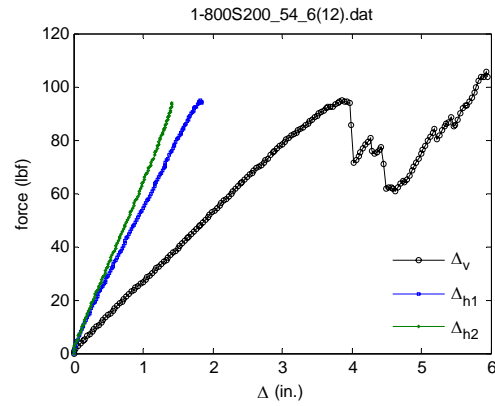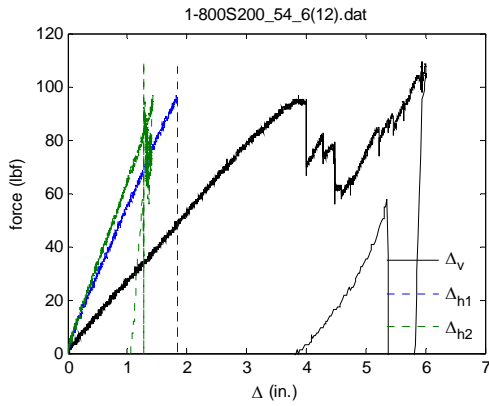
Figure 10.7

Test Date: 2/6/07 Initials: ETD,YG,RHS   *Notes*:
Joist ID: 800S200-54   Initial warp was .5".
Assembly ID: 1-PL-12-6-12-02   1 of 5 screws offset near web.
Sheathing: Plywood, L= 12in.   2 of 5 screws over driven.
Fastener: #6 @ 12 in.   Crack on compression side observed.
datafile: 1-800S200_54_5(12)
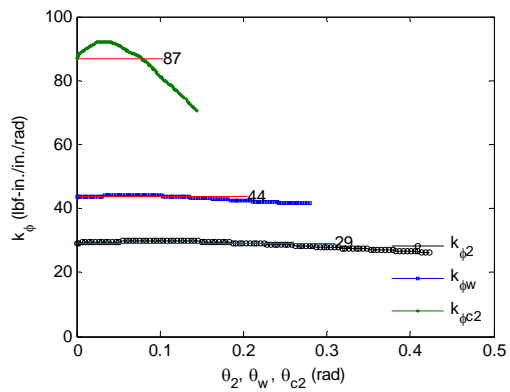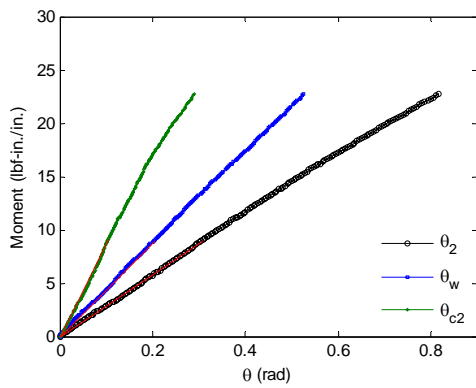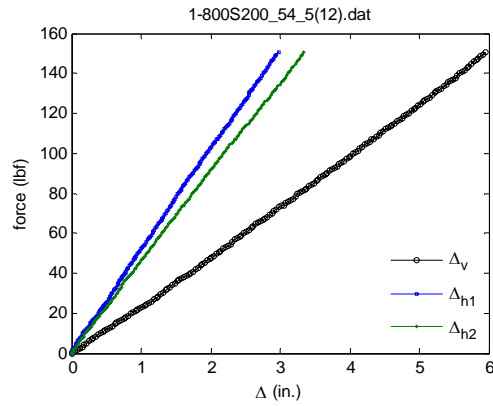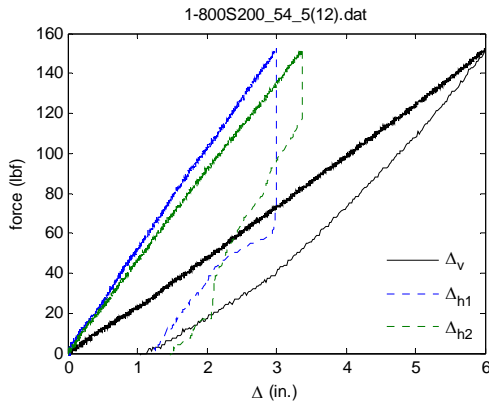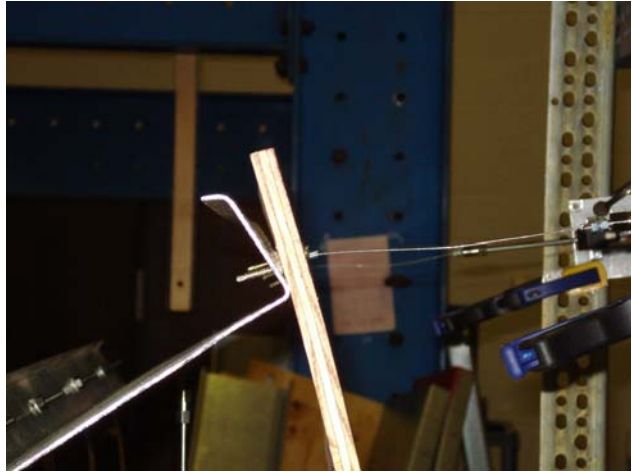
Figure 10.8

Test Date: 2/16/07 Initials: ETD,YG,RHS
Joist ID: 800S200-54
Assembly ID: 2-PL-12-6-12-01
Sheathing: Plywood, L = 12in.
Fastener: #6 @ 12in.
datafile: 2-800S200_54_11(12)

Notes:
Initial warp was .5".
1 of 5 screws offset near web
3 of 5 screws over driven.
No cracks observed on plywood.
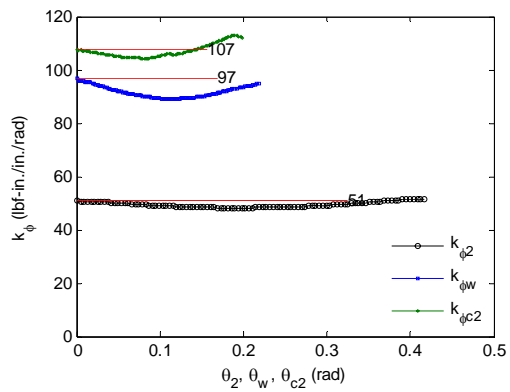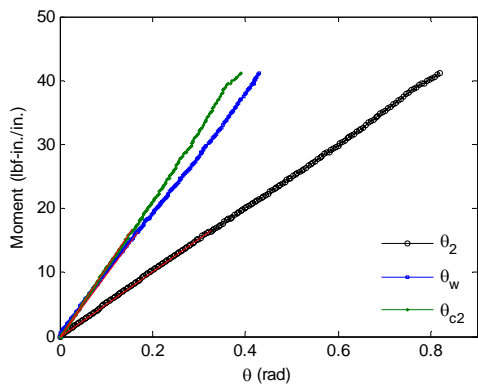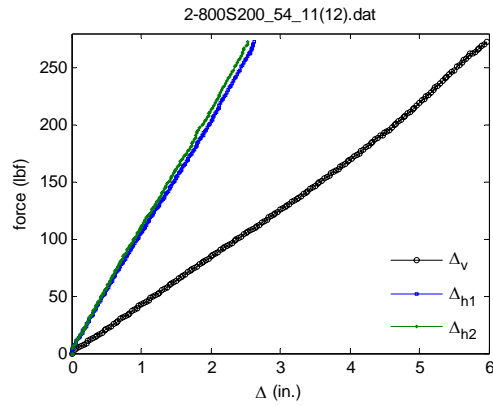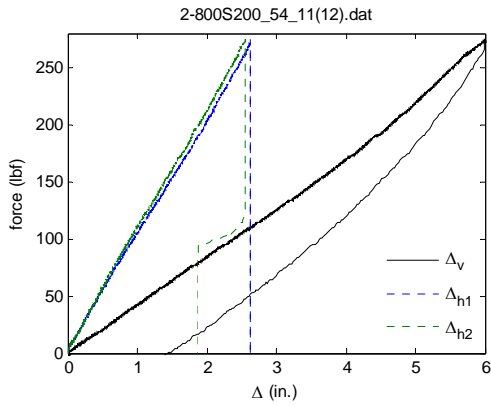
Figure 10.9

Test Date: 3/12/07 Initials: ETD,YG,RHS
Joist ID: 800S200-54
Assembly ID: 2-PL-12-6-12-01
Sheathing: Plywood, L = 12 in.
Fastener: #6 @ 12 in.
datafile: 2-800S200_54_11B

Notes:
Initial warp was .5".
1 of 5 screws offset near web
3 of 5 screws over driven.
No cracks observed on plywood.
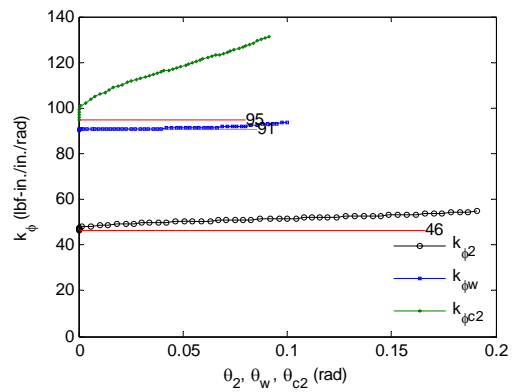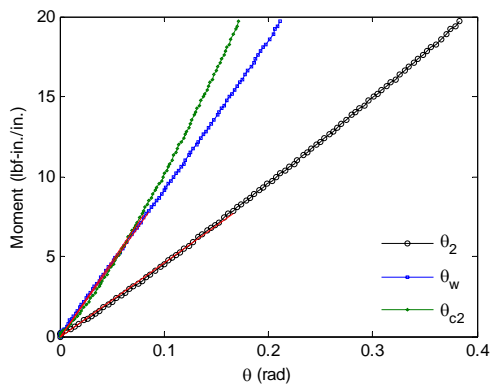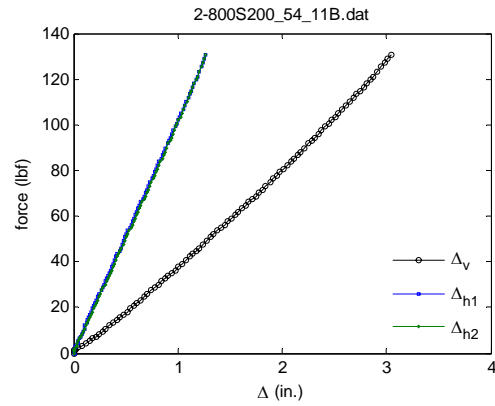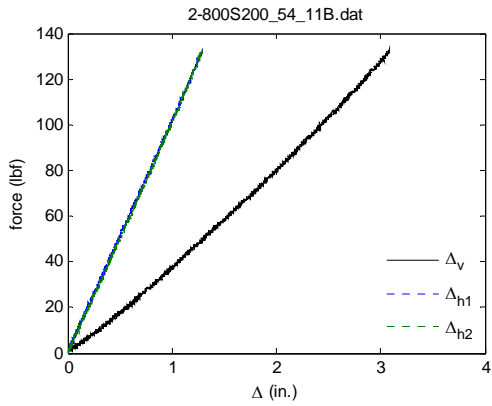
Figure 10.10

Test Date: 2/9/07   Initials: ETD,YG,RHS
Joist ID: 800S200-97
Assembly ID: 1-PL-12-10-12-01
Sheathing: Plywood, L = 12 in.
Fastener: #10 @ 12 in.
datafile: 1-800S200_97_1(12)

Notes:
Initial warp was .5".
2 of 5 screws offset near lip with
2 of 5 screws over driven.
Cracks on compression side of plywood
observed.
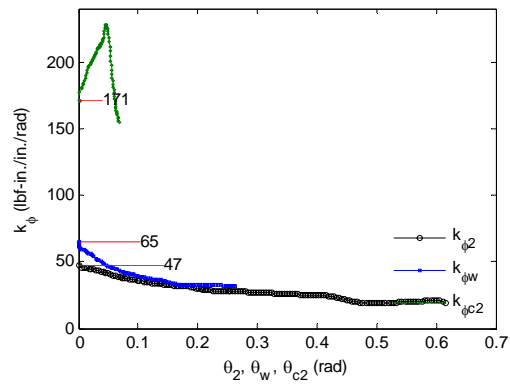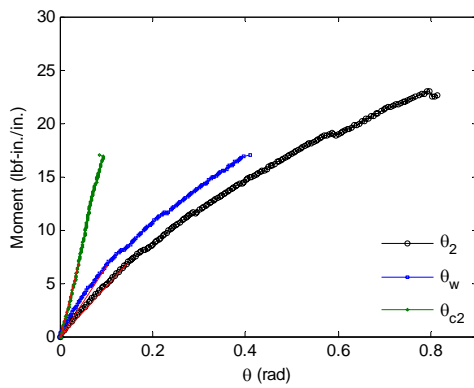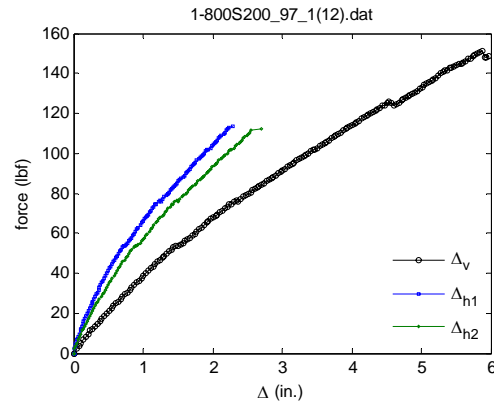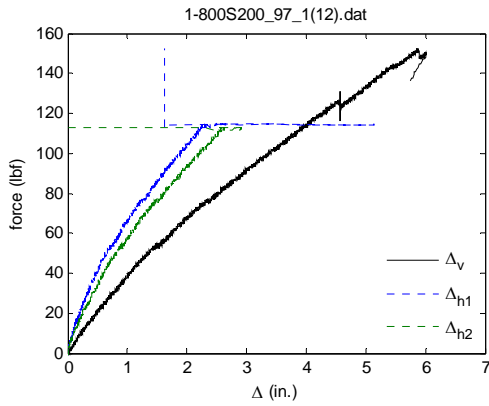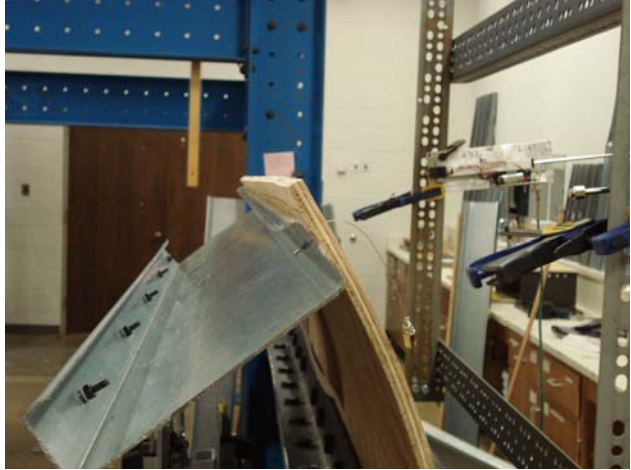
Figure 10.11

Test Date: 3/12/07 Initials: ETD,YG,RHS   *Notes*:
Joist ID: 800S200-97   Re-test of 1-PL-12-10-12-01
Assembly ID: 1-PL-12-10-12-01
Sheathing: Plywood, L = 12 in.
Fastener: #10 @ 12 in.
datafile: 1-800S200_97_1B
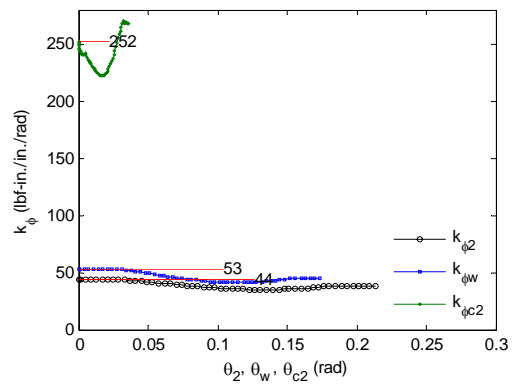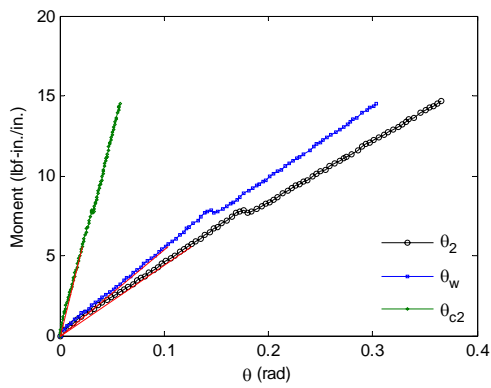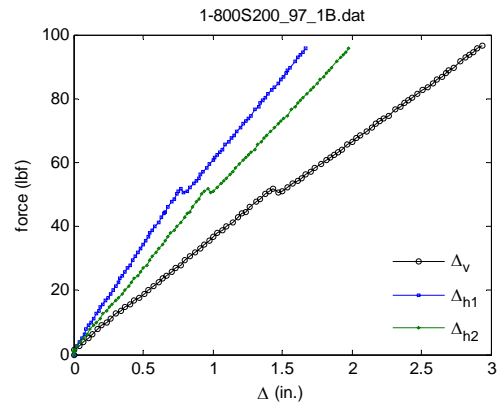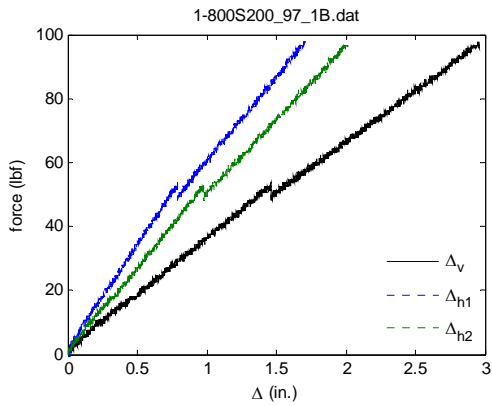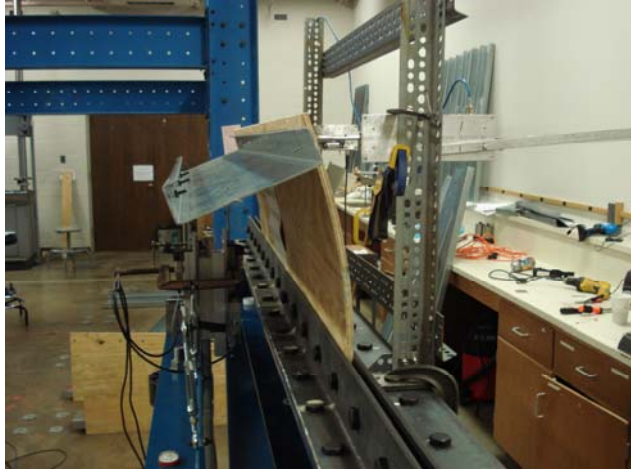
Figure 10.12

Test Date: 2/12/07 Initials: ETD,YG,RHS   *Notes*:
Joist ID: 800S200-97   Initial warp was .8".
Assembly ID: 1-PL-12-10-12-02   3 of 5 screws offset near lip and
Sheathing: Plywood, L = 12 in.   1 of 5 screws offset near web while
Fastener: #10 @ 12 in.   no screws were over driven.
datafile: 1-800S200_97_2(12)   No cracks were observed.
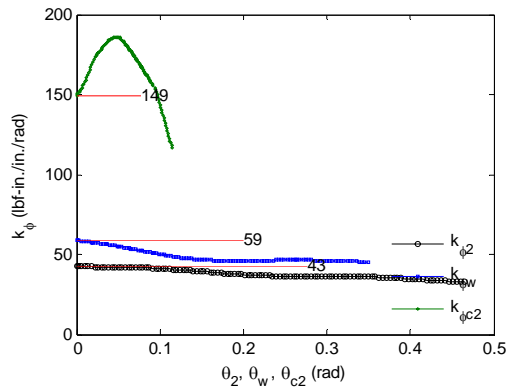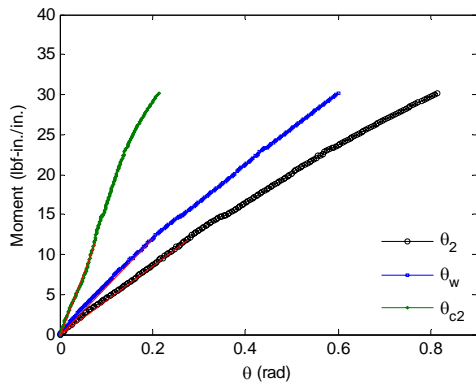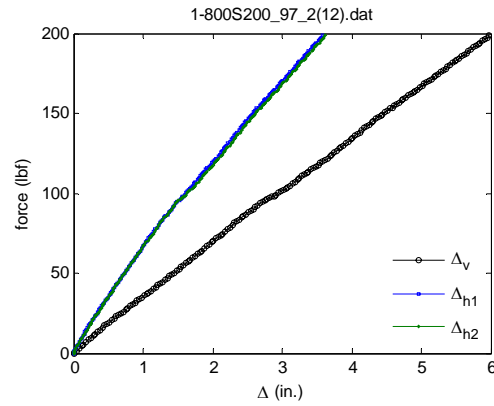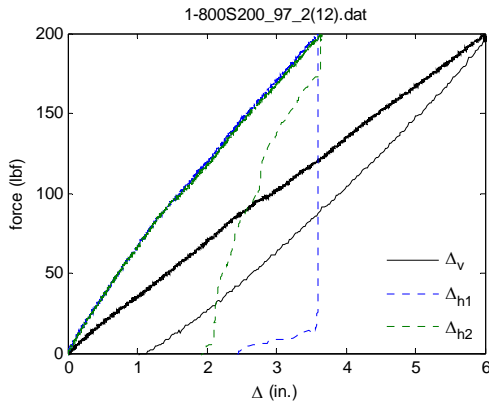
Figure 10.13

Test Date: 2/22/07 Initials: ETD,YG,RHS   *Notes*:
Joist ID: 800S200-97   Initial warp was 1".
Assembly ID: 1-PL-12-10-12-03   No screws offset with
Sheathing: Plywood, L = 12 in.   2 of 5 screws over driven.
Fastener: #10 @ 12 in.   Cracks on compression side observed.
datafile: 1-800S200_97_3(12)

Figure 10.14

Test Date: 3/12/07 Initials: ETD,YG,RHS   *Notes*:
Joist ID: 800S200-97   Initial warp was .125".
Assembly ID: 1-PL-12-10-12-03   No screws offset with
Sheathing: Plywood, L = 12 in.   2 of 5 screws over driven.
Fastener: #10 @ 12 in.   Cracks on compression side observed.
datafile: 1-800S200_97_4B

Figure 10.15

Test Date: 2/22/07 Initials: ETD,YG,RHS   *Notes*:
Joist ID: 800S200-97   Initial warp was .125".
Assembly ID: 2-PL-12-10-12-02   5 of 5 screws offset near web with
Sheathing: Plywood, L = 12 in.   2 of 5 screws over driven.
Fastener: #10 @ 12 in.   Cracks on tension side observed.
datafile: 2-800S200_97_15(12)
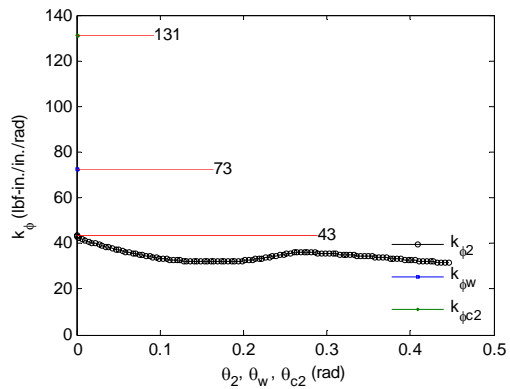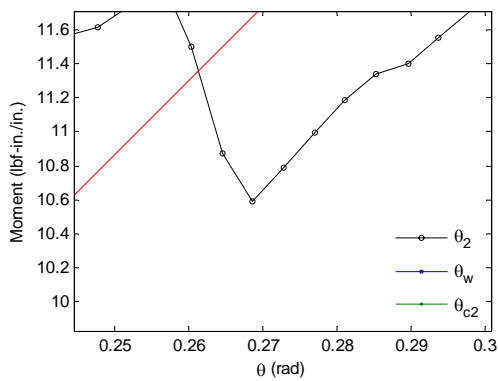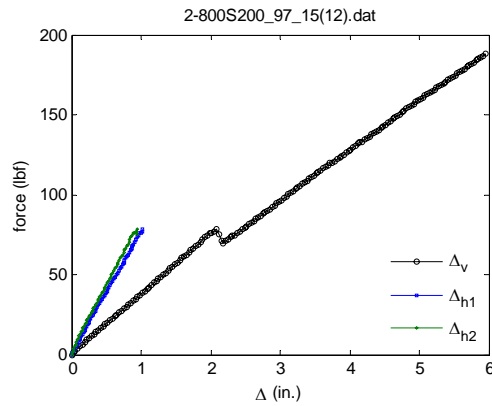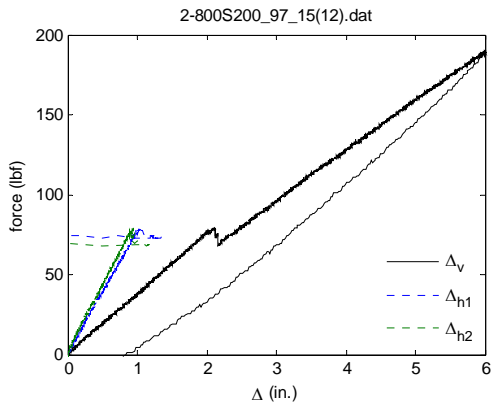
Figure 10.16

Test Date: 3/12/07 Initials: ETD,YG,RHS   *Notes*:
Joist ID: 800S200-97   Initial warp was .125".
Assembly ID: 2-PL-12-10-12-02   5 of 5 screws offset near web with
Sheathing: Plywood, L = 12 in.   2 of 5 screws over driven.
Fastener: #10 @ 12 in.   Cracks on tension side observed.
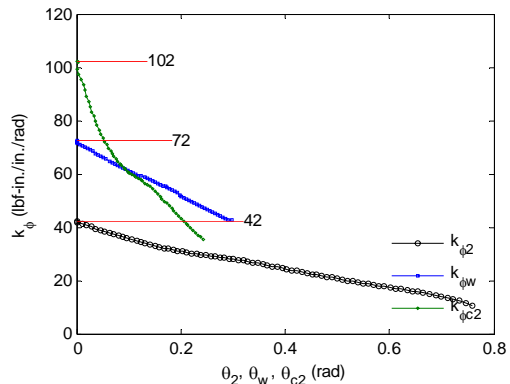datafile: 2-800S200_97_15B
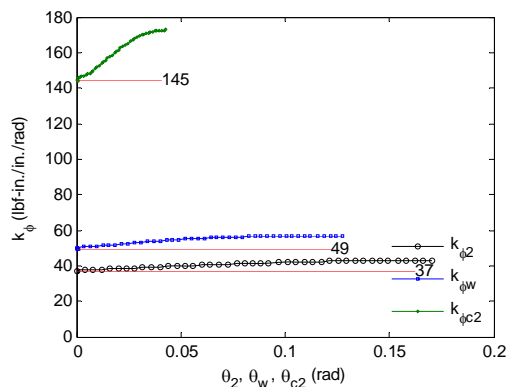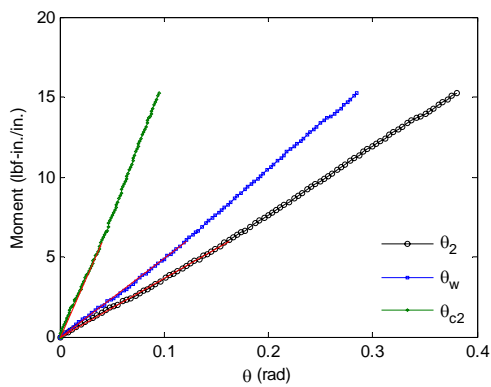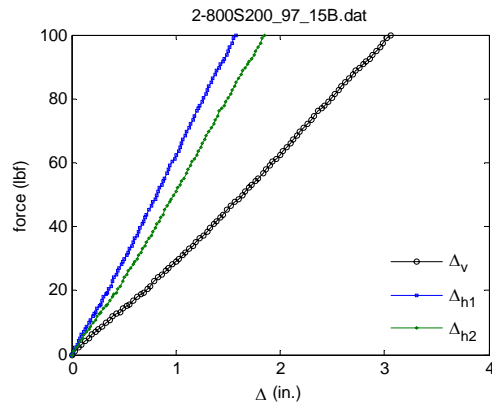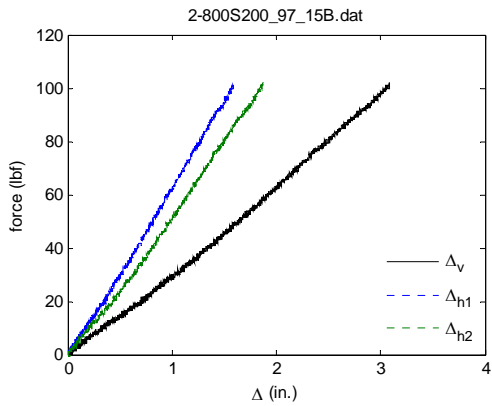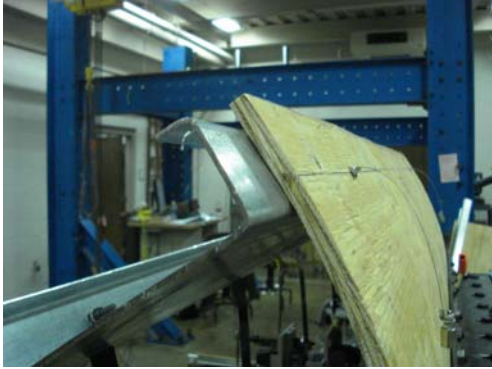
Figure 10.17

Test Date: 3/13/07 Initials: ETD,YG,RHS
Joist ID: 800S200_97
Assembly ID: 4-PL-12-10-6-02
Sheathing: Plywood, L = 12 in.
Fastener: #10 @ 6 in.
datafile: 4-800S200_97_17

Notes:
3 of 9 screws offset near web and
3 of 9 screws offset near lip with
0 of 9 screws over driven.
No initial cracks were observed.
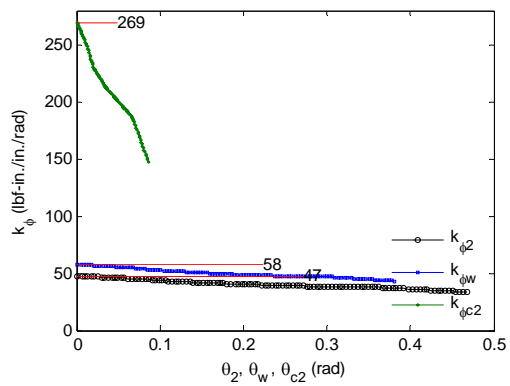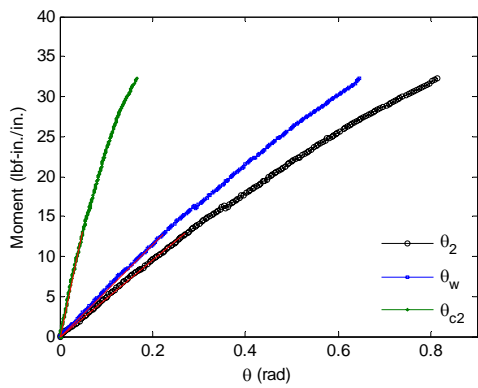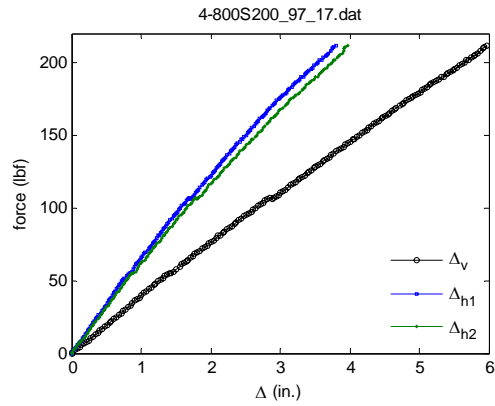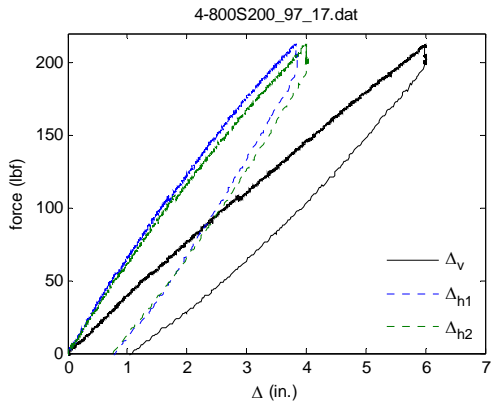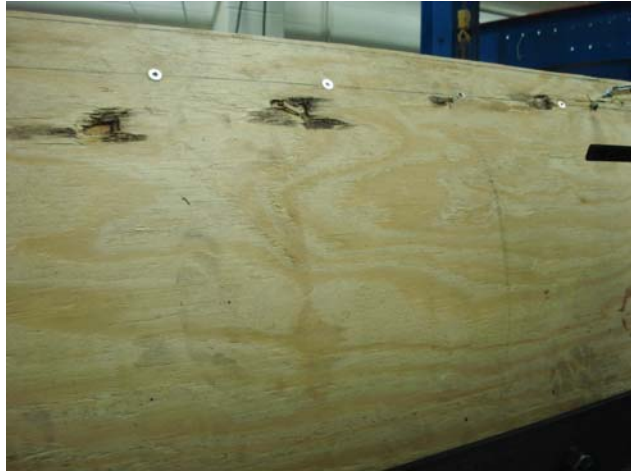
Figure 10.18

Test Date: 3/13/07 Initials: ETD,YG,RHS   *Notes*:
Joist ID: 800S250-54   Initial warp was .25".
Assembly ID: 3-PL-12-10-12-01   2 of 5 screws offset near web with
Sheathing: Plywood, L = 12 in.   no screws over driven.
Fastener: #10 @ 12 in.   No initial cracks observed.
datafile: 3-800S250_54_01
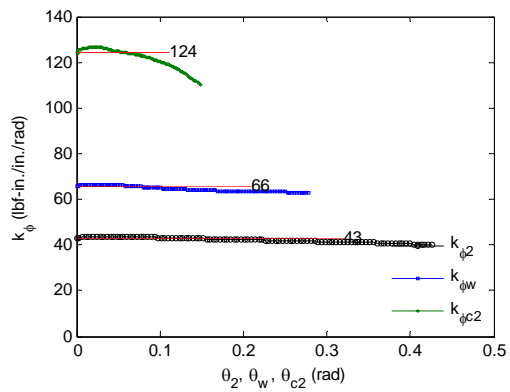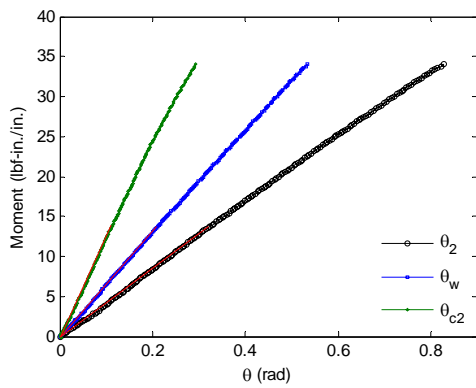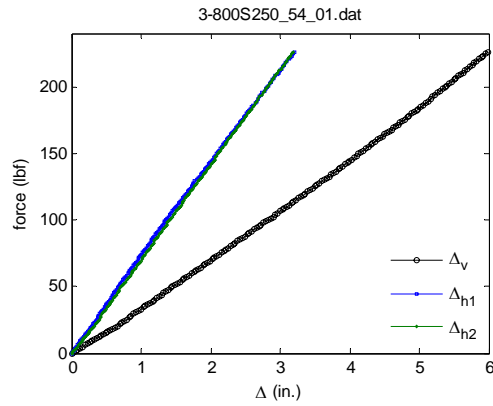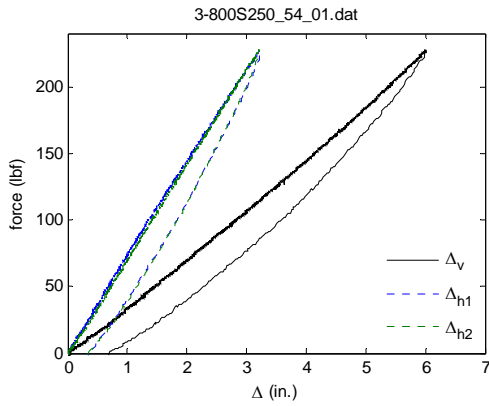
Figure 10.19

Test Date: 3/13/07 Initials: ETD,YG,RHS   *Notes*:
Joist ID: 800S250-54   Initial warp was .25".
Assembly ID: 3-PL-12-6-12-01   3 of 5 screws offset near lip with
Sheathing: Plywood, L = 12 in.   4 of 5 screws over driven.
Fastener: #6 @ 12 inches   Large cracks on tension side of plywood
datafile: 3-800S250_54_02   observed.
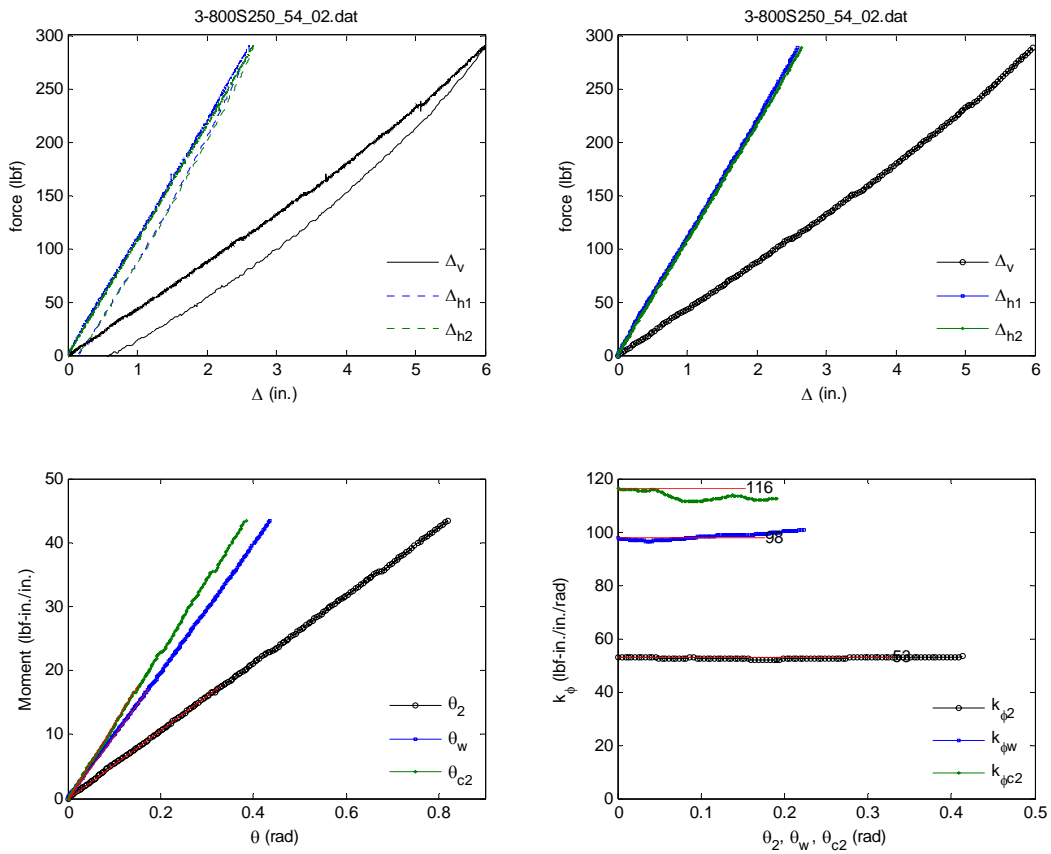
Figure 10.20

Test Date: 3/14/07 Initials: ETD,YG,RHS *Notes*:

Joist ID: 800S200-54   7 of 9 screws offset near lip with

Assembly ID: 4-PL-12-6-6-01   5 of 9 screws over driven.

Sheathing: Plywood, L = 12 in.   No cracks observed.

Fastener: #6 @ 6 in.

datafile: 4-800S200_54_7

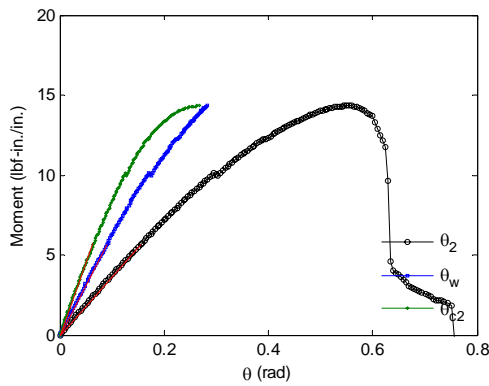

Figure 10.21

Test Date: 3/16/07 Initials: ETD,YG,RHS
Joist ID: 800S200-54
Assembly ID: 4-PL-12-6-6-02
Sheathing: Plywood, L = 12 in.
Fastener: #6 @ 6 in.
datafile: 4-800S200_54_10

Notes: 3 of 9 screws offset near lip and 3 of 9 screws offset near web with 6 of 9 screws over driven. 1/8" crack near base on tension side of plywood and crack on compression side of plywood observed.
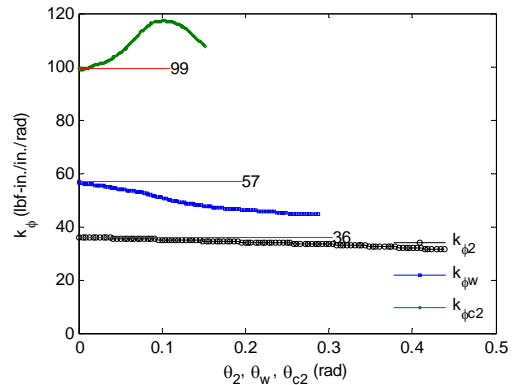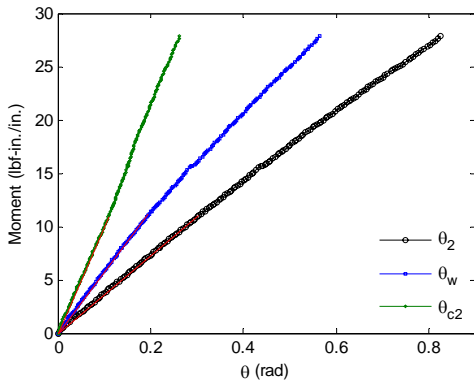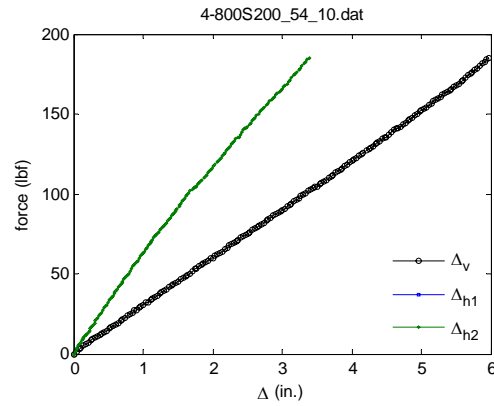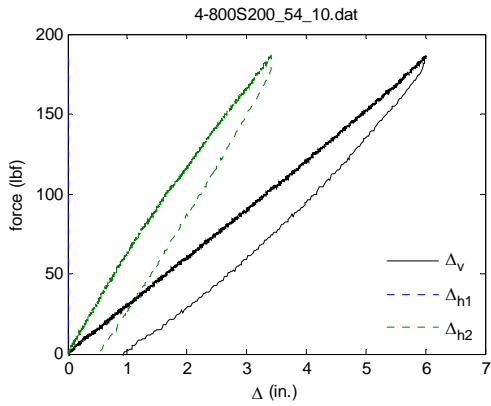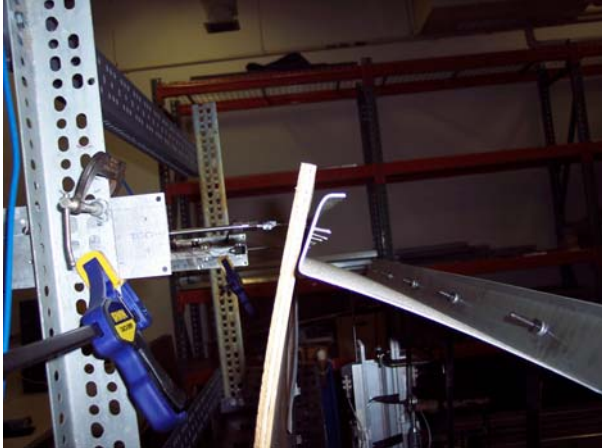
Figure 10.22

Test Date: 3/20/07 Initials: ETD,YG,RHS *Notes*: 5 of 5 screws offset near web with 1 of 5 screws over driven. Large crack on tension side of plywood observed.

Joist ID: 800S200-54

Assembly ID: 3-PL-12-10-12-02

Sheathing: PL
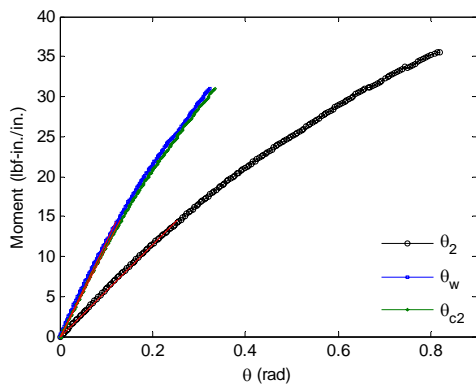
Fastener: #10 Spacing: 12 inches
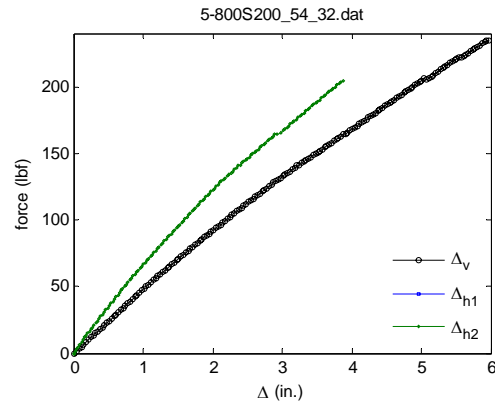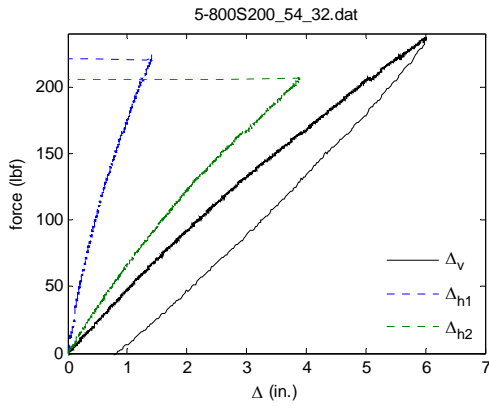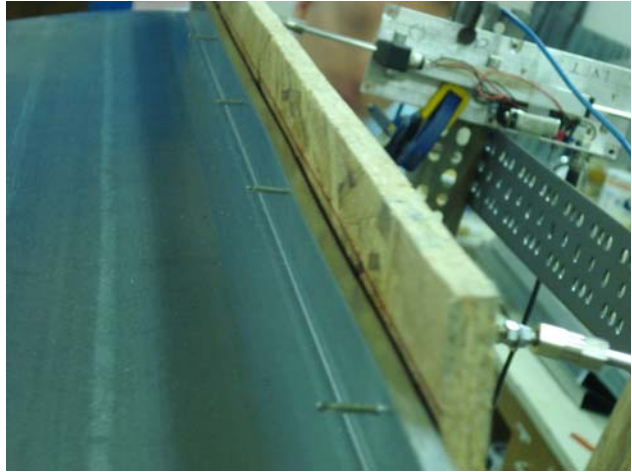
datafile: 3-800S200_54_05
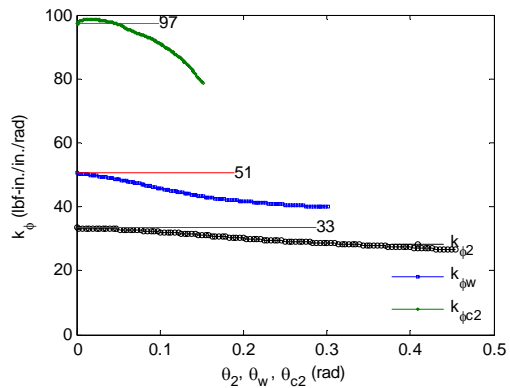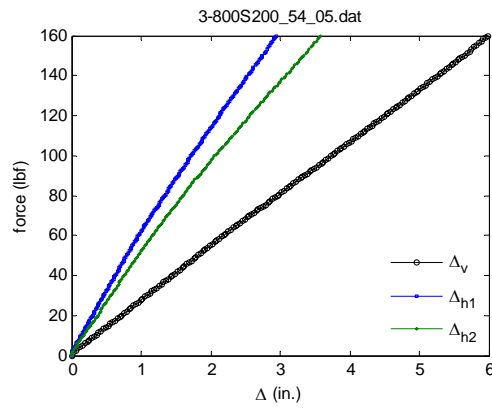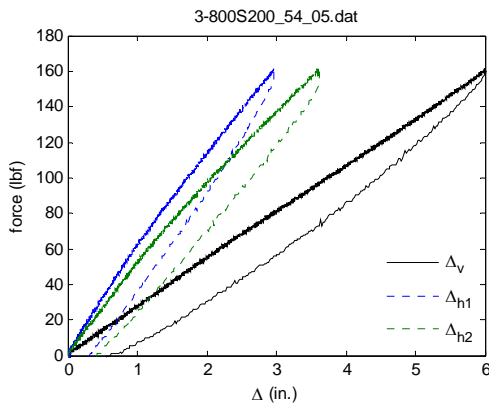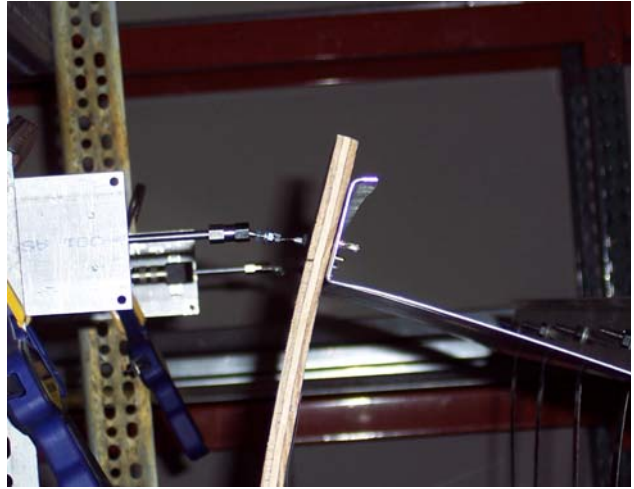
Figure 10.23

Test Date: 3/21/07 Initials: ETD,YG,RHS
Joist ID: 1200S200-97
Assembly ID: 7-PL-12-10-12-01
Sheathing: PL
Fastener: #10 Spacing: 12 inches
datafile: 7-1200S200_97_02

Notes: Initial warp of .125". 2 of 5 screws offset near web with 0 of 5 screws over driven. Large knot in plywood compression side observed
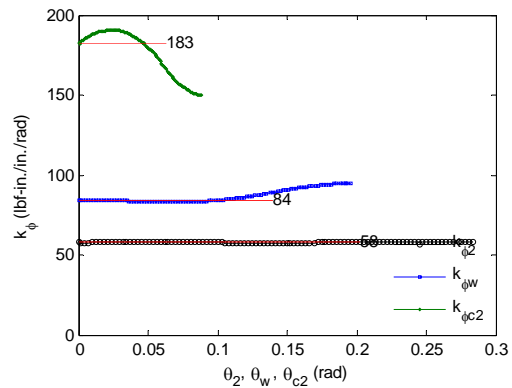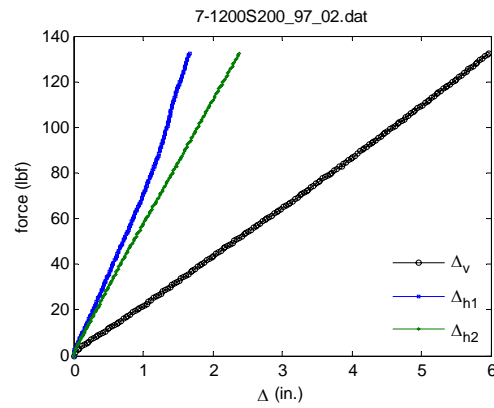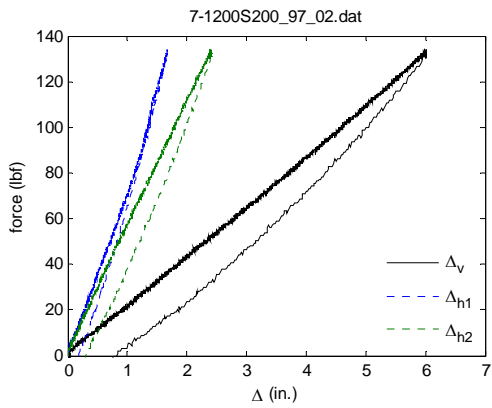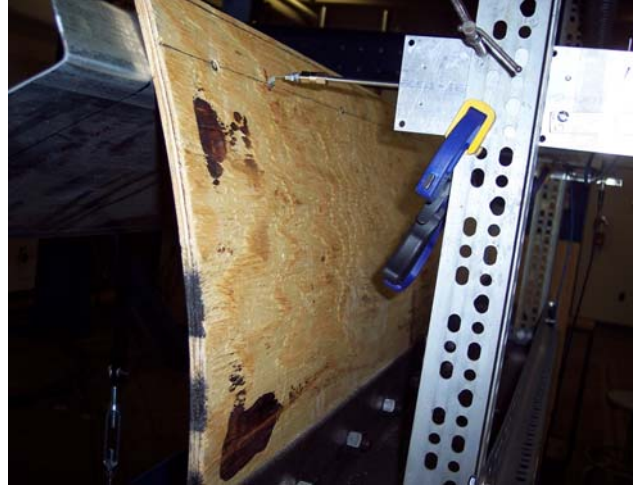
Figure 10.24

Test Date: 3/22/07   Initials: ETD,YG,RHS   *Notes*:
Joist ID: 1200S200-54
Assembly ID: 7-PL-12-6-12-01
Sheathing: PL
Fastener: #6   Spacing: 12 inches
datafile: 7-1200S200_54_01
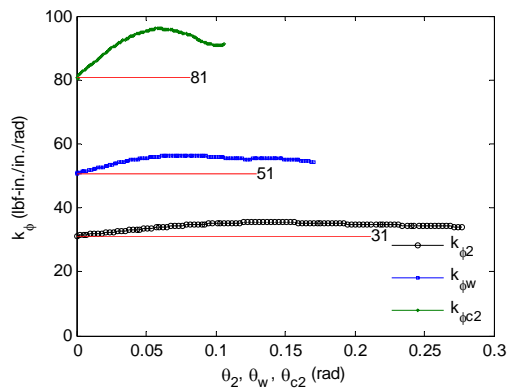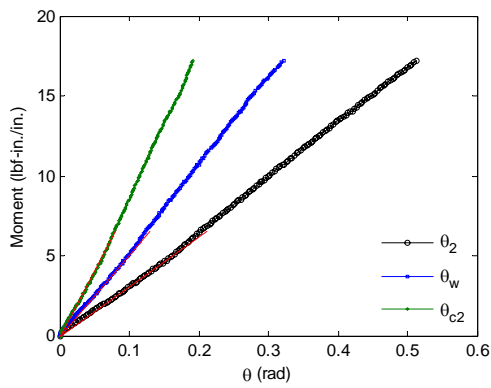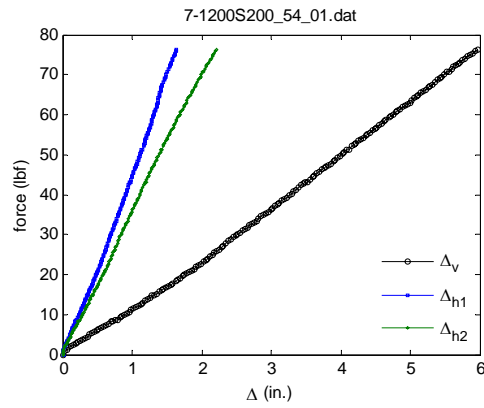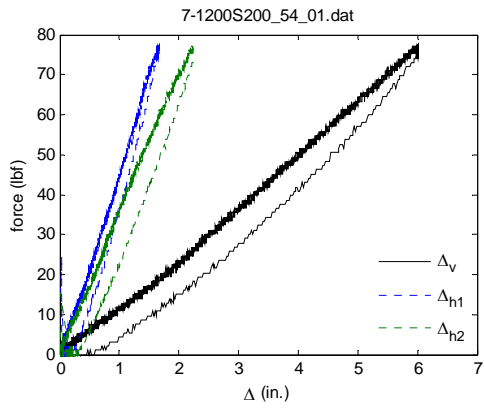
Figure 10.25

Test Date: 3/22/07 Initials: ETD,YG,RHS
Joist ID: 1200S200-54
Assembly ID: 7-PL-12-6-12-02
Sheathing: PL
Fastener: #6 Spacing: 12 inches
datafile: 7-1200S200_54_02

*Notes*: 0" initial warp was measured. 0 of 5 screws offset with 1 of 5 screws over driven. No cracks were observed on the plywood.
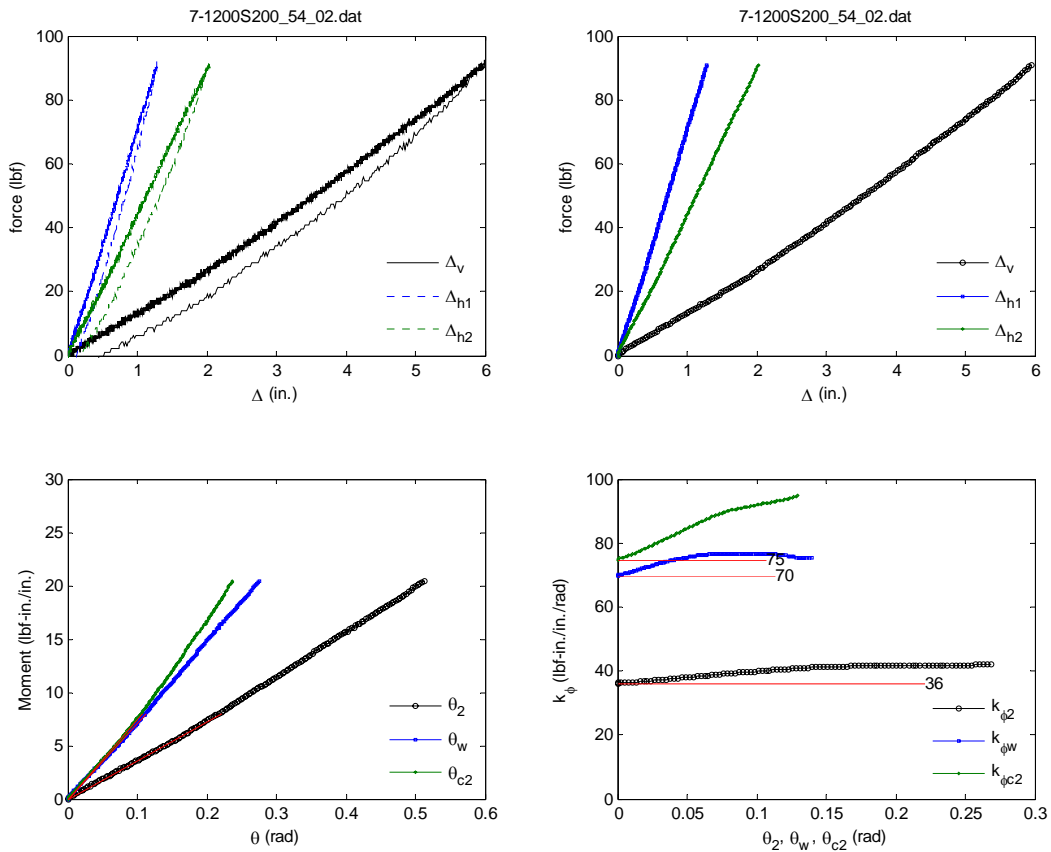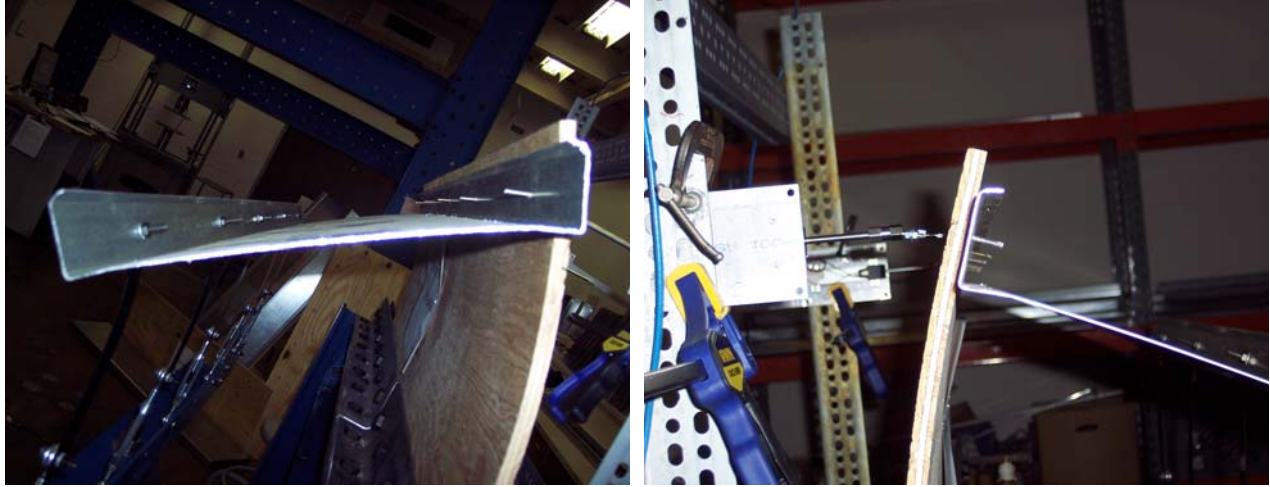
Figure 10.26

Test Date: 3/26/07 Initials: ETD,YG,RHS   *Notes*: Initial warp was 0". 2 of 5 screws offset
Joist ID: 1   near web with 0 of 5 screws over driven.
Assembly ID: 7-PL-12-10-12-02   Cracks less than 6" long on tension side of
Sheathing: PL   plywood observed.
Fastener: #10   Spacing: 12 inches
datafile: 7-1200S200_97_01
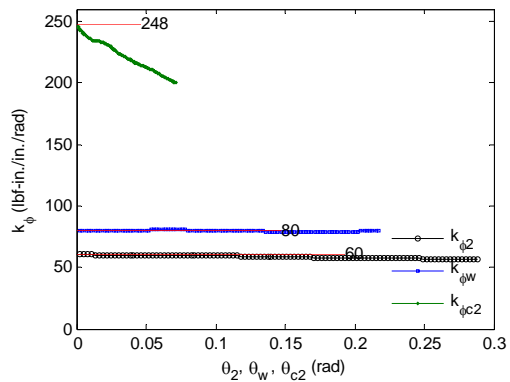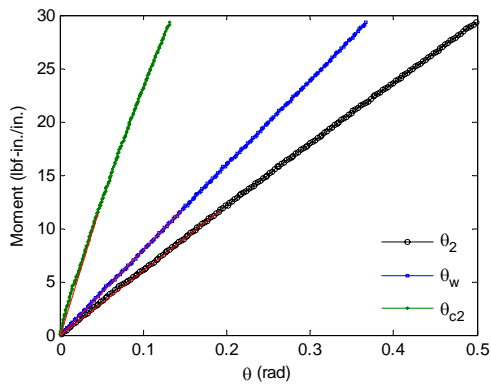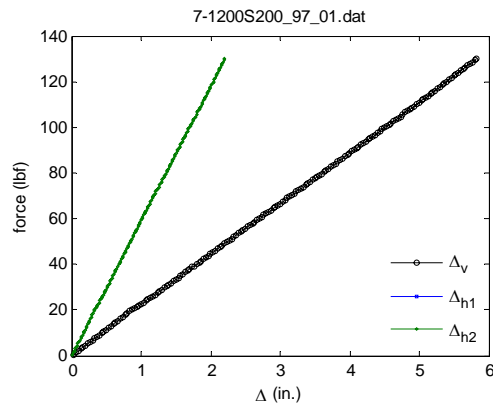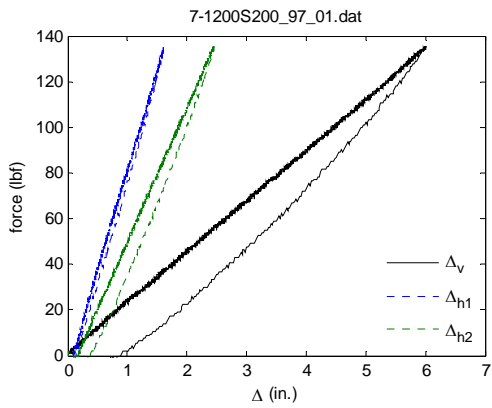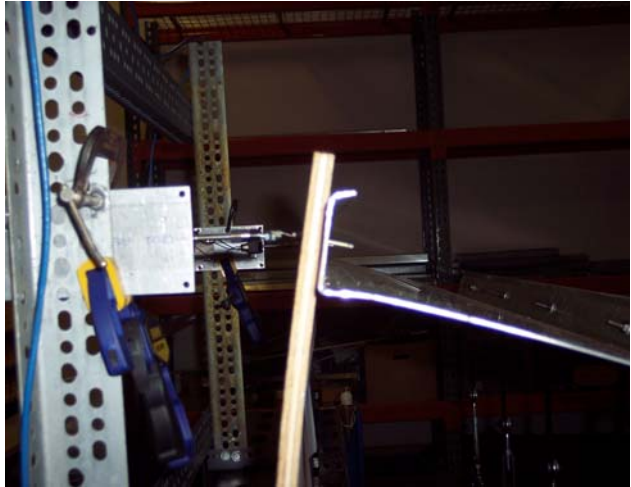
Figure 10.27

Test Date: 3/27/07 Initials: ETD,YG,RHS   *Notes:* 3 of 5 screws offset near lip with 0 of
Joist ID: 1   5 screws over driven. 6" long crack on
Assembly ID: 8-PL-12-6-12-01   tension side of plywood with knot on
Sheathing: PL   compression side observed.
Fastener: #6   Spacing: 12 inches
datafile: 8-362S162_33_01
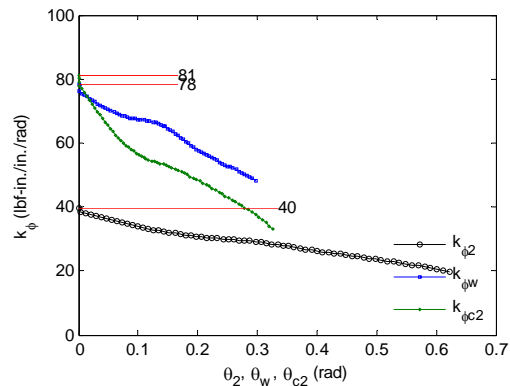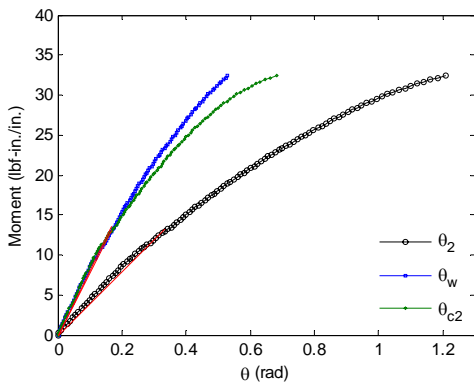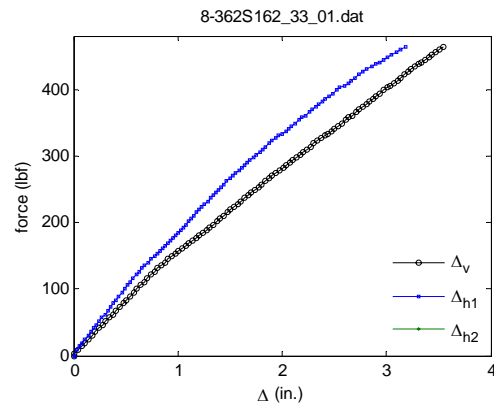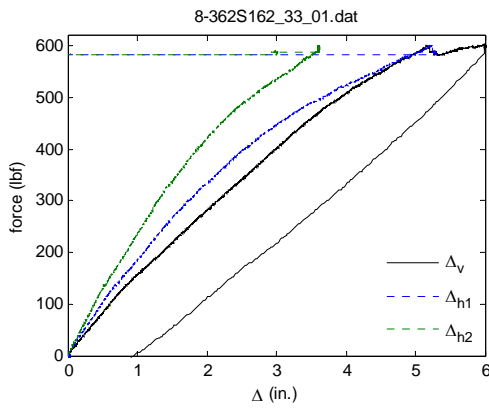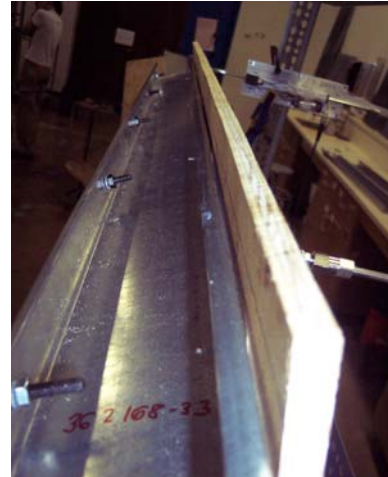
Figure 10.28

Test Date: 3/28/07 Initials: ETD,YG,RHS
Joist ID: 1
Assembly ID: 8-PL-12-6-12-02
Sheathing: PL
Fastener: #6 Spacing: 12 inches
datafile: 8-362S162_68_01

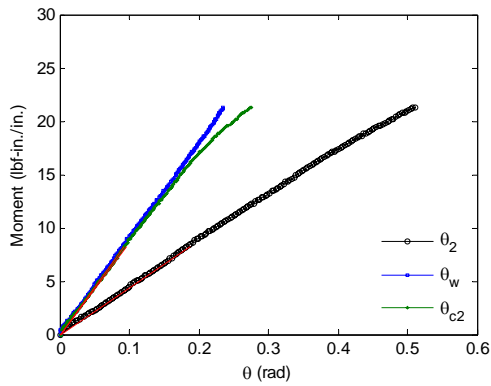*Notes*: Initial warp was .25". 1 of 5 screws offset near lip with 1 of 5 screws over driven. Knots on compression side of plywood observed.
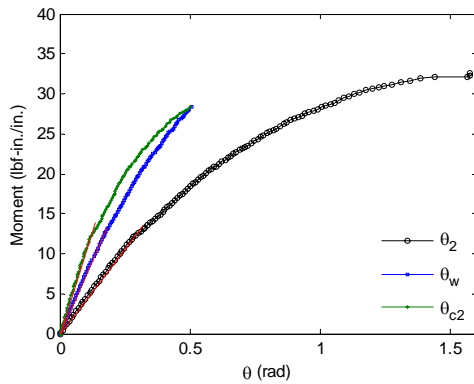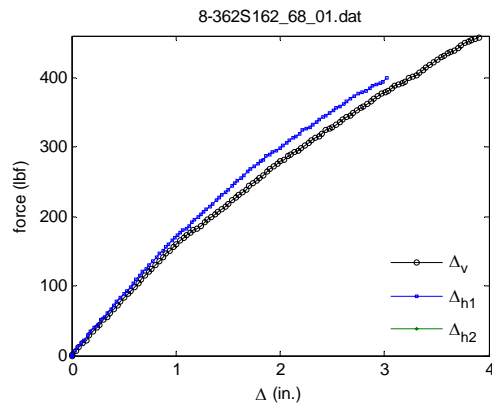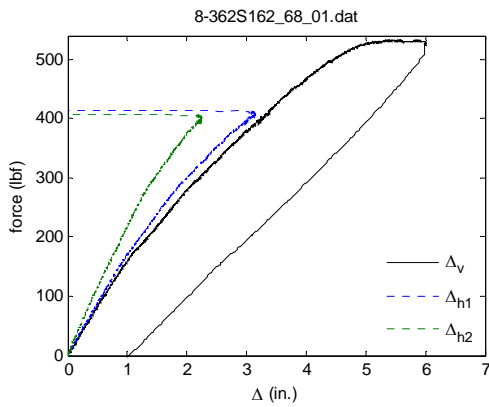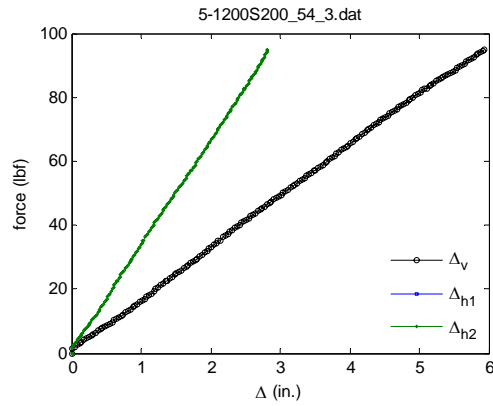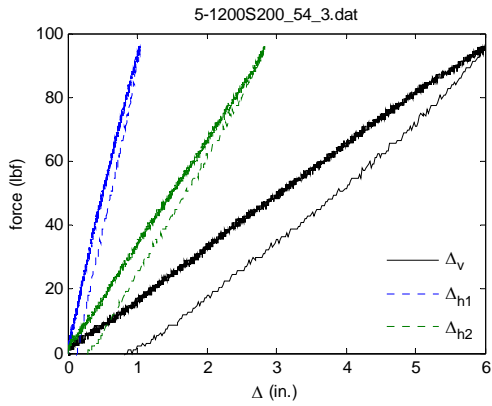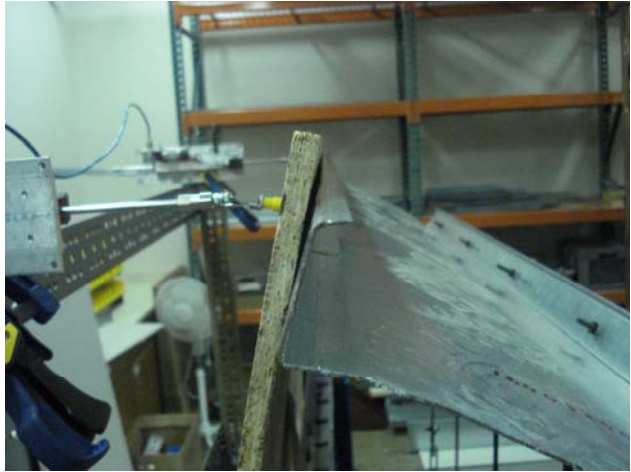

Figure 10.29

Test Date: 4/02/07 Initials: ETD,YG,RHS
Joist ID: #20
Assembly ID: 5-OSB-24-10-12-01
Sheathing: OSB
Fastener: #10   Spacing: 12 inches
datafile: 5-800S200_97_20

Notes: Initial warp was .25". 3 of 5 screws offset near web. All 5 fasteners pulled through wood.
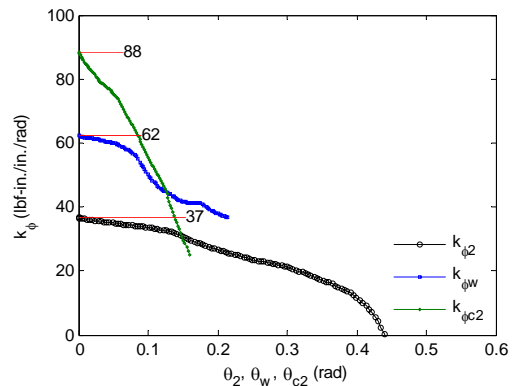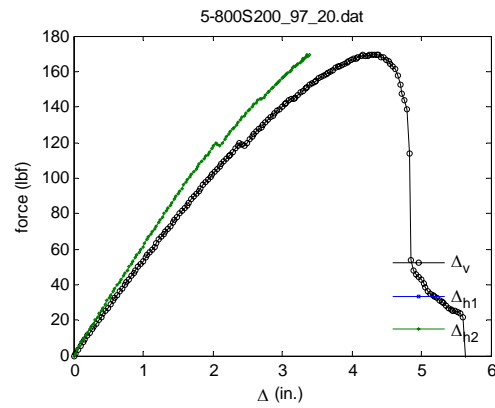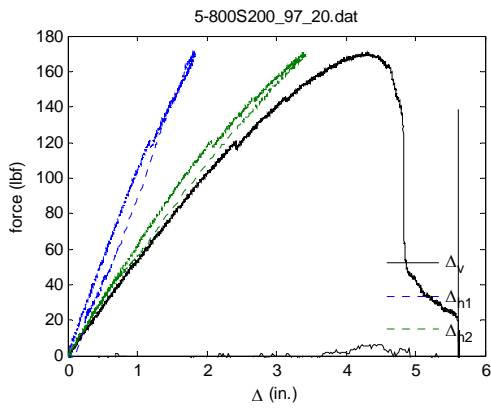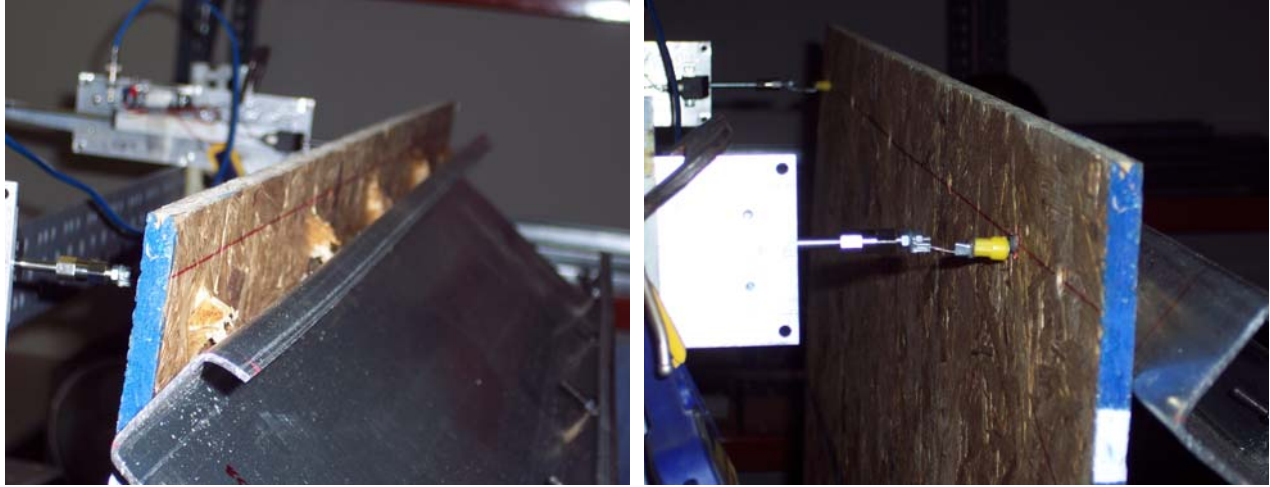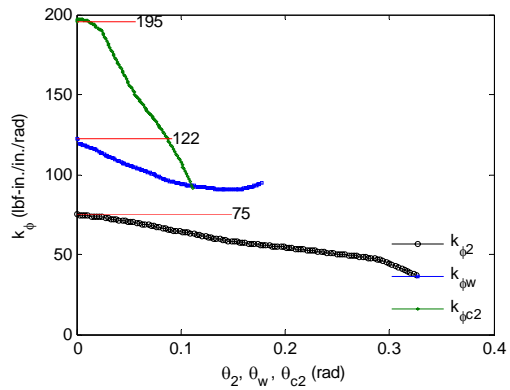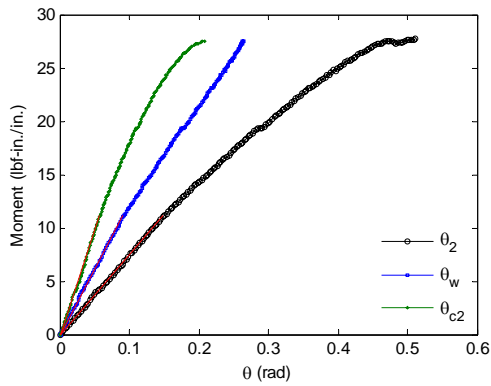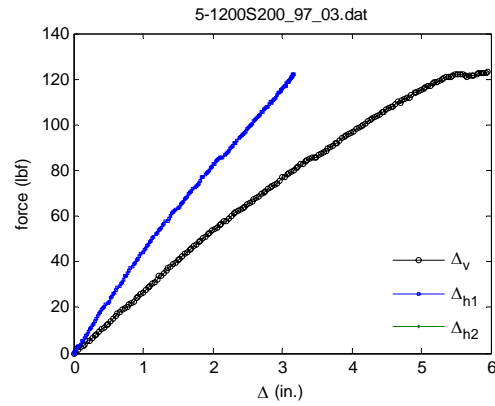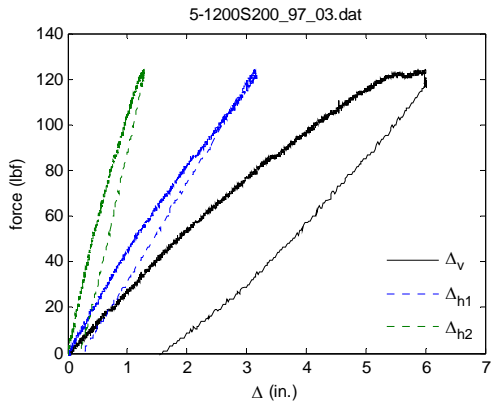

Figure 10.30

Test Date: 4/03/07 Initials: ETD,YG,RHS
Joist ID: 32
Assembly ID: 5-OSB-24-6-12-01
Sheathing: OSB
Fastener: #6 Spacing: 12 inches
datafile: 5-800S200_54_32

Notes: Initial warp was .125". 1 of 5 screws offset near lip with 2 of 5 screws over driven. Web bending along with flange joist separation observed.
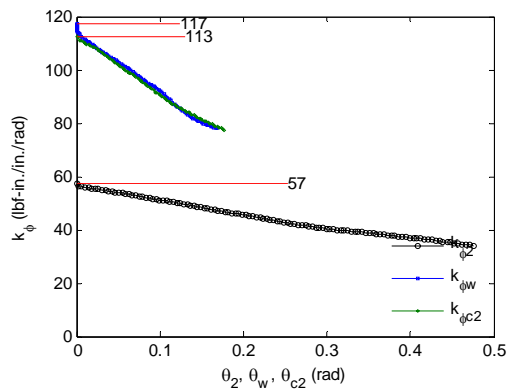
Figure 10.31

Test Date: 4/03/07 Initials: ETD,YG,RHS *Notes*: Initial warp was 0". 5 of 5 screws offset
Joist ID: 31   near web with 0 of 5 screws over driven. 1
Assembly ID: 5-OSB-24-10-12-01   screw observed to pull through.
Sheathing: OSB
Fastener: #6   Spacing: 12 inches
datafile: 5-800S200_54_31
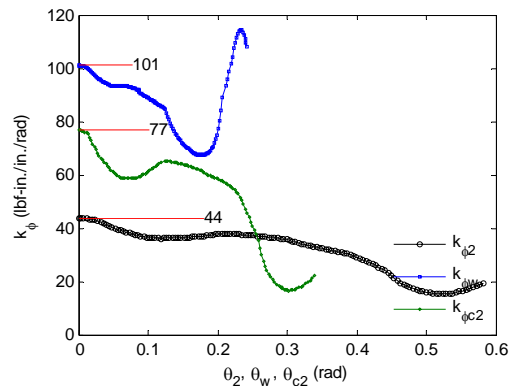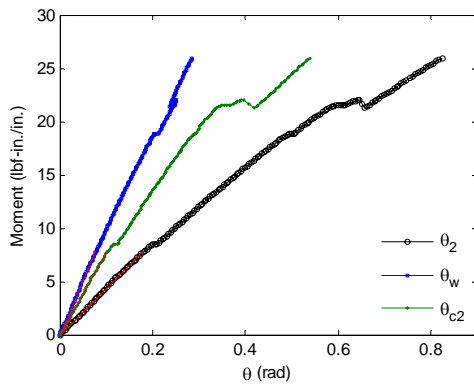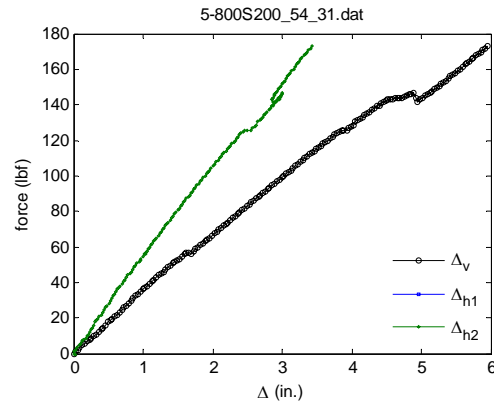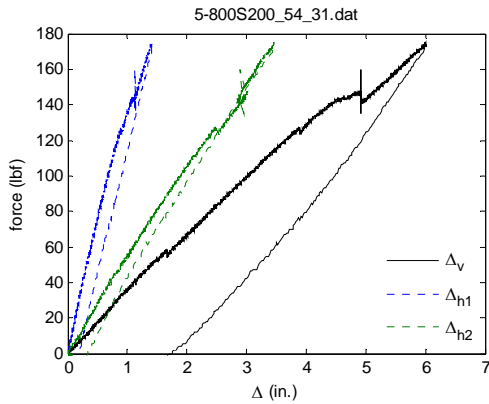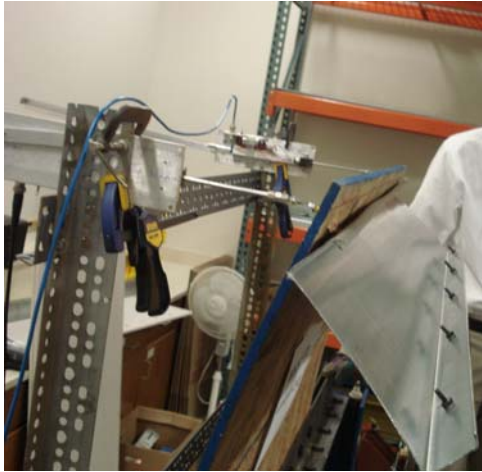
Figure 10.32

Test Date: 4/03/07 Initials: ETD,YG,RHS   *Notes*: Initial warp was 0". 2 of 5 screws offset
Joist ID: 3   near web with 2 of 5 screws over driven.
Assembly ID: 5-OSB-24-6-12-02   Cracks on compression side observed.
Sheathing: OSB
Fastener: #6   Spacing: 12 inches
datafile: 5-1200S200_54_3
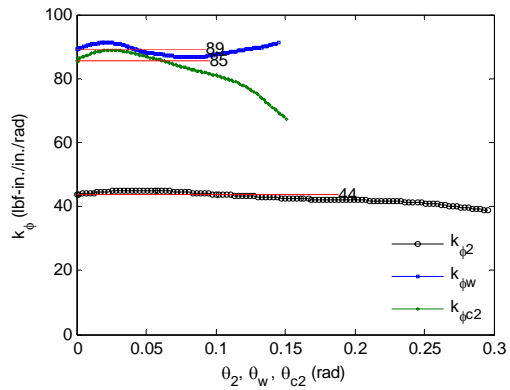
Figure 10.33

Test Date: 4/04/07 Initials: ETD,YG,RHS
Joist ID: 3
Assembly ID: 5-OSB-24-10-12-02
Sheathing: OSB
Fastener: #10 Spacing: 12 inches
datafile: 5-1200S200_97_03

Notes: Initial warp was .25". 1 of 5 screws offset near lip with 2 of 5 screws overdriven. 4 screws were observed to pull inward. Flange joist separation observed also.

Figure 10.34

Test Date: 4/04/07 Initials: ETD,YG,RHS
Joist ID: 21
Assembly ID: 6-GYP-12-10-12-01
Sheathing: GYP
Fastener: #10 Spacing: 12 inches
datafile: 6-800S200_97_21

Notes: Initial warp was 0". 3 of 5 screws offset near lip with 4 of 5 screws overdriven. Cracking was heard with all screws pulled through. Fracture at fastener connections and along top of gypsum board observed.
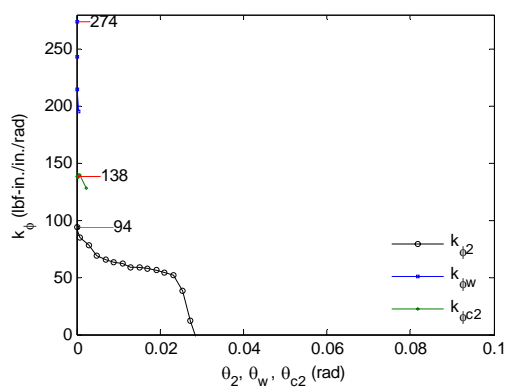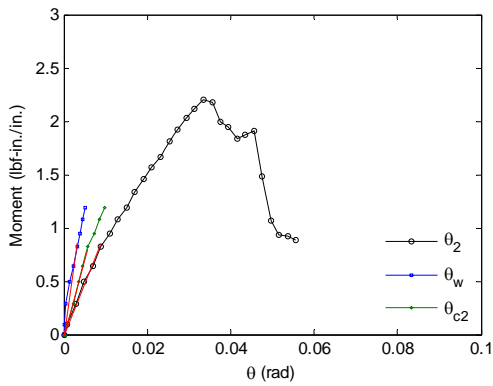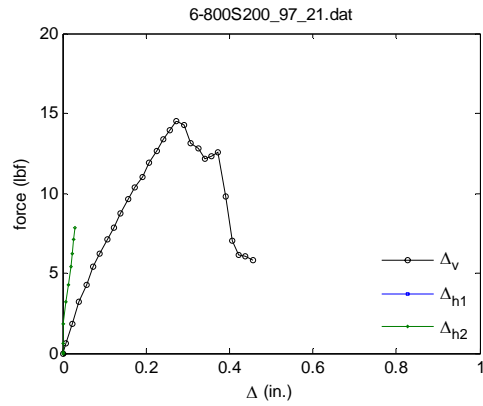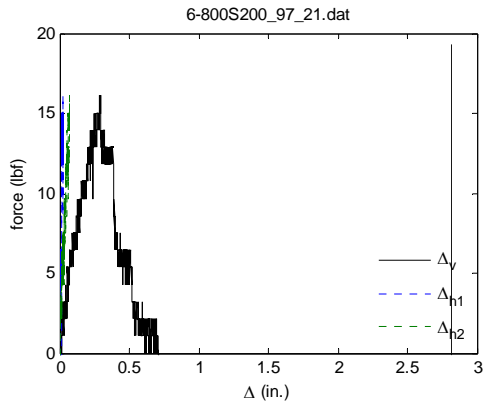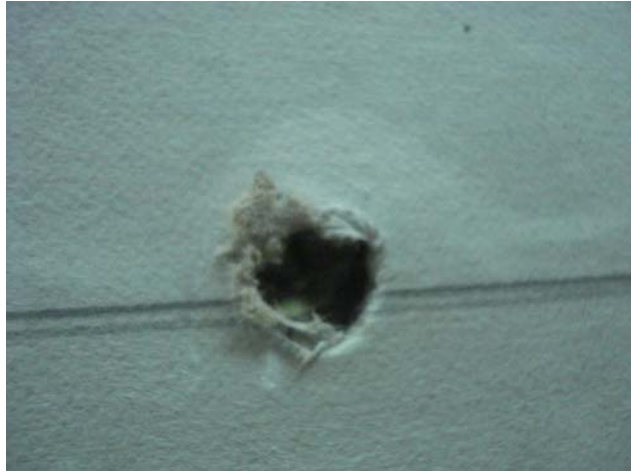

Figure 10.35

Test Date: 4/05/07 Initials: ETD,YG,RHS
Joist ID: 2
Assembly ID: 8-GYP-12-6-12-01
Sheathing: GYP
Fastener: #6 Spacing: 12 inches
datafile: 8-362S162_33_02

Notes: Initial warp was 0". 2 of 5 screws offset near lip with 1 of 5 screws overdriven. Fracture at fastener connections and along top of gypsum board observed.
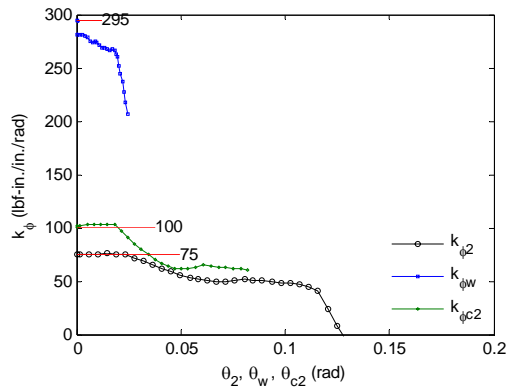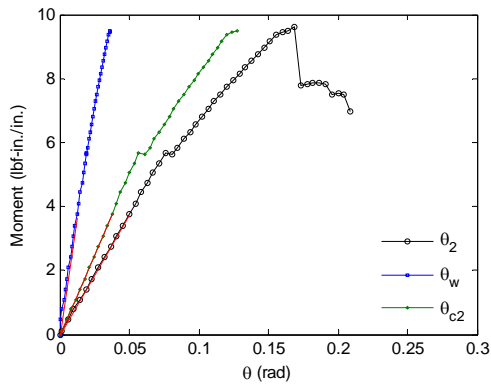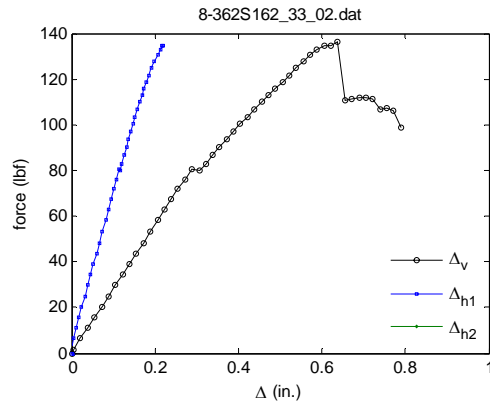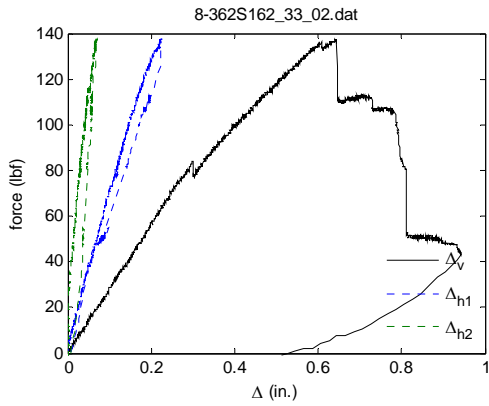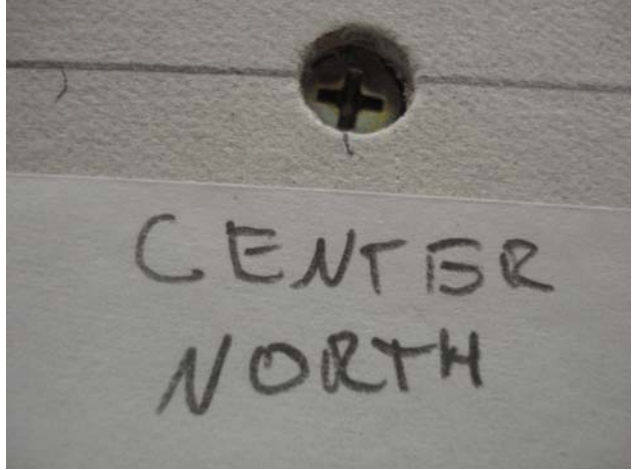

Figure 10.36

Test Date: 4/05/07 Initials: ETD,YG,RHS
Joist ID: 16
Assembly ID: 8-GYP-12-10-12-01
Sheathing: GYP
Fastener: #10   Spacing: 12 nches
datafile: 8-800S200_97_16

Notes: Initial warp was 0". 0 of 5 screws offset with 2 of 5 screws overdriven. Fracture at fastener connections and along top of gypsum board observed.

Figure 10.37

Test Date: 4/05/07 Initials: ETD,YG,RHS

Notes: Initial warp was 0". 0 of 5 screws offset with 1 of 5 screws overdriven. Fracture at fastener connections and along top of gypsum board observed.

Joist ID: 2
Assembly ID: 8-GYP-12-6-12-02
Sheathing: GYP
Fastener: #6 Spacing: 12 nches
datafile: 8-362S162_68_02

Figure 10.38

Test Date: 4/05/07 Initials: ETD,YG,RHS

Joist ID: 30

Assembly ID: 6-GYP-12-6-12-01

Sheathing: GYP

Fastener: #6 Spacing:12 inches

datafile: 6-800S200_54_30

Notes: Initial warp was 0". 4 of 5 screws offset near web with 0 of 5 screws over driven. Fracture at fastener connections and along top of gypsum board observed.

Figure 10.39

Test Date: 4/06/07 Initials: ETD,YG,RHS
Joist ID: 34
Assembly ID: 6-GYP-12-10-12-01
Sheathing: GYP
Fastener: #10   Spacing: 12 inches
datafile: 6-800S200_54_34

Notes: Initial warp was 0". 0 of 5 screws offset with 1 of 5 screws over driven. Fracture at fastener connections and along top of gypsum board observed.
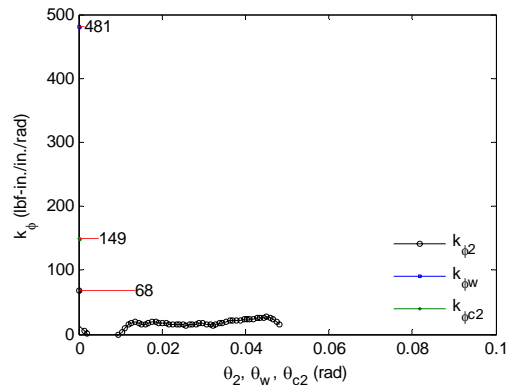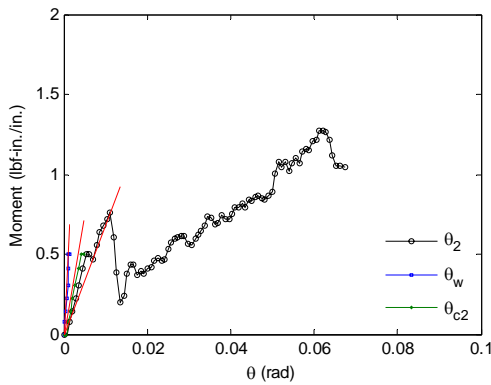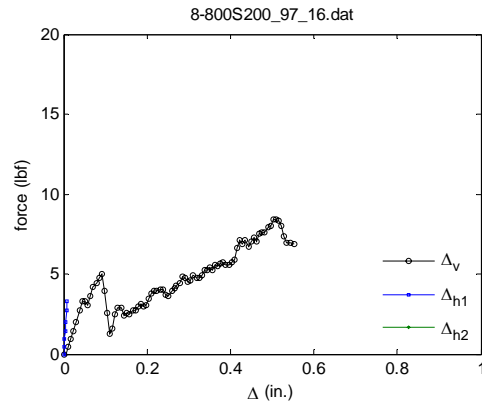

Figure 10.40

Test Date: 4/06/07 Initials: ETD,YG,RHS
Joist ID: 33
Assembly ID: 6-GYP-24-10-12-01
Sheathing: GYP
Fastener: #10 Spacing: 12 inches
datafile: 6-800S200_54_33

Notes: Initial warp was 0". 1 of 5 screws offset near lip and 4 of 5 screws offset near web with 1 of 5 screws over driven. Fracture at fastener connections and along top of gypsum board observed.
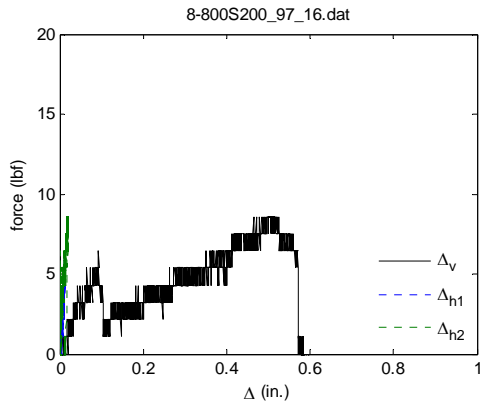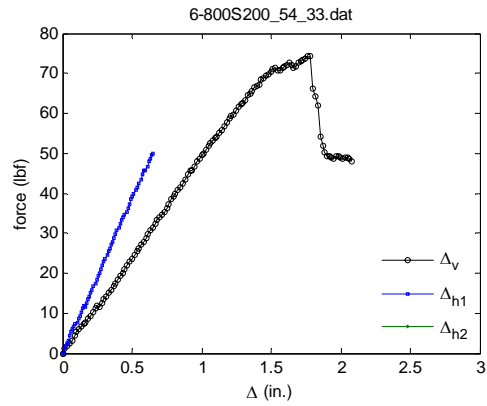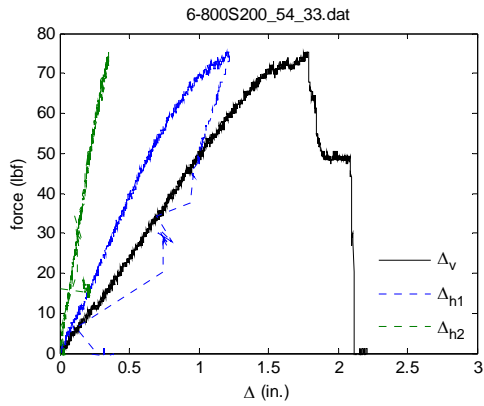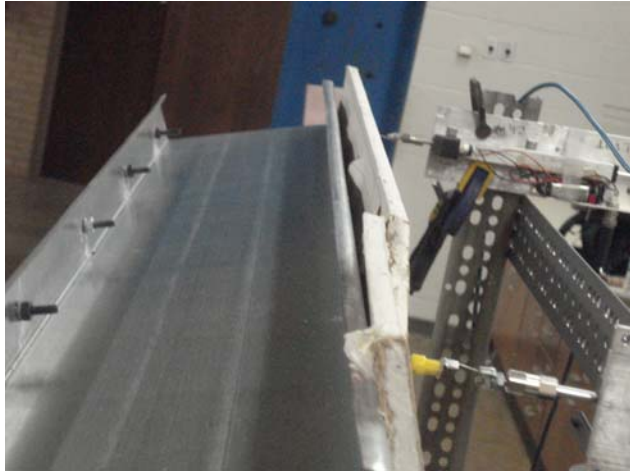

Figure 10.41

Test Date: 4/06/07 Initials: ETD,YG,RHS

Joist ID: 35

Assembly ID: 6-GYP-24-6-12-01

Sheathing: GYP

Fastener: #6 Spacing: 12 inches

datafile: 6-800S200_54_35

Notes: Initial warp was 0". 0 of 5 screws offset with 0 of 5 screws over driven. Fracture at fastener connections and along top of gypsum board observed.
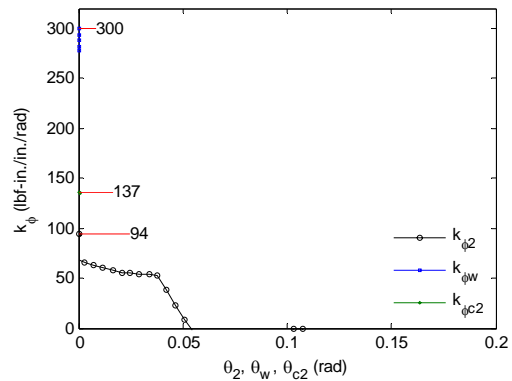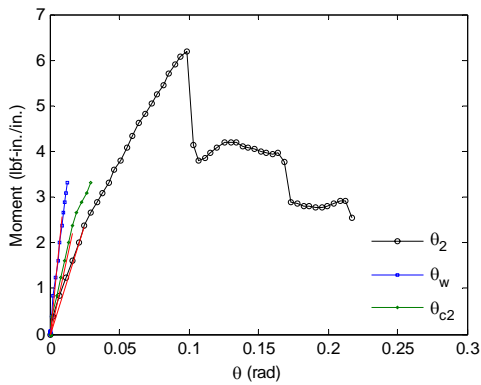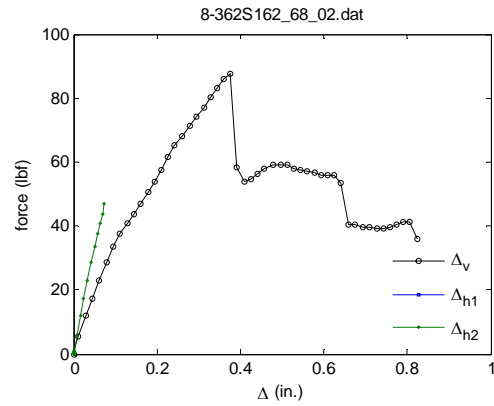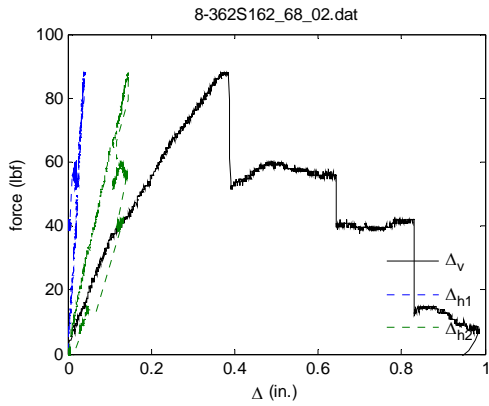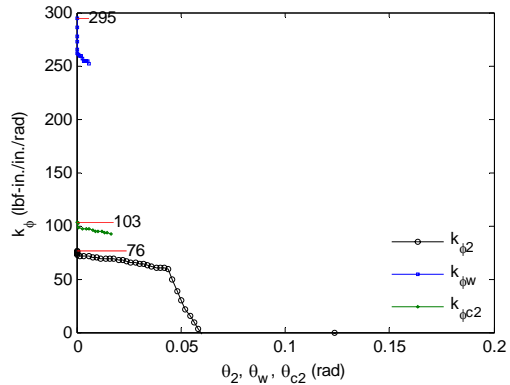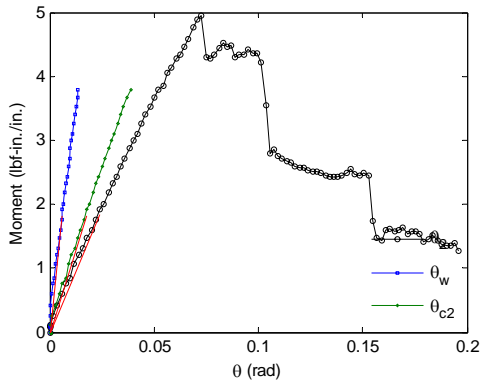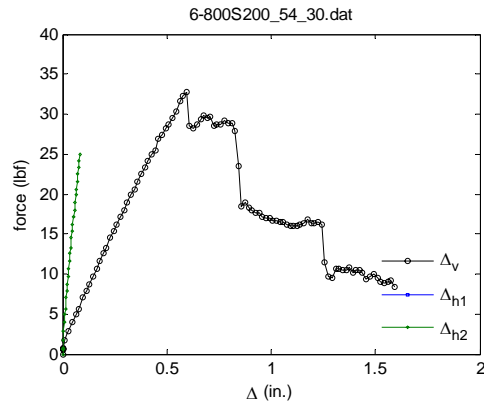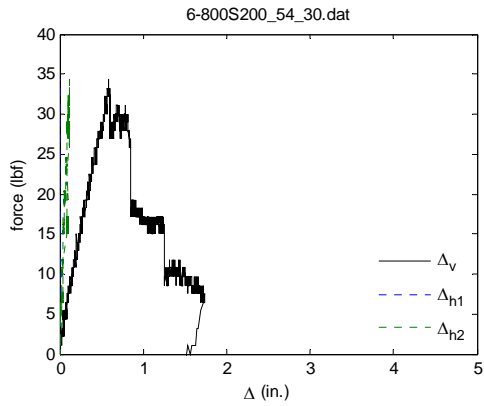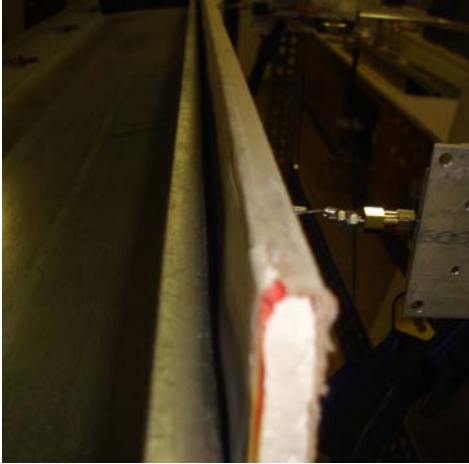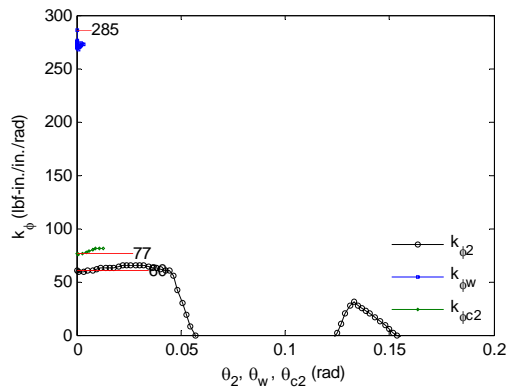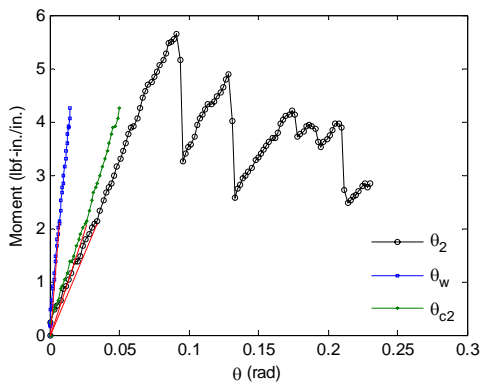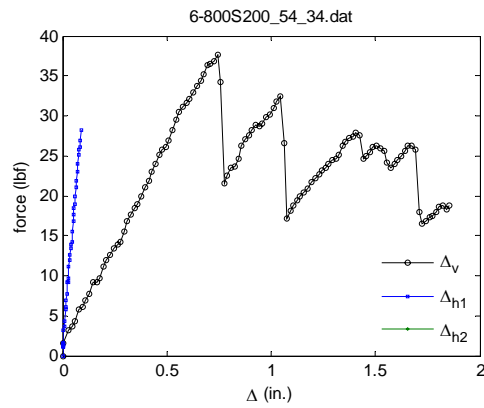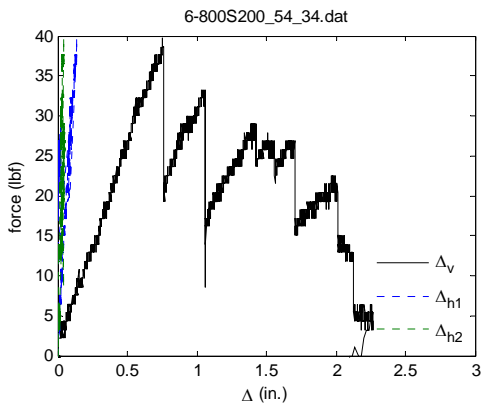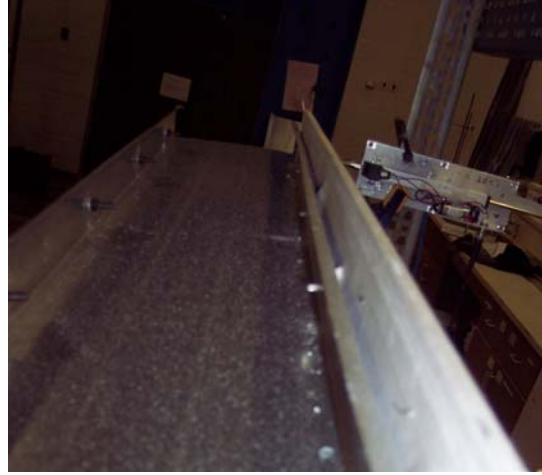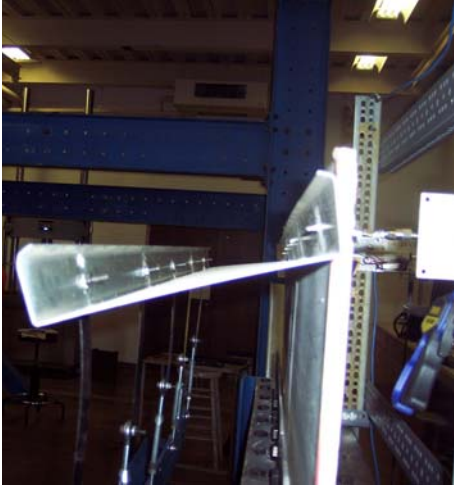

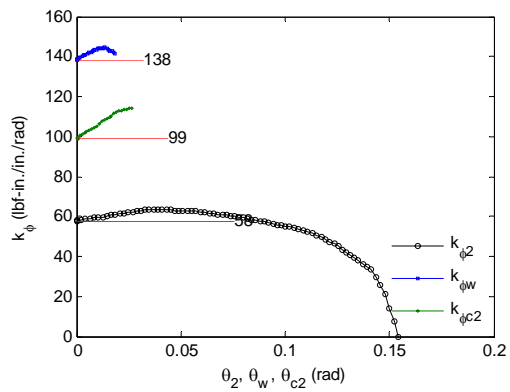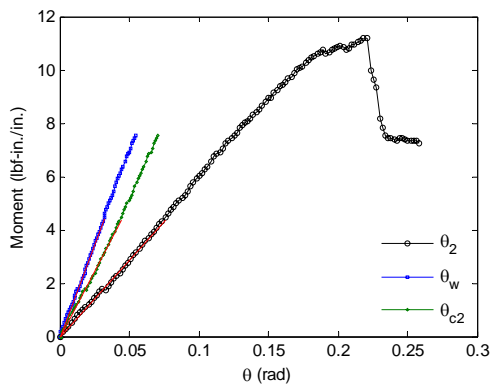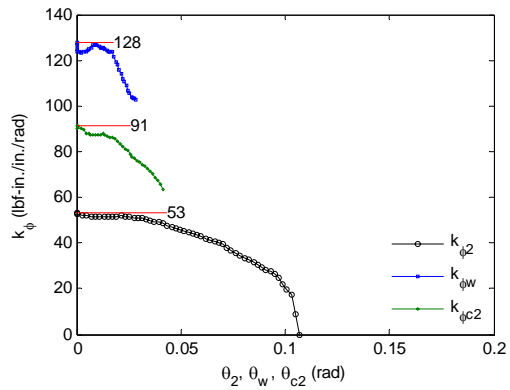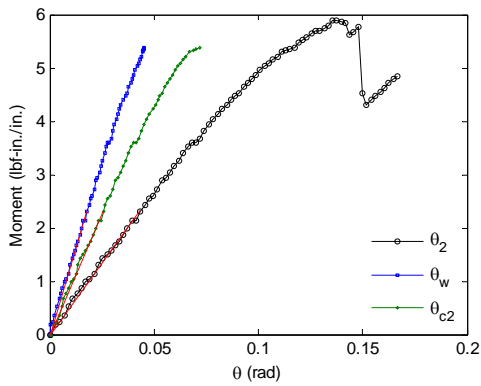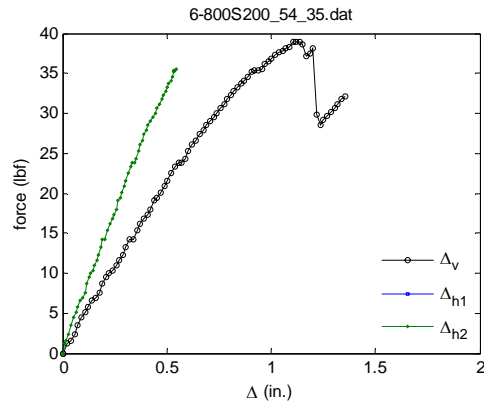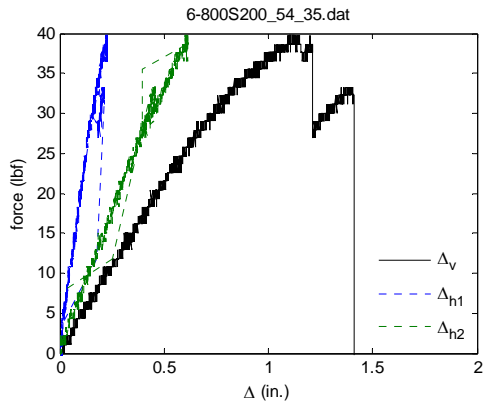Figure 10.42

11   DESIGN EXAMPLE: DISTORTIONAL BUCKLING INCLUDING k_ϕ

Section 11

Example Calculation for Distortional Buckling of Beams via AISI C3.1.6

A distortional buckling (DB) check was added to the *North American Specification for the Design of Cold-Formed Steel Structural Members*, herein referred to as the *Specification*. The DB check was approved as Ballot CS04-227B in 2005 and added a new section C3.1.6 to the *Specification*.

Given: SSMA section and a bracing stiffness

Required: Nominal capacity in distortional buckling per C3.1.6

Comment: At the conclusion of this example the calculated capacity is compared against the local buckling and lateral-torsional capacity to consider if the DB provisions of C3.1.6 control the design.

Dimensions:

section name:	$\text{name} := \text{"600S162-54 (50ksi)"}$
out-to-out web depth:	$h_o := 6 \cdot in$
out-to-out flange width:	$b_o := 1.625 \cdot in$
out-to-out lip length:	$D := 0.50 \cdot in$
inside radius:	$r_i := 0.0849$
design thickness:	$t := 0.0566 \cdot in$
section modulus (S_{xx})	$S_f := 0.953 \cdot in^3$

Material properties:

yield stress:	$f_y := 50 \cdot ksi$
elastic modulus:	$E := 29500 \cdot ksi$
Poisson's ratio:	$\nu := 0.3$
shear modulus:	$G := \dfrac{E}{2 \cdot (1 + \nu)}$

Bracing:

rotational restraint $k_\phi := 0.5 \cdot \dfrac{kip \cdot in}{rad \cdot in}$

This will need to be updated to reflect results herein and method of findi... k_ϕ from $k_{\phi w}$ and $k_{\phi c}$.

Determination of M_n for distortional buckling per C3.1.6

The nominal strength in the distortional buckling limit state in Specification C3.1.6 follows the same expressions as the Direct Strength Method found in Appendix 1 of the Specification Eq. 1.2.2-8 through 1.2.2-10. See the Appendix 1 commentary for further discussion. Following the notation of Specification C3.1.6 Mn is found via:

$$M_{nd} := \begin{cases} M_y & \text{if } \lambda_d \le 0.673 \\ \left[1 - 0.22 \cdot \left(\dfrac{M_{crd}}{M_y} \right)^{0.5} \right] \left(\dfrac{M_{crd}}{M_y} \right)^{0.5} \cdot M_y & \text{if } \lambda_d > 0.673 \end{cases}$$

(Eq. C3.1.6-1)
(Eq. C3.1.6-2)

where $\lambda_d := \sqrt{\dfrac{M_y}{M_{crd}}}$ (Eq. C3.1.6-3)

and M_y is the yield moment and M_{crd} is the elastic distortional buckling moment.

M_{crd} is the gross section modulus times the elastic distortional buckling stress, F_d, and C3.1.6 provides 3 methods for finding F_d: C3.1.6(a), (b), and (c). C3.1.6(a) is a conservative approximation that does not account for bracing, C3.1.6(c) employs rational elastic buckling analysis such as finite strip, this is the preferred approach, but is numerical in nature so explicit expressions cannot be provided, C3.1.6(b) provides a lengthy hand calculation but includes the influence of bracing in the solution and is thus illustrated here.

Determination of elastic distortional buckling stress, Fd, per C3.1.6(b)

The distortional buckling stress is found via

$$F_d := \beta \, \frac{k_{\phi fe} + k_{\phi we} + k_\phi}{k_{\phi fg} + k_{\phi wg}} \qquad\qquad (C3.1.6\text{-}10)$$

These stiffness terms "k" represent the elastic (subscript 'e') and geometric (g) rotational stiffness of the flange (f) and web (w) as described in C4.7. Calculation of these terms is rather involved. However, Table C-C3.1.6(b)-1 in the C3.1.6 commentary for DB of beams gives canned expressions for all of the variables if the section is a lipped channel or lipped zed - so it is not as bad as the following pages of expressions might indicate. β accounts for moment gradient.

Using Table C-C3.16(b) the properties of the flange are calculated, the table uses centerline dimensions for the flange

centerline flange dimensions: $b := b_o - t$ $d := D - \dfrac{t}{2}$ also note $\theta := \dfrac{\pi}{2}$ (lip angle)

Properties of the Flange Only:
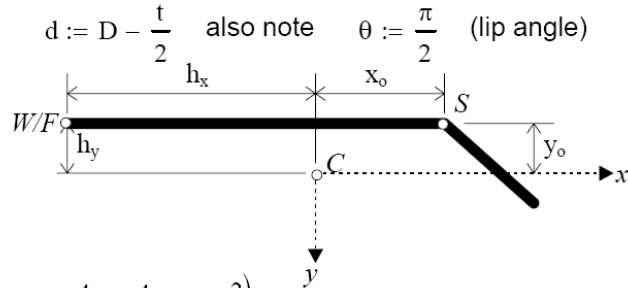
$A_f := (b + d)\cdot t$ $\qquad A_f = 0.115 \text{ in}^2$

$J_f := \dfrac{1}{3}\cdot b\cdot t^3 + \dfrac{1}{3}\cdot d\cdot t^3$ $\quad J_f = 1.233 \times 10^{-4} \text{ in}^4$

$I_{xf} := \dfrac{t\cdot\left(t^2\cdot b^2 + 4\cdot b\cdot d^3 - 4\cdot b\cdot d^3\cdot\cos(\theta)^2 + t^2\cdot b\cdot d + d^4 - d^4\cdot\cos(\theta)^2\right)}{12\cdot(b + d)}$ $\qquad I_{xf} = 1.66 \times 10^{-3} \text{ in}^4$

$I_{yf} := \dfrac{t\cdot\left(b^4 + 4\cdot d\cdot b^3 + 6\cdot d^2\cdot b^2\cdot\cos(\theta) + 4\cdot d^3\cdot b\cdot\cos(\theta)^2 + d^4\cdot\cos(\theta)^2\right)}{12\cdot(b + d)}$ $\qquad I_{yf} = 0.031 \text{ in}^4$

$I_{xyf} := \dfrac{t\cdot b\cdot d^2\cdot\sin(\theta)\cdot(b + d\cdot\cos(\theta))}{4\cdot(b + d)}$ $\qquad I_{xyf} = 3.796 \times 10^{-3} \text{ in}^4$

$I_{of} := \dfrac{t\cdot b^3}{3} + \dfrac{b\cdot t^3}{12} + \dfrac{t\cdot d^3}{3}$ $\qquad I_{of} = 0.075 \text{ in}^4$

$x_{of} := \dfrac{b^2 - d^2\cdot\cos(\theta)}{2\cdot(b + d)}$ x distance from the centroid to the shear center. $\qquad x_{of} = 0.603 \text{ in}$

$y_{of} := \dfrac{-d^2\cdot\sin(\theta)}{2\cdot(b + d)}$ y distance from the centroid to the shear center. $\qquad y_{of} = -0.055 \text{ in}$

$h_{xf} := \dfrac{-\left(b^2 + 2\cdot d\cdot b + d^2\cdot\cos(\theta)\right)}{2(b + d)}$ x distance from the centroid to the web/flange juncture. $\qquad h_{xf} = -0.966 \text{ in}$

$h_{yf} := \dfrac{-d^2\cdot\sin(\theta)}{2\cdot(b + d)}$ y distance from the centroid to the web/flange juncture. $\qquad h_{yf} = -0.055 \text{ in}$

$C_{wf} := 0\cdot\text{in}^6$ $\qquad C_{wf} = 0 \text{ in}^6$

Determination of elastic distortional buckling stress, Fd, per C3.1.6(b) (CONTINUED)

in the following expressions the web dimension h is the out-to-out dimension: $h := h_o$

Determine the critical half-wavelength at which distortional buckling occurs per C3.1.6-16:

$$L_{cr} := \left[\frac{4 \cdot \pi^4 \cdot h \cdot \left(1 - \nu^2\right)}{t^3} \cdot \left[I_{xf} \cdot \left(x_{of} - h_{xf}\right)^2 + C_{wf} - \frac{I_{xyf}^2}{I_{yf}} \cdot \left(x_{of} - h_{xf}\right)^2 \right] + \frac{\pi^4 \cdot h^4}{720} \right]^{0.25} \quad {}_{[} = 13.639 \, in$$

Determine the elastic and "geometric" rotational spring stiffness of the flange per C3.1.6-11,12:

$$k_{\phi fe} := \left(\frac{\pi}{L_{cr}} \right)^4 \cdot \left[E \cdot I_{xf} \cdot \left(x_{of} - h_{xf}\right)^2 + E \cdot C_{wf} - E \cdot \frac{I_{xyf}^2}{I_{yf}} \cdot \left(x_{of} - h_{xf}\right)^2 \right] + \left(\frac{\pi}{L_{cr}} \right)^2 \cdot G \cdot J_f$$

$k_{\phi fe} = 0.318 \, kip$

$$k_{\phi fg} := \left(\frac{\pi}{L_{cr}} \right)^2 \cdot \left[A_f \left[\left(x_{of} - h_{xf}\right)^2 \cdot \left(\frac{I_{xyf}}{I_{yf}} \right)^2 - 2 \cdot y_{of} \cdot \left(x_{of} - h_{xf}\right) \cdot \left(\frac{I_{xyf}}{I_{yf}} \right) + h_{xf}^2 + y_{of}^2 \right] + I_{xf} + I_{yf} \right]$$

$k_{\phi fg} = 7.811 \times 10^{-3} \, in^2$

Determine the elastic and "geometric" rotational spring stiffness of the web per C3.1.6-13,14:

$$k_{\phi we} := \frac{E \cdot t^3}{12 \cdot \left(1 - \nu^2\right)} \cdot \left[\frac{3}{h} + \left(\frac{\pi}{L_{cr}} \right)^2 \cdot \frac{19 \cdot h}{60} + \left(\frac{\pi}{L_{cr}} \right)^4 \cdot \frac{h^3}{240} \right] \qquad k_{\phi we} = 0.296 \, kip$$

per definitions in C3.1.6(b) the stress gradient in the web term $\xi_{web} := 2$

$$k_{\phi wg} := \frac{h \cdot t \cdot \pi^2}{13440} \cdot \frac{\left[45360 \cdot \left(1 - \xi_{web}\right) + 62160\right] \cdot \left(\frac{L_{cr}}{h} \right)^2 + 448 \cdot \pi^2 + \left(\frac{h}{L_{cr}} \right)^2 \cdot \left[53 + 3 \cdot \left(1 - \xi_{web}\right)\right] \cdot \pi^4}{\pi^4 + 28 \cdot \pi^2 \cdot \left(\frac{L_{cr}}{h} \right)^2 + 420 \cdot \left(\frac{L_{cr}}{h} \right)^4}$$

$k_{\phi wg} = 1.804 \times 10^{-3} \, in^2$

Moment gradient term, β, is conservatively taken as 1.0 $\beta := 1$

Typically the moment gradient term has a smaller influence than the rotational restraint (k_ϕ) on the buckling stress F$_d$, further, the moment gradient must occur in relatively short length (near L$_{cr}$) to have a substantial influence, therefore Eq. C3.1.6-15, β, is set to 1.0.

Determine the distortional buckling stress:

$$F_d := \beta \frac{k_{\phi fe} + k_{\phi we} + k_\phi}{k_{\phi fg} + k_{\phi wg}} \qquad F_d = 115.803 \, ksi$$

← this is where kφ comes in!

Determination of M_n for distortional buckling per C3.1.6

$M_{crd} := S_f F_d$ $M_{crd} = 110.361 \text{ kip}\cdot\text{in}$ (Eq. C3.1.6-4)

$M_y := S_f f_y$ $M_y = 47.65 \text{ kip}\cdot\text{in}$ (Eq. C3.1.6-5)

$\lambda_d := \sqrt{\dfrac{M_y}{M_{crd}}}$ $\lambda_d = 0.657$ (Eq. C3.1.6-3)

$$M_{nd} := \begin{vmatrix} M_y & \text{if } \lambda_d \leq 0.673 \\[2mm] \left[\left[1 - 0.22\cdot\left(\dfrac{M_{crd}}{M_y}\right)^{0.5}\right]\left(\dfrac{M_{crd}}{M_y}\right)^{0.5}\cdot M_y\right] & \text{if } \lambda_d > 0.673 \end{vmatrix}$$

       (Eq. C3.1.6-1)
       (Eq. C3.1.6-2)

$M_{nd} = 47.65 \text{ kip}\cdot\text{in}$

Using this worksheet and combining the resuls for the same section using CFS v5.02 the following summary table for a typical section was generated.

Updated versions of this Table discussed in Section 2 of report

M_n for SSMA 600S162-54 (50ksi) Beam

Distortional buckling per C3.1.6(b)		Local and lateral-torsional per AISI 2004 (calc per CFS 5.02)					
		M_n 46.4	46.4	41.6	28.0	16.3	(kip-in)
M_n	k_ϕ	L 0	2	4	6	8	(ft)
40.0	0.0	40.0	40.0	40.0	28.0	16.3	
42.0	0.1	42.0	42.0	41.6	28.0	16.3	
44.0	0.2	44.0	44.0	41.6	28.0	16.3	
46.0	0.3	46.0	46.0	41.6	28.0	16.3	
47.0	0.4	46.4	46.4	41.6	28.0	16.3	
47.6	0.5	46.4	46.4	41.6	28.0	16.3	
47.6	0.6	46.4	46.4	41.6	28.0	16.3	
47.6	0.7	46.4	46.4	41.6	28.0	16.3	
47.6	0.8	46.4	46.4	41.6	28.0	16.3	
47.6	0.9	46.4	46.4	41.6	28.0	16.3	
47.6	1.0	46.4	46.4	41.6	28.0	16.3	
(kip-in)	(kip/rad)						

▮ indicates regions where distortional buckling is predicted to control the strength

Summary: if the braced length is small and the rotational restraint small DB may control..

This example could be the beginning of CFSEI technical note on DB calculation?

12   RECOMMENDED AISI-COS PROVISIONS/CHANGES

** Draft 13 May 2007 **

It is recommended to modify the commentary to C3.1.6 in the *Specification*, as follows:

The primary difficulty in calculating the strength in distortional buckling is to efficiently estimate the elastic distortional buckling stress, F_d. Recognizing the complexity of this calculation this section provides three alternatives: C3.1.6(a) provides a conservative prediction for unrestrained C- and Z-sections, C3.1.6(b) provides a more comprehensive method for C- and Z-Section members and any open section with a single web and single edge stiffened compression flange, and C3.1.6(c) offers the option to use rational elastic buckling analysis, e.g., see the Appendix 1 commentary. The equations of C3.1.6(a) assume the compression flange is unrestrained; however, the methods of C3.1.6(b) and (c) allow for a rotational restraint, k_ϕ, to be included to account for attachments which restrict flange rotation.

While it is always conservative to ignore the rotational restraint, k_ϕ, in many cases it may be beneficial to include this effect. Due to the large variety of possible conditions, no specific method is provided for determining the rotational restraint. Instead, per Section A1.1 of the *Specification,* k_ϕ may be estimated by testing or rational engineering analysis. Test determination of k_ϕ may use AISI TS-1-02 (AISI 2002). K from this method is a lower bound estimate of k_ϕ. ~~The member lateral deformation may be removed from the measured lateral deformation to provide a more accurate estimate of k_ϕ.~~

For members with profiled steel panels providing k_ϕ: Testing on 8 and 9.5 in. (203 and 241 mm) deep Z-sections with a thickness between 0.069 (1.75 mm) and 0.118 in. (3.00 mm), through-fastened 12 in. (205 mm) o.c., to a 36 in. (914 mm) wide, 1 in. (25.4 mm) and 1.5 in. (38.1 mm) high steel panels, with up to 6 in. (152 mm) of blanket insulation between the panel and the Z-section, results in a k_ϕ between 0.15 to 0.44 kip-in./rad./in. (0.667 to 1.96 kN-mm/rad./mm) (MRI 1981). Additional testing on C- and Z-sections with pairs of through-fasteners provides considerably higher rotational stiffness: for 6 and 8 in. (152 and 203 mm) deep C-sections with a thickness between 0.054 and 0.097 in. (1.27 and 2.46 mm), fastened with pairs of fasteners on each side of a 1.25 in. (31.8 mm) high steel panel flute at 12 in. (305 mm) o.c., k_ϕ is 0.4 kip-in./rad./in. (1.78 kN-mm/rad./mm); and for 8.5 in. (216 mm) deep Z-sections with a thickness between 0.070 and 0.120 in. (1.78 to 3.05 mm), fastened with pairs of fasteners on each side of 1.25 in. (31.8 mm) high steel panel flute at 12 in. (305 mm) o.c., k_ϕ is 0.8 kip-in./rad./in. (3.56 kN-mm/rad./mm) (Yu and Schafer 2003, Yu 2005).

~~Examples of rational engineering analysis to estimate the rotational stiffness are provided in the Direct Strength Method Design Guide (2006). For a flexural member, k_ϕ can be approximated as:~~

~~$$k_\phi \approx EI/(W/2) \quad (C\text{-}C3.1.6\text{-}1)$$~~

~~where E is the modulus of the attached material, I is the moment of inertia of the engaged attachment, and W is the member spacing. The primary complication in such a method is determining how much of the attachment (decking, sheathing, etc.) is engaged when the flange attempts to deform. For the Z-sections tested in Yu (2005) experimental k_ϕ is 0.8 kip-in./rad./in. (3.56 kN-mm/rad./mm). Using an estimate of EI/(W/2) the rational engineering values are k_ϕ of 9 kip-in./rad./in. (40.0 kN-mm/rad./mm) if the entire panel, flutes and all, are engaged; k_ϕ of 1.2 kip-in./rad./in. (5.34 kN-mm/rad./mm) if only the corrugated bottom panel, but not the flutes, is engaged; and k_ϕ of 0.003 kip-in./rad./in. (0.0133 kN-mm/rad./mm) if plate bending of the t =~~

0.019 in. (0.483 mm) panel occurs. The observed panel engagement is between the last two estimates, and assuming the corrugated bottom pan, but not the 1.25 in. (31.8 mm) high flutes is engaged is reasonable.

For members with wood sheathing attached, little experimental information is available. The problem has been studied numerically using the same paired fastener detail as in Yu's (2005) and Yu and Schafer (2003) tests but replacing the steel panel with a simulated wood member, thickness = 0.5 in. (12.7 mm), E = 1000 ksi (6900 MPa), and μ = 0.3. The calculated k_ϕ is 5.1 kip-in./rad./in. (22.7 kN-mm/rad./mm) for 6 and 8 in. (152 to 203 mm) deep C-sections with a thickness between 0.054 and 0.097 in. (1.37 and 2.46 mm); and k_ϕ is 4.1 kip-in./rad./in. (18.2 kN-mm/rad./mm) for 8.5 in. (216 mm) deep Z-sections with thickness between 0.070 and 0.120 in. (1.78 mm and 3.05 mm). From calculations assuming a fully engaged ½ in. (12.7 mm) thick wood sheet on top of C- or Z-section members spaced 12 in. (305 mm) apart, k_ϕ is predicted to be 1.7 kip-in./rad./in. (7.56 kN-mm/rad./mm). Thus, use of EI/(W/2) provides a reasonably conservative approximation, with I calculated assuming the full engagement of wood sheet.

For members with plywood, OSB, or gypsum sheathing testing reported in Schafer et al. (2007) provides a methodology for using AISI TS-1-02 testing to separate the rotational stiffness into a sheathing and a connection component. This methodology has been adopted in the xxx AISI-COFS standard (2000x).

13 RECOMMENDED AISI-COFS PROVISIONS/CHANGES

<center>**DRAFT 11 May 2007 for discussion**</center>

Calculation of the nominal distortional buckling strength in bending, M_{nd}, per C3.1.6(b) or (c) of the *Specification*, or per Appendix 1 of the *Specification*, may utilize the beneficial system affect of sheathing fastened to the compression flange of flexural members (e.g., floor joists) through the calculation of the rotational stiffness provided to the bending member, k_ϕ.

The rotational stiffness k_ϕ is determined via

$$k_\phi = (1/k_{\phi w} + 1/k_{\phi c})^{-1} \tag{x.1}$$

where the sheathing rotational restraint $k_{\phi w}$ is calculated

for interior joists with fastened sheathing on both sides as
$$k_{\phi w} = EI_w/L_1 + EI_w/L_2 \tag{x.2}$$
for exterior joists, or joists with fastened sheathing on one side as
$$k_{\phi w} = EI_w/L_1 \tag{x.2}$$

and:

EI_w = sheathing bending rigidity, for plywood and OSB use EI_w values of APA (2004) as given in Table x.2(a), for gypsum board use minimum EI_w values of GA (2001) as given in Table x.2(b); note gypsum may be used for serviceability only, not for ultimate strength

L_1, L_2 = one half the joist spacing to the first and second sides respectively, as illustrated in Figure x.1

where the connection rotational restraint $k_{\phi c}$ is calculated

for fasteners spaced 12 in. o.c. or closer in plywood, OSB, or gypsum
$$k_{\phi c} = \text{values per Table x.2} \tag{x.2}$$

<center>Table x.1</center>
<center>(a) Plywood and OSB bending rigidity per APA, Panel Design Spec. (2004)</center>
<center>divide table values by 12 to convert to lbf-in.^{2}/in. of panel width</center>

RATED PANELS DESIGN CAPACITIES

Span Rating	Stress Parallel to Strength Axis				Stress Perpendicular to Strength Axis			
	Plywood			OSB	Plywood			OSB
	3-ply	4-ply	5-ply		3-ply	4-ply	5-ply	
PANEL BENDING STIFFNESS, EI (lb-in.²/ft of panel width)								
24/0	66,000	66,000	66,000	60,000	3,600	7,900	11,000	11,000
24/16	86,000	86,000	86,000	78,000	5,200	11,500	16,000	16,000
32/16	125,000	125,000	125,000	115,000	8,100	18,000	25,000	25,000
40/20	250,000	250,000	250,000	225,000	18,000	39,500	56,000	56,000
48/24	440,000	440,000	440,000	400,000	29,500	65,000	91,500	91,500
16oc	165,000	165,000	165,000	150,000	11,000	24,000	34,000	34,000
20oc	230,000	230,000	230,000	210,000	13,000	28,500	40,500	40,500
24oc	330,000	330,000	330,000	300,000	26,000	57,000	80,500	80,500
32oc	715,000	715,000	715,000	650,000	75,000	165,000	235,000	235,000
48oc	1,265,000	1,265,000	1,265,000	1,150,000	160,000	350,000	495,000	495,000

<center>(b) Gypsum board bending rigidity (modified to APA units) Gypsum Assoc., GA-235-01 (2001)</center>

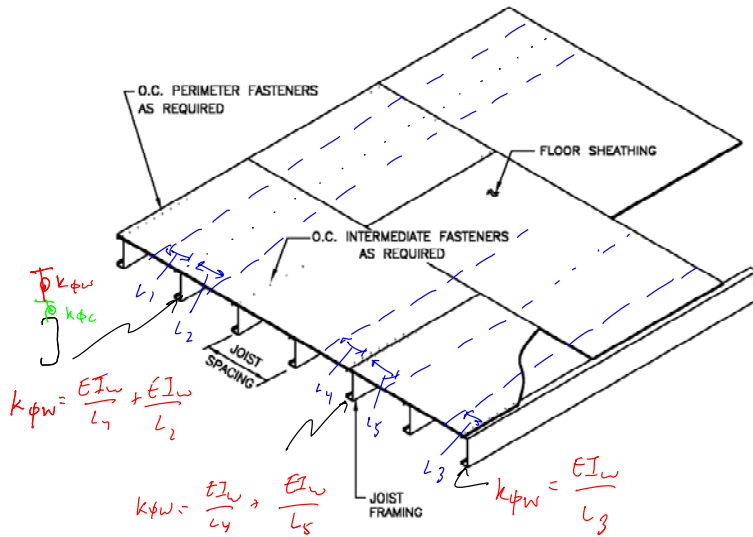| Effective Stiffness (EI)*		
(typical range)		
Board Thickness (in.)	Lb-in²/in of width	N-mm²/mm of width
1/2	1500 to 4000	220,000 to 580,000
5/8	3000 to 8000	440,000 to 1,160,000
* EI is dependent on board density, relative humidity, type of board, paper type, direction of board during testing and the amount of handling prior to measurement. In general the value of EI follows the following relationships: Type X Gypsum Board > Regular Gypsum Board; Denser Gypsum Board > Less Dense Gypsum Board; Machine Direction > Cross Direction; Low Relative Humidity > High Relative Humidity		

Detail F32
Floor Sheathing Connection Detail

O.C. PERIMETER FASTENERS AS REQUIRED

FLOOR SHEATHING

O.C. INTERMEDIATE FASTENERS AS REQUIRED

JOIST SPACING

JOIST FRAMING

$\textcircled{1} k_{\phi w}$
$\textcircled{2} k_{\phi c}$

$k_{\phi w} = \dfrac{E I_w}{L_1} + \dfrac{E I_w}{L_2}$

$k_{\phi w} = \dfrac{t I_w}{L_4} + \dfrac{E I_w}{L_5}$

$k_{\phi w} = \dfrac{E I_w}{L_3}$

L_1 L_2 L_4 L_5 L_3

Figure x.1 Illustration of L_1, L_2 for sheathing rotational restraint

Table x.2 Connection rotational restraint

t (mils)	t (in.)	$k_{\phi c}$ (lbf-in./in./rad)	$k_{\phi c}$ (N-mm/mm/rad)
18	0.018	78	348
27	0.027	83	367
30	0.03	84	375
33	0.033	86	384
43	0.043	94	419
54	0.054	105	468
68	0.068	123	546
97	0.097	172	766

(handwritten, right of upper rows) no testing in this range, but extension using formula in note (2) recommended.

(handwritten, right of lower rows) testing over this range, but bulk of testing at 054 and 097, use over full range recommended.

(1) fasteners spaced 12 in. o.c. or less

(2) values based on $k_{\phi c} = 0.00035 E t^2 + 75$

with E in psi, t in in., $k_{\phi c}$ in lbf-in./in./rad